DESIGN OF PATTERN RECONFIGURABLE ANTENNA

EMPLOYING RF-MEMS SWITCHES

A THESIS SUBMITTED TO
THE GRADUATE SCHOOL OF NATURAL AND APPLIED SCIENCES
OF
MIDDLE EAST TECHNICAL UNIVERSITY

BY

ÇAĞLAR GÖK

IN PARTIAL FULFILLMENT OF THE REQUIREMENTS
FOR
THE DEGREE OF MASTER OF SCIENCE
IN
ELECTRICAL AND ELECTRONIC ENGINEERING

AUGUST 2022

Approval of the thesis:

DESIGN OF PATTERN RECONFIGURABLE ANTENNA EMPLOYING RF-MEMS SWITCHES

submitted by **ÇAĞLAR GÖK** in partial fulfillment of the requirements for the degree of **Master of Science** i**n Electrical and Electronic Engineering, Middle East Technical University** by,

Prof. Dr. Halil Kalıpçılar
Dean, Graduate School of **Natural and Applied Sciences** _____

Prof. Dr. İlkay Ulusoy
Head of the Department, **Electrical and Electronics Engineering** _____

Assoc. Prof. Dr. Lale Alatan
Supervisor, **Electrical and Electronics Engineering** _____

Examining Committee Members:

Prof. Dr. Sencer Koç
Electrical and Electronics Engineering, METU _____

Assoc. Prof. Dr. Lale Alatan
Electrical and Electronics Engineering, METU _____

Assist. Prof. Dr. Ahmet Cemal Durgun
Electrical and Electronics Engineering, METU _____

Prof. Dr. Vakur B. Ertürk
Electrical and Electronics Engineering, Bilkent University _____

Prof. Dr. Birsen Saka
Electrical and Electronics Engineering, Hacettepe University _____

Date: 17.08.2022

I hereby declare that all information in this document has been obtained and presented in accordance with academic rules and ethical conduct. I also declare that, as required by these rules and conduct, I have fully cited and referenced all material and results that are not original to this work.

Name Last name : Çağlar Gök

Signature :

ABSTRACT

DESIGN OF PATTERN RECONFIGURABLE ANTENNA EMPLOYING RF-MEMS SWITCHES

Gök, Çağlar
Master of Science, Electrical and Electronic Engineering
Supervisor : Assoc. Prof. Dr. Lale Alatan

August 2022, 123 pages

In this thesis, the design, simulations, fabrication and measurements of reconfigurable antennas for use in 5G Massive MIMO systems are presented. 26 GHz is chosen as the operating frequency and RF-MEMS switches are used as control elements for pattern reconfiguration. As a first step, a patch antenna is designed based on the excitation of different operation modes of different resonators. A circular patch in the center and a ring resonator structure around it are used to create different radiation patterns by utilizing different modes of each resonator. The antenna is designed to have two feeds; the feed points are located at two opposite sides of the antenna. Two different radiation patterns, namely broadside and conical beams, are obtained depending on whether the antenna ports are fed in phase or out of phase. To increase the number of different radiation modes and to obtain radiation patterns that are not symmetric, two slots are opened in the ground plane of the antenna. Through the RF-MEMS switches placed inside these slots, one of the slots are short circuited and asymmetric radiation patterns are obtained for both in-phase and out of phase feeding. Due to the prolongation of the manufacturing process in METU MEMS Center, in order to validate the reconfiguration concept proposed in

this thesis, the design is repeated by using a commercially available dielectric substrate and by choosing a lower frequency band (the sub-6 GHz band) so that the antenna can be manufactured by using LPKF PCB Prototyping machine. To provide in-phase and out of phase excitation of antenna ports, a rat-race coupler is also designed. The antenna is manufactured together with the rat-race coupler and measured.

Keywords: Reconfigurable Antennas, RF-MEMS Switches, Pattern Reconfigurable Antennas, Phased Array Antennas

ÖZ

RF-MEMS ANAHTARLARI KULLANILARAK IŞIMA ÖRÜNTÜSÜ YAPILANDIRILABİLEN ANTEN TASARIMI

Gök, Çağlar
Yüksek Lisans, Elektrik ve Elektronik Mühendisliği
Tez Yöneticisi: Doç. Dr. Lale Alatan

Ağustos 2022, 123 sayfa

Bu tezde, 5G Massive MIMO sistemlerinde kullanılmak üzere yeniden yapılandırılabilir antenlerin tasarımı, simülasyonları, üretimi ve ölçümleri sunulmaktadır. Çalışma frekansı olarak 26 GHz seçilmiştir ve ışıma örüntüsünün yeniden yapılandırması için kontrol elemanları olarak RF-MEMS anahtarları kullanılmıştır. İlk adım olarak, farklı rezonatörlerin farklı çalışma modlarını uyarmasına dayalı olarak bir yama anteni tasarlanmıştır. Her rezonatörün farklı modlarını kullanarak farklı ışıma örüntüleri oluşturmak için merkezde dairesel bir yama ve etrafındaki halka rezonatör yapısı kullanılır. Anten iki beslemeye sahip olacak şekilde tasarlanmıştır; besleme noktaları antenin karşılıklı iki tarafında bulunur. Anten portlarının fazda veya faz dışı beslenmesine bağlı olarak, enine ışıma ve konik ışıma olmak üzere iki farklı ışıma modeli elde edilir. Farklı ışıma modlarının sayısını artırmak ve simetrik olmayan ışıma desenleri elde etmek için antenin yer düzleminde iki yarık açılır. Bu yarıkların içine yerleştirilen RF-MEMS anahtarları sayesinde yuvalardan biri kısa devre edilerek hem faz içi hem de faz dışı besleme için asimetrik ışıma desenleri elde edilir. ODTÜ MEMS Merkezi'ndeki üretim sürecinin uzaması nedeniyle, bu tezde önerilen yeniden yapılandırma konseptini doğrulamak için, ticari olarak mevcut bir dielektrik alt tabaka kullanılarak

ve daha düşük bir frekans bandı (6-GHz altındaki bant) seçilerek tasarım tekrarlanmıştır. Böylece anten LPKF PCB Prototipleme makinesi kullanılarak üretililmiştir. Anten bağlantı noktalarının faz içi ve faz dışı uyarımını sağlamak için, bir hibrit halka bağlayıcı da tasarlanmıştır. Anten, hibrit halka bağlayıcı ile birlikte üretilmiş ve ölçülmüştür.

Anahtar Kelimeler: Yapılandırılabilen Antenler, RF-MEMS Anahtarlar, Işıma Örüntüsü Yapılandırılabilen Antenler, Faz Dizili Antenler

To My Family

ACKNOWLEDGMENTS

I would like to deeply thank my advisor Assoc. Prof. Dr. Lale Alatan for her sincere friendship, support, and kindly attitude during my master's degree education. Thanks to her, I have never felt lonely on this journey. Her guidance and full support in all research and thesis stages helped me to conclude this thesis.

I also would like to thank Assoc. Prof. Dr. Mehmet Ünlü and Prof. Dr. Hamza Kurt for their inspiration during last two years in my undergraduate study in TOBB University of Economics and Technology. Being a part of their research group was a great honour for me.

I would like to thank ASELSAN Inc. for providing the technical facilities and resources during the thesis period.

I would like to thank Mustafa Kuloğlu for his valuable comments and contributions during the thesis process. I also thank Yunus Emre Taşkır and Beytullah Bozkır for their help during the pattern measurements in anechoic chamber.

I would like to thank Feza Turgay Çelik and Muhammed Tonga for their inspiration and support from the beginning to the end of the work. I also thank Yağmur Karahan, Elif Damla Gültekin, and Tutku Bakan for their support and friendship.

Finally, I would like to thank my dear family deeply. I will always be grateful to my father Hikmet Gök, my mother Kıymet Gök, and my sister Gizem Gök for their understanding and loving support. Without them, this work would not have come about.

This work is partially supported by the Scientific and Technological Research Council of Turkey (TUBITAK) under Grant 218E039.

TABLE OF CONTENTS

LIST OF TABLES

TABLES

LIST OF FIGURES

FIGURES

LIST OF ABBREVIATIONS

ABBREVIATIONS

5G	Fifth Generation Mobile Network
RF-MEMS	Radio Frequency Microelectromechanical Systems
GPS	Global Positioning System
MIMO	Multiple Input Multiple Output
TM	Transverse Magnetic
PEC	Perfect Electric Conductor
PMC	Perfect Magnetic Conductor
CPW	Coplanar Waveguide
GCPW	Grounded Coplanar Waveguide
HRS	High Resistivity Silicon
HFSS	High Frequency Structural Simulator

LIST OF SYMBOLS

SYMBOLS	
Θ	Elevation Angle [degree]
ϕ	Azimuth Angle [degree]
$\boldsymbol{\omega}$	Angular Frequency [rad/sn]
λ_0	Wavelength in the free space [m]
μ_0	Permeability of free space [H/m]
ε_r	Relative permittivity of the dielectric
J_n	Bessel function of the first kind in nth order
tan δ	Loss tangent

CHAPTER 1

INTRODUCTION

In wireless communication systems, radar systems, GPS, and imaging systems, antennas are critical elements. Antennas have certain parameters such as operating frequency, radiation pattern, and polarization. These parameters differ according to the usage area of the antenna. In the light of developing new technologies, especially in new generation communication systems, these parameters need to be changed dynamically on the same antenna. Based on this need, reconfigurable antenna technologies have started to be developed.

The reconfigurable antenna is the antenna that can dynamically change some characteristic features of the antenna according to changing conditions [1]. Such antennas are often preferred over wireless communication systems because they can change their polarization, radiation patterns, or operating frequencies. Through an internal mechanism placed inside the antenna, the current distributions on the antenna can be reshaped, and specific features of the antenna can be reconstructed in this way. The reconstruction process on the antenna can be electrical, mechanical, or material-based [2]. Electrical reconfiguration is one of the most preferred restructuring methods in new generation communication systems. In this reconfiguration method, electronic switching mechanisms such as radio frequency microelectromechanical system (RF-MEMS) switches, PIN diodes, or varactors are used to redistribute the surface currents on the antenna and change the radiation characteristics of the antenna [2].

Increasing speed, lower latency, and higher capacity requirements in communication systems create new design demands in antenna technologies. To meet this demand

through spatial diversity in massive MIMO array systems, antennas whose radiation patterns can be reconfigured are utilized.

1.1 Motivation and Problem Definition

Array antennas are structures formed by at least two antenna elements. Array antennas are used to achieve high gain and narrow beam performance that cannot be achieved with a single antenna element. Antenna elements must be arranged with a certain geometry and stimulated with an appropriate feeding method. Phased array antennas can rotate the radiation pattern electronically without the need to rotate the antenna mechanically. They are also known as electronically scanned arrays. Thanks to the phase shifters placed behind each antenna element and the progressive phase shift applied to these phase shifters, the radiation pattern of the array can be rotated in the desired direction.

Array antenna patterns can be found by multiplying the array factor and the element pattern. The array factor is a function of the positions of the antennas in the array and the excitation coefficients used, and it is not preferable to change it. Even if the array factor is maximized in any desired direction, the overall pattern will still depend on the pattern of the elements. For this reason, rotating the radiation patterns of the antenna elements used in the array in the same direction with the maximum radiation direction of the array would improve the array performance. Hence the aim of this thesis is to design pattern reconfigurable antenna that will be used in an array and the pattern will be reconfigured according to the beam steering direction of the array. As the application area, small cell massive MIMO array for 5G, operating at 26 GHz is chosen.

There are some limitations in the design to be made. First, the size of the antenna element to be designed should be less than $\lambda/2$, since it will be used in an array. Secondly, since the physical size of the antenna will be small due to the high operating frequency, RF-MEMS switches are chosen to be the control elements to

reconfigure the pattern of the antenna. The designed antenna will be manufactured at METU MEMS center. Hence the design should be compatible with the production abilities available at METU MEMS Center. For example, the micromachining technology at METU MEMS Center does not allow the production of shortening vias. Therefore the design should avoid the use of shorting vias or probe fed structures. In the next section, pattern reconfigurable antenna structures proposed in literature will be summarized and some of them will be evaluated in terms of their compliance with the requirements mentioned above.

1.2 Literature Review

Antenna design, whose radiation pattern can be reconfigured, has been one of the most researched subjects in recent years. Many studies have been carried out in this area, especially due to the development of 5G technology and the increasing need for new antenna technologies.

When the literature is examined, it is seen that some studies are handled using the parasitic element method [3]-[6]. In [3], the structure consists of three strips placed parallel to each other, as shown in Figure 1.1 and only the center strip is excited. There are gaps and switching mechanisms on the right and left strips, which are excited parasitically. With the help of the switches placed between these gaps, the lengths of the strips on the right or left can be changed to form a Yagi-Uda antenna. When the left strip is switched, the longer left strip works like a reflector and removes the radiated electromagnetic fields from itself. The shorter right strip works like a director and directs the emitted electromagnetic fields towards itself. Although this study successfully steers the antenna pattern, the large physical dimensions seem to be a major drawback to be used as an array element.

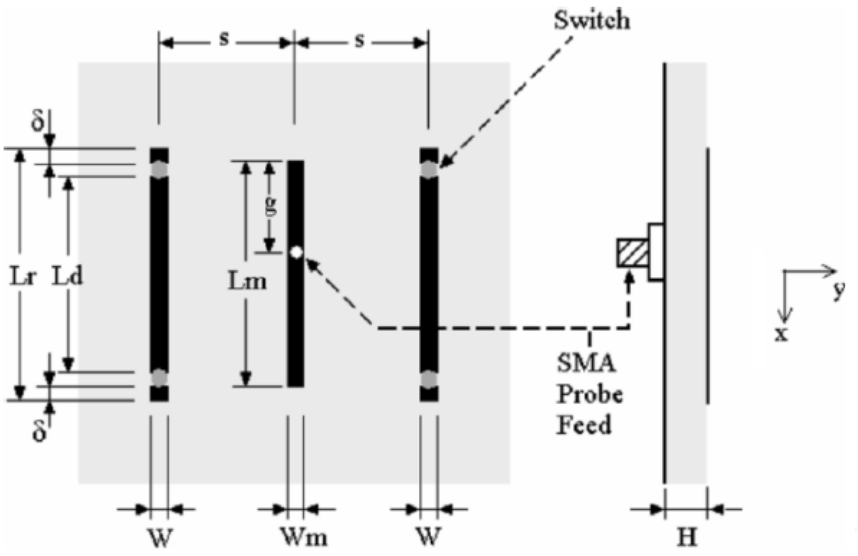

Figure 1.1: Physical structure of the reconfigurable microstrip parasitic array [3]

In [7], a pattern reconfigurable microstrip patch antenna is proposed for wearable antenna applications. The proposed rectangular microstrip antenna structure is presented in Figure 1.2. The switches between the feed line and the antenna patch can control the radiation pattern. The antenna has broadside radiation when switch 1 and switch 2 are in the open position. When one of the switches is turned off, main beam rotates 30˚ from broadside, in the opposite direction of the closed switch. The circular slots at the end of the U-slot are used for impedance matching. Resonance at the same frequency was obtained for all switch positions. At the beginning of this thesis, this antenna structure is tried to be adapted for the design of the antenna considered in this work. Although a similar pattern reconfiguration is achieved, the resonance frequency of the antenna shifted according to switch positions. Although antenna dimensions are aimed to be optimized to obtain pattern reconfiguration at the same frequency, it could not be achieved. Therefore, other pattern reconfigurable antenna structures are explored.

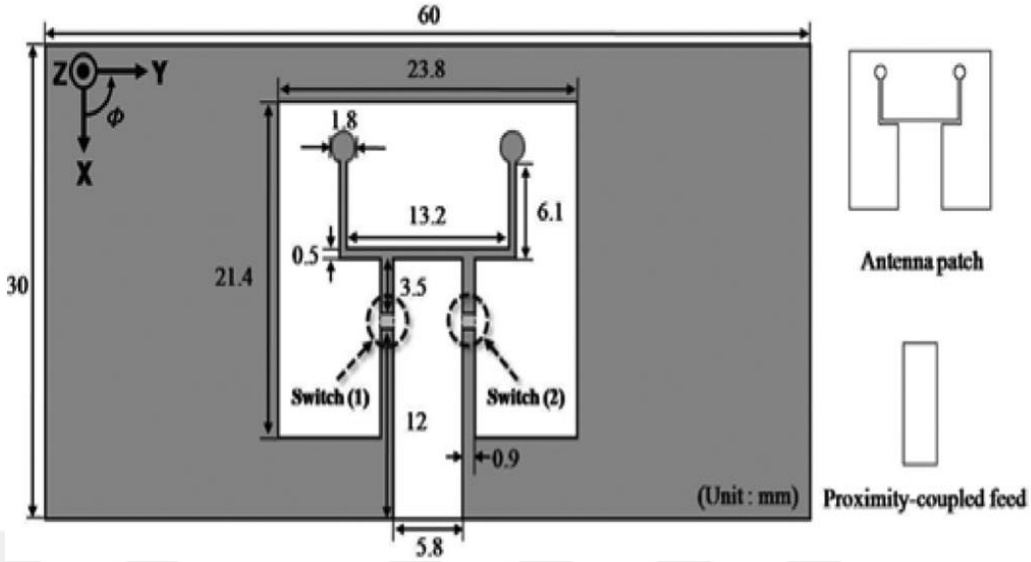

Figure 1.2: Geometry of the proposed antenna [7]

Another method proposed in the literature for pattern reconfiguration is based on the characteristic mode theory [8]-[10]. In these studies, different characteristic modes are stimulated using either capacitive coupling elements as in [8] and [9] or inductive coupling elements as suggested in [10]. The structures of capacitive and inductive coupling elements are presented in Figures 1.3(a) and (b), respectively. When these structures are examined, it has been evaluated that it is not possible to use such excitation structures for antennas that will operate at 26 GHz and be produced with micromachining technology.

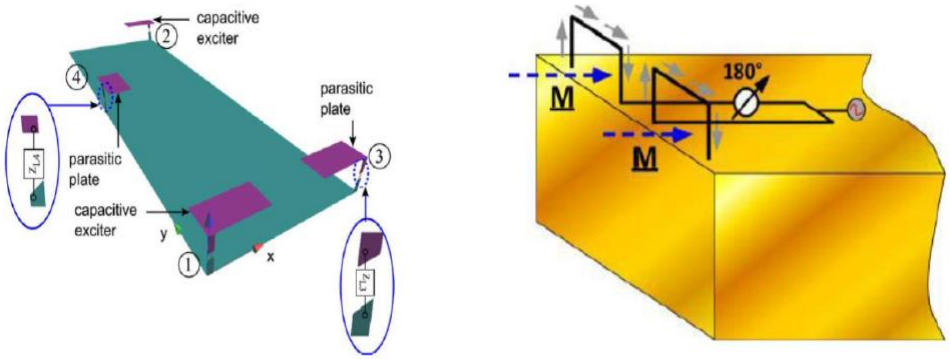

(a) (b)

Figure 1.3: Coupling structures a) capacitive [8], b) inductive [10]

In [11]-[12], the pattern reconfiguration property is presented by integrating two shorted quarter-wave patch antennas. In [12], the patches are excited with the slot-coupled feeding technique, as shown in Figure 1.4. The shorting plane connected from the middle of the patch to the ground plane combines two shorted quarter-wave patch antennas. The antenna is fed by a rat-race coupler that provides in-phase or out of phase excitation of two patches. Since two antennas have opposite polarizations, out of phase excitation results in conical beam and in-phase excitation provides broadside radiation. However, such a structure is not possible to be used in our design since the micromachining facilities at METU MEMS Center does not allow the fabrication of shorting vias or planes.

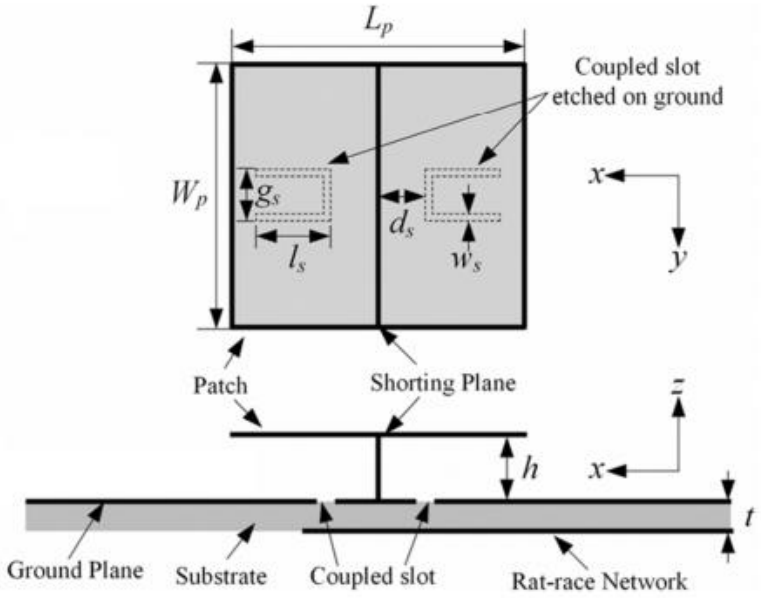

Figure 1.4: Shorted Patch Antenna [12]

In [13], the antenna structure which is both pattern and frequency reconfigurable, is presented. The proposed antenna can dynamically change its operating frequency and radiation pattern. Longitudinal slits are opened on the antenna, and PIN diodes are placed in these slots for switching purposes, as shown in Figure 1.5. The electrical length of the antenna can change through PIN diode switches. In this way,

the antenna can radiate at different frequencies. The proposed antenna can radiate at 4.5 GHz, 4.8 GHz, 5.2 GHz, and 5.8 GHz frequencies according to the ON and OFF status of the switches. In addition, it can rotate the main beam direction to -30 degrees and 30 degrees in xz plane, through the switching mechanism.

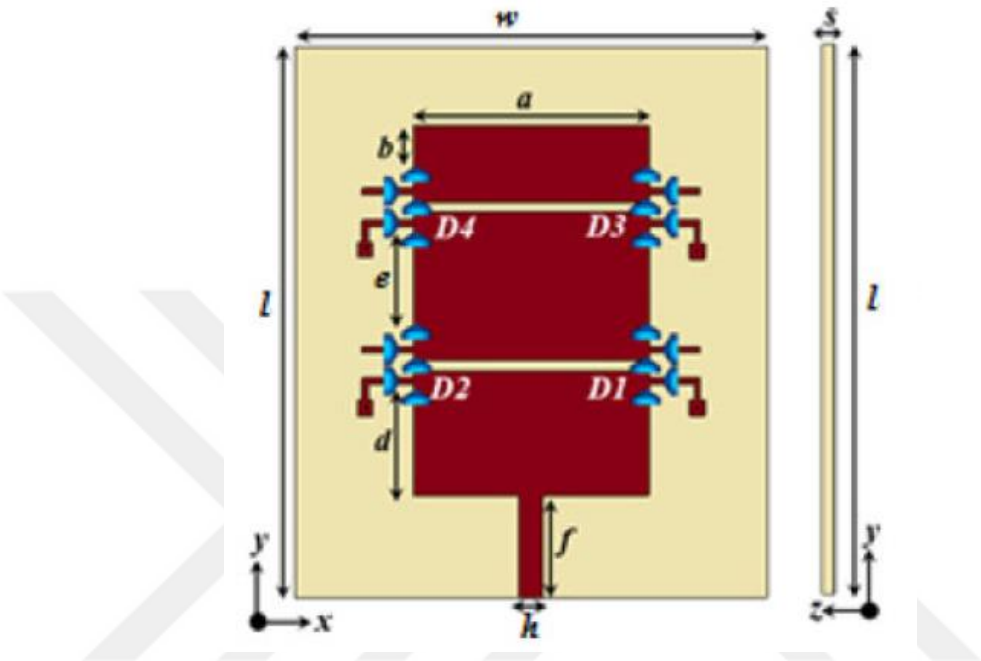

Figure 1.5: Frequency and pattern reconfigurable antenna [13]

Circular patch antennas are generally operated at the dominant TM_{11} mode that provides broadside radiation. In recent years it is shown that conical beams can be obtained by exciting TM_{01} and/or TM_{02} modes of circular patch antennas by utilizing shorting vias [14, 15]. Such circular patch antennas are refered as monopolar patch antenna. Various pattern reconfigurable circular patch antennas are proposed in literature [16-18] that switch between conical beam and broadside radiation modes at the same frequency by utilizing stacked patches or complicated feeding structures. However, since monopolar patch structure involves shorting vias, fabrication of such a frequency reconfigurable antenna is also not possible at METU MEMS Center.

In [19], a multi-mode microstrip antenna structure consisting of a concentric circular patch and two circular rings is proposed. The sizes of each resonator are adjusted so

that TM_{11}, TM_{21}, and TM_{31} modes are excited at the same frequency for the circular patch, the inner ring, and the outer ring, respectively. To excite these modes, one, two, and three probe feeds are used for TM_{11}, TM_{21}, and TM_{31} modes, respectively. In addition to these three different radiation modes, numerous radiation patterns are obtained by different combinations of these modes with various phase differences and amplitude ratios. Although the proposed structure provides high diversity in radiation patterns, the size of the antenna is large, and the feed network is complicated for array applications.

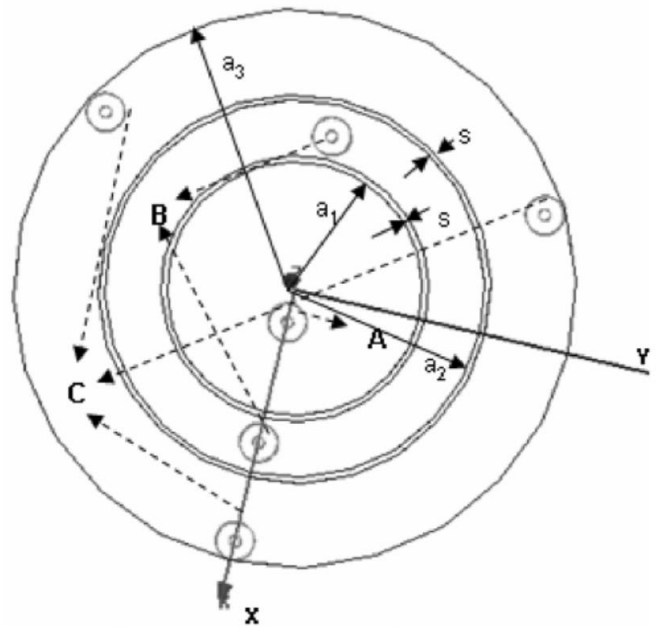

Figure 1.6: Geometry of a multimode concentric circular microstrip patch antenna [19]

In [20], only the circular patch and one concentric ring are studied to reduce the antenna size. It is shown that the feed of the circular patch can be eliminated, and it can be excited by the probe feeds of the ring antenna through electromagnetic coupling in the gap between the ring and the circular patch. It is shown in [20] that when two feeds of the ring are in phase, TM_{21} mode is excited in the ring, whereas TM_{11} is excited when they are out of phase. Consequently, the antenna could switch between conical and broadside radiation modes. Moreover, by changing the phase

difference between the feeds, the main radiation direction of the antenna can be steered between -40 degrees and +40 degrees from the broadside. However, when this antenna is used in a large array application, it is not practical to steer the main radiation direction of the element by using an additional phase shifter for each element.

1.3 Objectives and Structure of the Thesis

After this literature survey, the antenna structure proposed in [20] is evaluated to be the best candidate to start the design of the antenna aimed in this thesis. The antenna presented in [20] provides only two different radiation modes: conical beam and broadside radiation. However, in this thesis other radiation modes like $\pm 20^0$-30^0 from broadside and modified conical beam that radiates more efficiently in one half plane and has suppressed radiation in the other half plane are targeted. To achieve such asymmetric radiation modes, it is clear that the symmetry of the antenna needs to be disturbed. To introduce asymmetry to the antenna geometry, first slots are opened on the patch, but these slots did not affect the radiation pattern of the antenna considerably. In addition, the slots opened on the patch also shifted the resonant frequency of the antenna. Thereupon, slots are opened in the ground plane of the antenna, and it is observed that the radiation pattern changes with the introduction of the slots. As a result of simulation studies where RF-MEMS switches are modelled by conducting strips, it is observed that slots can be short circuited by using a couple of RF-MEMS switches in the slot. Hence, the design of the antenna proceeded in that direction. All electromagnetic simulations in this study are performed by using Finite Element Method based commercially available software ANSYS HFSS.

A pattern reconfigurable antenna operating at 26 GHz and suitable to be manufactured at METU MEMS Center is designed. However, due to the prolongation of the manufacturing process, in order to validate the reconfiguration concept proposed in this thesis, the design is repeated by using a commercially available dielectric substrate and by choosing a lower frequency band (the sub-6 GHz

band) so that the antenna can be manufactured by using LPKF PCB Prototyping machine. To provide in-phase and out of phase excitation of antenna ports, a rat-race coupler is also designed. The antenna is manufactured together with the rat-race coupler and measured.

The content of the thesis can be listed as follows:

In Chapter 2, design considerations of circular microstrip patch antennas are presented. In addition, the most commonly used microstrip antenna feeding methods are described.

In Chapter 3, the design of the ringed circular patch antenna operating in the mm-wave band and compatible with manufacturing facilities at METU MEMS Center is introduced. Then design stages for improving the pattern reconfiguration ability of the antenna by introducing slots into its ground plane are given.

It was mentioned that due to the prolongation of the manufacturing process of the mm waveband antenna, the antenna design was repeated for the sub-6 GHz frequency band. In Chapter 4, the design of this antenna together with the design of rat-race coupler and its integration with the antenna are introduced.

In Chapter 5, the fabrication process and measurement results of the antenna designed in the sub-6 GHz frequency band are presented. The obtained simulation results and the measurement results are compared and interpreted.

In Chapter 6, the conclusion and future works are presented. Also, the contribution of this research work is summarized.

CHAPTER 2

MICROSTRIP PATCH ANTENNAS

Microstrip antennas are usually made by placing a ground plane on one side of a dielectric substrate and a conductive patch on the other side. The patch shape can be square, rectangular, triangular, or circular [21]. Since the antenna designed in this thesis consists of circular and ring shaped patches, their analyses will be considered in this chapter.

2.1 Cavity Model Analysis of Circular Microstrip Patch Antennas

A circular microstrip patch antenna geometry is given in Figure 2.1.

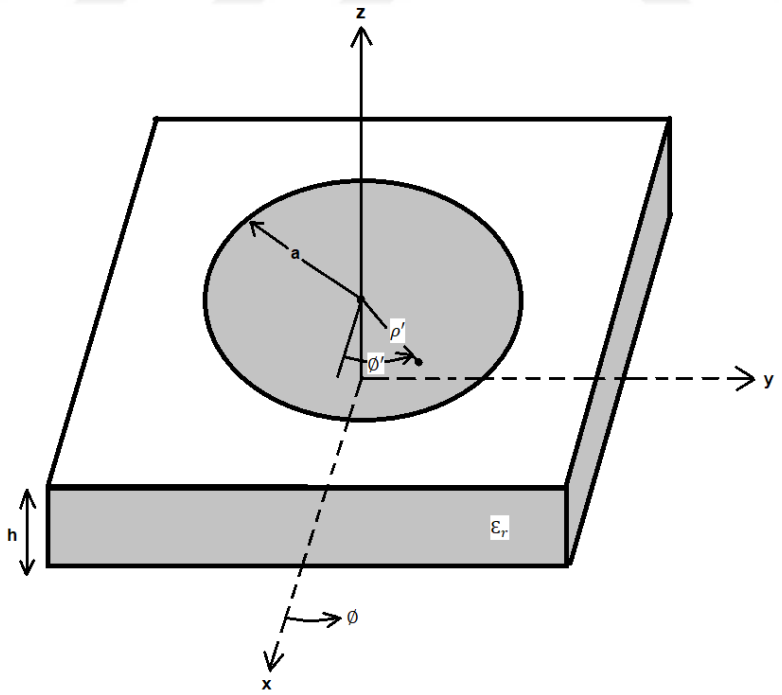

Figure 2.1: Geometry of circular microstrip patch antenna

Cavity model analysis is a commonly used method to examine fields excited by a microstrip antenna. In this method, the patch antenna can be considered as a cylindrical cavity with two Perfect Electric Conductor (PEC) walls on the top and bottom and Perfect Magnetic Conductor (PMC) walls on the edges of the patch. Some assumptions are made in the cavity model. Firstly, only the z component of the electric field exists in the cavity region and is independent of the z coordinate for all frequencies. This assumption is based on the fact that the thickness of the patch antenna is very small relative to the wavelength. The PMC wall assumption at the edges of the patch is based on the fact that the tangential component of the magnetic field is vanishingly small at the edges [22]. Electric and magnetic fields within the cavity are found by solving the wave equation, which is stated for the electric field as;

$$(\boldsymbol{\nabla}^2 + k^2)E_Z = 0 \qquad (2\text{-}1)$$

where wave number k can be expressed in terms of free space wavelength $\boldsymbol{\lambda}_0$, and dielectric constant ε_r as;

$$k = \frac{2\pi}{\boldsymbol{\lambda}_0}\sqrt{\varepsilon_r} \qquad (2\text{-}2)$$

When the wave equation (2.1) is solved subject to the boundary conditions given above, the electric and magnetic fields can be written as follows [22].

$$E_\rho = E_\phi = H_z = 0 \qquad (2\text{-}3)$$

$$E_Z = E_0 J_n(k\rho')\cos(n\emptyset') \qquad (2\text{-}4)$$

$$H_\rho = j\frac{E_0}{\omega\boldsymbol{\mu}_0}\frac{1}{\rho}J_n(k\rho')\sin(n\emptyset') \qquad (2\text{-}5)$$

$$H_{\emptyset} = j\frac{E_0}{\omega \boldsymbol{\mu}_0} J_n{}'(k\rho')\sin(n\emptyset') \qquad (2\text{-}6)$$

where '= $\partial/\partial\rho$ and $\emptyset'$ is the azimuth angle in xy plane measured from x-axis and $J_n(k\rho)$ is the Bessel functions of the first kind of order n. The boundary condition of the PMC type limits the values that the wavenumber (k) can take. This constraint can be expressed as:

$$H_{\emptyset}|_{\rho'=a} = j\frac{E_0 k}{\omega \boldsymbol{\mu}_0} J_n'(ka)\sin(n\emptyset) = 0 \qquad (2\text{-}7)$$

To satisfy the boundary conditions, $J_n'(ka)$ expression must be zero. m^{th} zero of the derivative of the n^{th} order Bessel function corresponds to TM_{nm} operation mode of the antenna and determines the wave number, k_{nm}, of the corresponding mode. The roots and the corresponding TM modes are given in Table 2.1.

Table 2.1: Roots of $J_n'(ka)$ [22]

Mode (n,m)	1,1	2,1	0,2	3,1	4,1	1,2
$k_{nm}a$	1.8411	3.0542	3.8317	4.2011	5.3170	5.3301

Fringing fields, a natural consequence of the radiation of patch antennas, make the antenna electrically larger. The effective radius of the circular patch antenna can be found by [22]:

$$a_e = a\left[1 + \frac{2h}{\pi a \varepsilon_r}\left[\ln\left(\frac{\pi a}{2h}\right) + 1.7726\right]\right]^{1/2} \qquad (2\text{-}8)$$

where; 'a_e' is the effective radius of the circular patch antenna

'h' is the thickness of the dielectric

'ε_r' is the relative permittivity of the dielectric

After k_{nm} is found by using the effective radius, the resonance frequency can be calculated as:

$$(f_{nm}) = \frac{k_{nm}}{2\pi\sqrt{\mu\varepsilon}} \qquad (2\text{-}9)$$

Field and current vectors for different TM_{nm} modes (m=1) are given in Figure 2.2 [22].

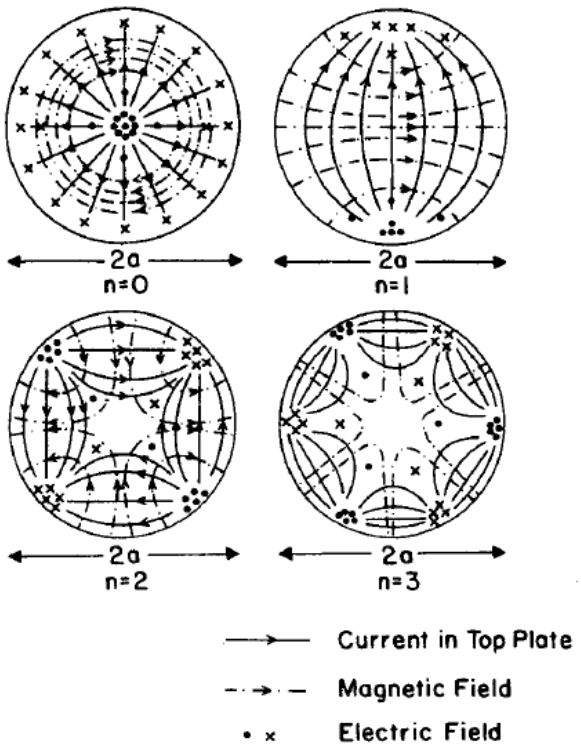

Figure 2.2: Fields and current patterns for different TM_{n1} modes [22].

As can be seen in Table 2.1, TM_{11} mode is the lowest order mode of the circular patch antenna, and from the current distribution it can be concluded that this mode provides broadside radiation. The second mode is the TM_{21} mode. This mode creates the monopole-like conical beam pattern. Generally, only a single feed is enough to excite dominat TM_{11} mode. However, the current distributions given in Figure 2.2 imply that two or larger number of feeds are required to excite higher order modes like TM_{21}. Therefore, before moving to the design of pattern reconfigurable antenna, different feeding techniques used for microstrip patch antennas will be summarized.

2.2 Feeding Techniques of Microstrip Patch Antennas

The feeding method is a critical parameter that affects the antenna input impedance and antenna characteristics. Selecting the feed type suitable for the designed antenna structure will allow the antenna to radiate more efficiently. There are basically five types of feeding techniques in patch antennas [22].

2.2.1 Microstrip Line Feeding

It is the feed type where the patch antenna and the feed line are on the same plane and are directly connected to each other [21]. It is frequently used because it is easy to manufacture, and the impedance matching can be easily achived by adjusting the feed location through an inset fed configuration as seen in Figure 2.3. On the other hand, since the feed line and the antenna are on the same substrate, unwanted radiation is possible with the increase in the dielectric thickness [22].

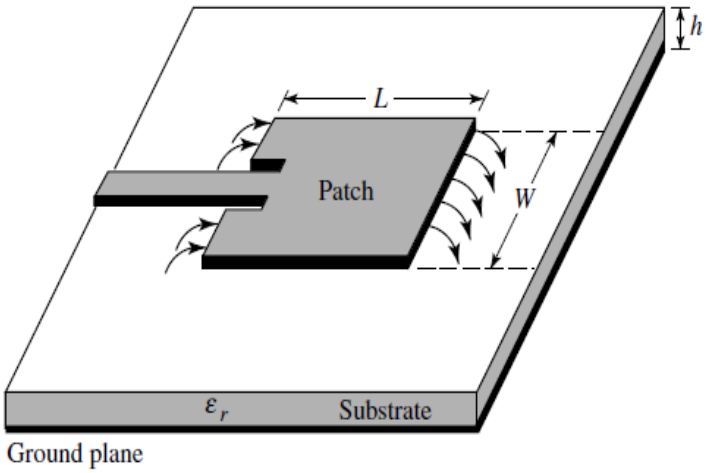

Figure 2.3: Microstrip line feeding [16]

2.2.2 Coaxial Probe Feeding

The coaxial feeding type is one of the most preferred feeding types because it is easy to manufacture, impedance matching can be done simply by changing the feed location, and it creates less unwanted radiation compared to the microstrip feeding type [21]. Outer conductor of the coaxial cable is connected to the ground plane, while the inner one is connected to the patch as shown in Figure 2.4.

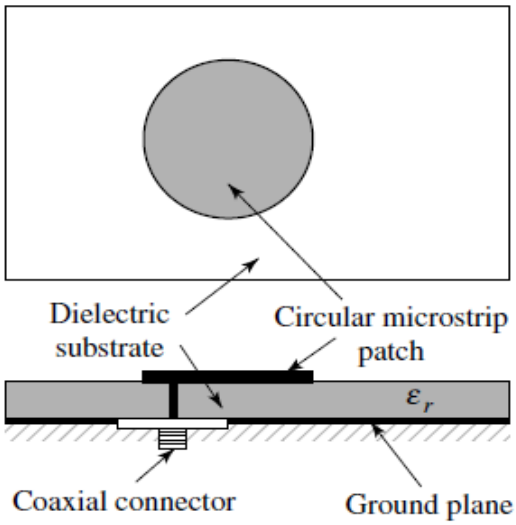

Figure 2.4: Coaxial probe feeding [21]

2.2.3 Proximity Coupling Feeding

Another method of feeding microstrip patch antennas is the proximity coupling method. In this method, two dielectric layers are used as shown in Figure 2.5. The lower dielectric has the feed line on it, while the upper dielectric has the patch on it. Thanks to the capacitive coupling formed between the feeding line and the patch, the patch is excited, and radiation occurs [22]. Although it provides more bandwidth than microstrip feed and coaxial feed, the antenna size increases due to its two-layer structure.

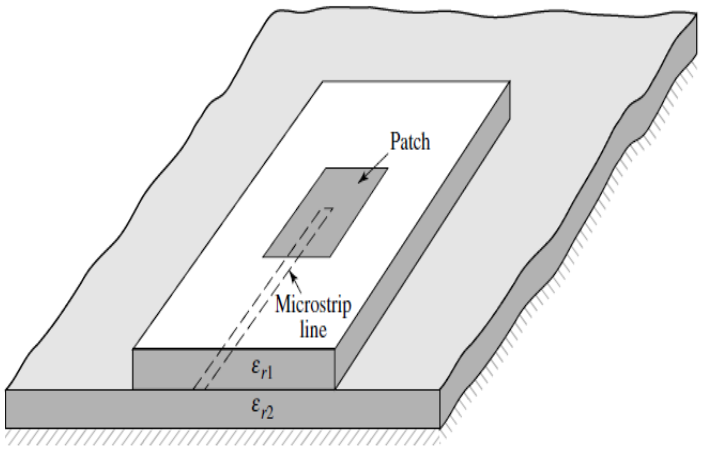

Figure 2.5: Proximity coupling feeding [21]

2.2.4 Aperture Coupled Feeding

One of the most important disadvantages of microstrip antennas is their narrow bandwidth. One of the methods used to eliminate this disadvantage is using the aperture coupled feeding technique. This feeding technique is the one that provides the most bandwidth compared to other techniques [22]. As shown in Figure 2.6, the two dielectric substrates are separated by a common ground plane which has a slot on it. There is a microstrip line under the lower dielectric layer, and this microstrip

line couples energy to the patch in the upper layer through the slot. One of its major drawbacks is the increase in antenna size, as it uses a two-layer structure.

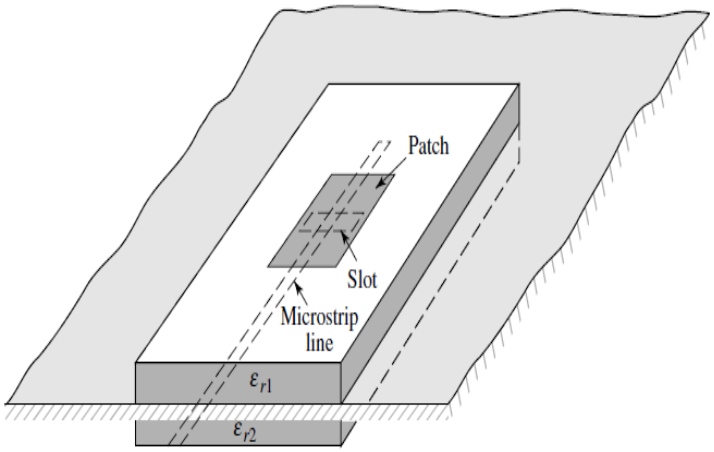

Figure 2.6: Aperture coupling feeding [21]

2.2.5 Coplanar Waveguide Feeding

Apart from the four feeding types described above, another feeding type used is the coplanar waveguide (CPW) feeding method. They are mostly preferred in systems where microwave circuits and patch antennas are used together [22]. In this feeding method, the CPW is etched into the ground plane of the patch antenna, and its coupling to the antenna is provided by slots that terminate the CPW feedline. Depending on the shape of the slot, the patch can be stimulated by inductively couple or capacitively coupled slots as shown in Figure 2.7. Its main advantage is that it is suitable for micromachining.

(a) (b)

Figure 2.7: (a) Inductively coupled and (b) capacitively coupled slot structures [23]

CHAPTER 3

DESIGN AND ANALYSIS OF RINGED CIRCULAR PATCH ANTENNA AT MM-WAVE BAND

This section presents the antenna design that can reconfigure the radiation pattern at 26 GHz. As mentioned in Chapter 1, in the literature many issues have been studied before on this subject. In the study proposed in [19] and shown in Figure 3.1, the innermost circular patch operates at TM_{11} mode (broadside radiation) with a single probe, TM_{21} (conical beam) mode is stimulated by two probes in the middle ring, and finally, by three probes in the outer ring TM_{31} mode is stimulated. The diameter of the center patch and the inner and outer radius of the middle ring and outer ring are chosen so that all modes are excited at the same frequency. From the results presented in [20], it was observed that the outermost ring did not contribute much to improve of the radiation pattern diversity. In order not to increase the antenna size too much, simulations of the structure consisting of only the inner circular patch and the ring in the middle are performed.

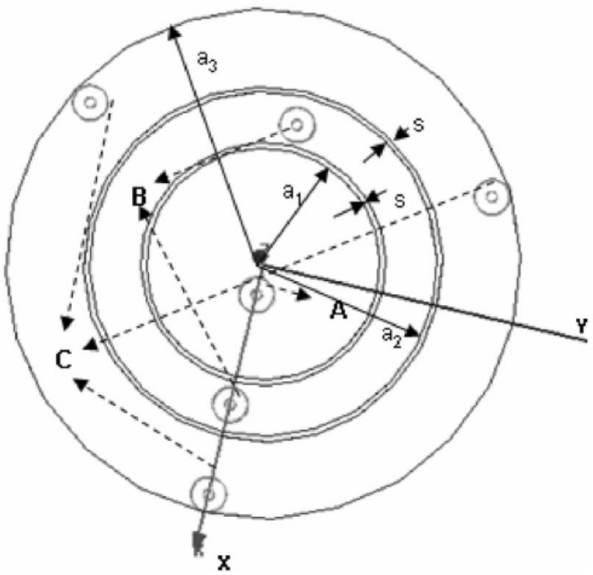

Figure 3.1: Geometry of a multimode concentric circular microstrip patch antenna [19]

Since this study aims to excite the antenna in two different operating modes using two different resonators, the antenna structure presented in [19] is the cornerstone of the design here. A critical point has been noticed in [20]. Without connecting a probe to the inner circular patch antenna, only the outer ring is fed with two probes, and the main beam direction changes when the phase difference between the probes is changed between 0 and 180 degrees. After seeing that the radiation pattern of the antenna can be shaped with a simple phase change, it is started to work on designing this antenna structure to operate at 26 GHz and to be produced by micromachining processes.

3.1 Antenna Structure at 26 GHz

Since the antenna will be produced by METU MEMS Center, the dielectric substrates used in the antenna were chosen to be compatible for fabrication by micromachining. As mentioned in the previous section, microstrip antennas can be excited by CPW feed lines via capacitively or inductively coupled slots. Simulations were made with both types of slots, and inductively coupled slot was preferred since it provided easier impedance matching. An antenna operating at 26 GHz has been obtained by examining the length of the inductive slot and the length of the antenna parametrically. However, when the radiation pattern is examined, it is observed that the radiation made by the antenna to the lower hemisphere is high. It is thought that this radiation is caused by the slot. For this reason, instead of CPW, a grounded coplanar waveguide (GCPW) with a metal plate at the bottom has been used in the design. Glass with a thickness of 0.5 mm, a dielectric constant (ε_r) of 4.6, and a loss tangent (tan δ) of 0.0002 is chosen as the substrate of the GCPW. The dielectric substrate of the antenna was chosen as 0.5 mm thick High Resistivity Silicon (HRS) (ε_r=11.7, tan δ=0.01). Since the dielectric constant of HRS is very high, the bandwidth of antennas designed on this material is very narrow. To increase the bandwidth, it is necessary to decrease the effective dielectric constant. For this purpose, the HRS substrate is micromachined to obtain an air gap of 0.2 mm

thickness. Then, the antenna is etched at the interface of HRS and the air cavity, as shown in Figure 3.2. The top views of the antenna and GCPW layers are shown in Figures 3.3(a) and 3.3(b), respectively.

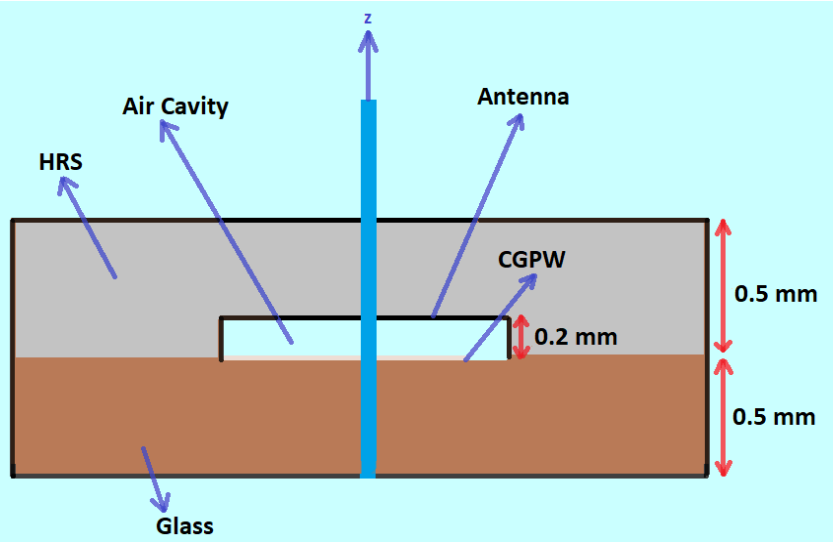

Figure 3.2: Side view of proposed antenna

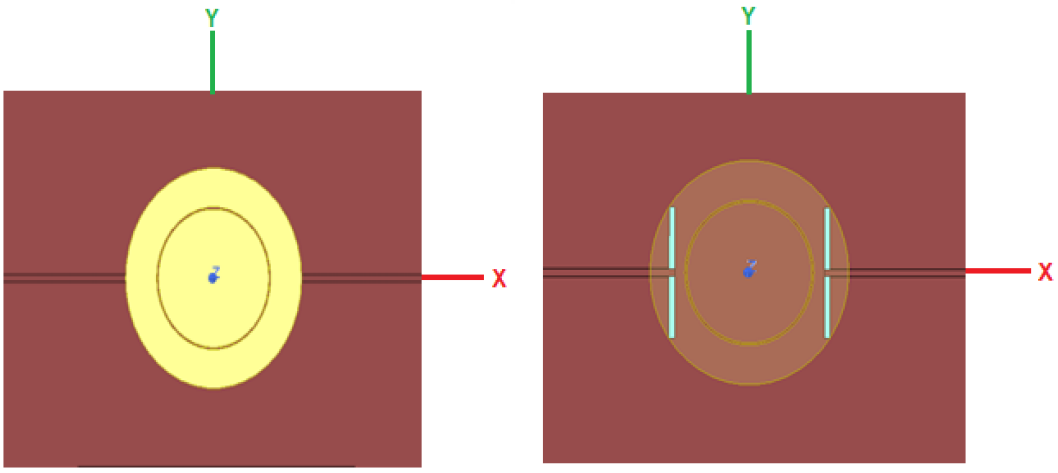

(a) (b)

Figure 3.3: Top views of (a) antenna layer and (b) GCPW layer

Throughout the thesis, to avoid confusion, the situation where the two excitation ports are fed in phase will be called "common mode", and the situation where they are fed with a 180˚ phase difference will be called "differential mode". The input return loss (S_{11}), and isolation between two ports (S_{12}) are presented in Figure 3.4. The parameters of the optimized antenna are listed in Table 3.1.

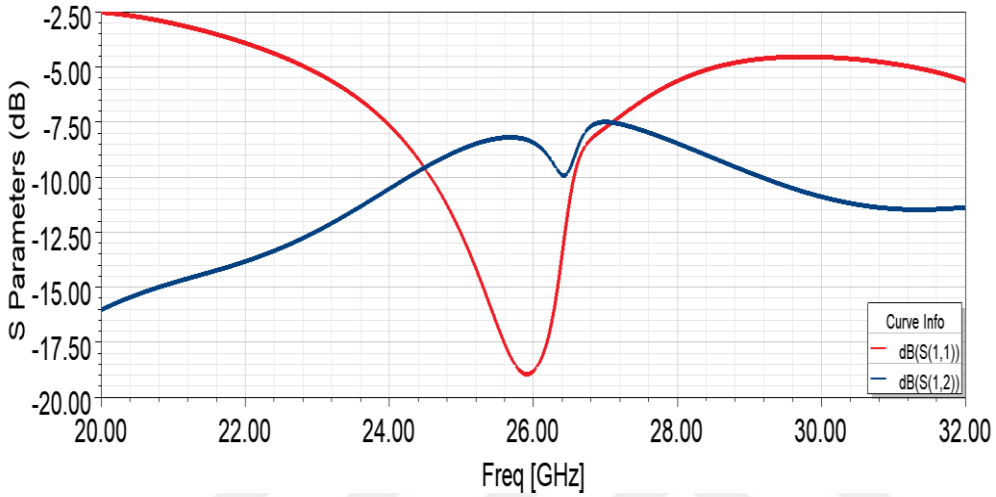

Figure 3.4: Input return loss, and isolation between two ports of ringed circular patch antenna

Table 3.1: Optimized parameters of ringed circular patch antenna

Parameters	Values
Radius of the circular patch	1.615 mm
Inner radius of the ring	1.665 mm
Outer radius of the ring	2.568 mm
50Ω GCPW signal line width	0.15 mm
Gap between 50Ω GCPW signal line and ground	0.02 mm
Inductive slot length	2.997 mm
Inductive slot width	0.15 mm

The largest dimension of the designed antenna is 2x2.568=5.136 mm. At 26 GHz, the wavelength is 11.53 mm. The antenna size is 0.445 wavelength. The current distributions for in-phase and out-of-phase feeding are shown in Figure 3.5 and Figure 3.6, respectively.

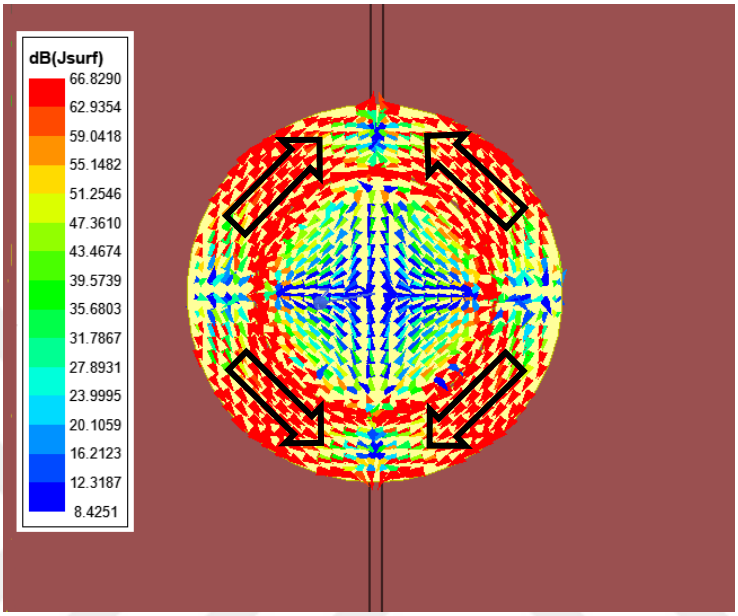

Figure 3.5: Current distribution for in-phase feeding

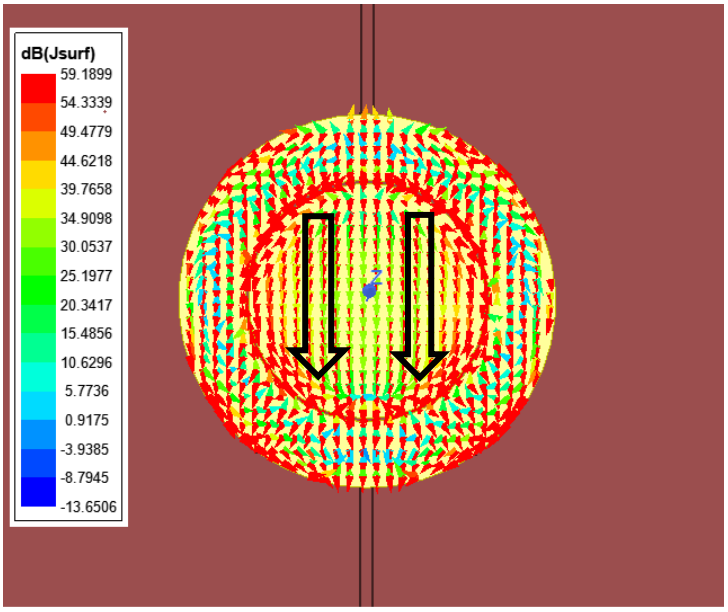

Figure 3.6: Current distribution for out-of-phase feeding

The radiation patterns at ϕ=0˚ plane obtained for cases where two ports are fed with 0˚ (in-phase) and 180˚ (out-of-phase) phase difference are presented in Figure 3.7 and Figure 3.8, respectively.

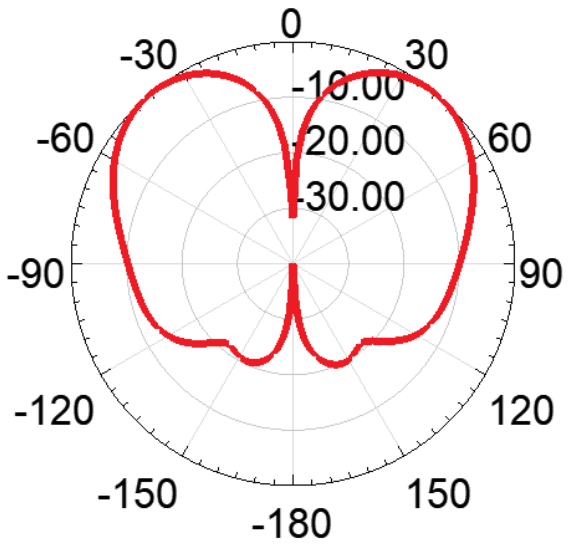

Figure 3.7: Normalized radiation pattern obtained when 0˚ phase differences are applied between two ports

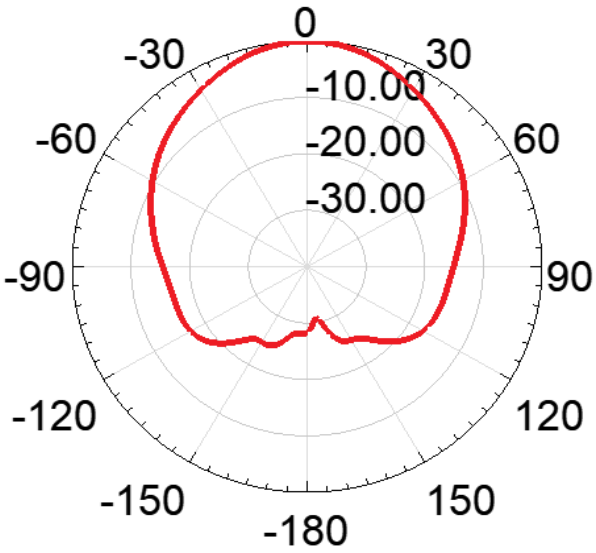

Figure 3.8: Normalized radiation pattern obtained when 180˚ phase differences are applied between two ports

As seen from Figure 3.7 and Figure 3.8, in-phase and out-of-phase excitation of the two feeds provided conical beam and broadside radiation, respectively. These results are also consistent with the current distributions in Figure 3.5 and Figure 3.6. Maximum gains of the antenna are given in Table 3.2 and Table 3.3.

Table 3.2: Maximum gain of the antenna for in-phase feeding

Feeding Type	Radiation Type	Angle at which maximum gain is seen (degrees)	Maximum Gain (dB)
In-Phase	Conical	±40	-1.63

Table 3.3: Maximum gain of the antenna for out-of-phase feeding

Feeding Type	Radiation Type	Angle of rotation from broadside (degrees)	Maximum Gain (dB)
Out-of-Phase	Broadside	0	7.05

As seen in Table 3.2 and Table 3.3, gains of the antenna are -1.63 and 7.05 dB for conical beam and broadside radiation, respectively. The gain has been observed as low and negative in the conical beam mode. In order to investigate the cause of this low gain, active s-parameters of ringed circular patch antenna for in-phase and out of phase feeding are studied and presented in Figure 3.9 and Figure 3.10, respectively. It can be observed that the active input return loss is below -10dB at 26 GHz for out of phase feeding, whereas it is about -6 dB at 26GHz for in-phase feeding. Hence it can be concluded that low isolation ($|S_{12}|$=-8.15 dB) causes coupling between two ports and this coupling affects the active return loss adversely for in-phase excitation. There are studies in the literature to decrease the coupling between two ports and increase the gain [24], but since it is out of the scope of this thesis, it will not be detailed. Only it should be noted that for a two-port antenna, the optimization of the antenna should be performed by considering both the input return loss and the isolation between the ports of the antenna. Since the active s-parameters

include effects of both of them, the antenna studied in the next chapter is designed by performing optimizations according to the active s-parameters for both types of excitations.

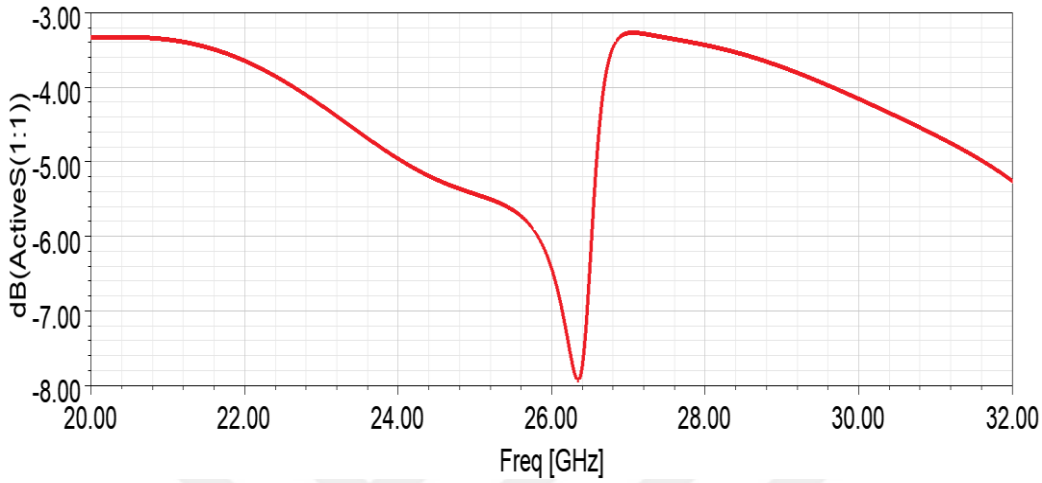

Figure 3.9: Active return loss graph for in-phase feeding

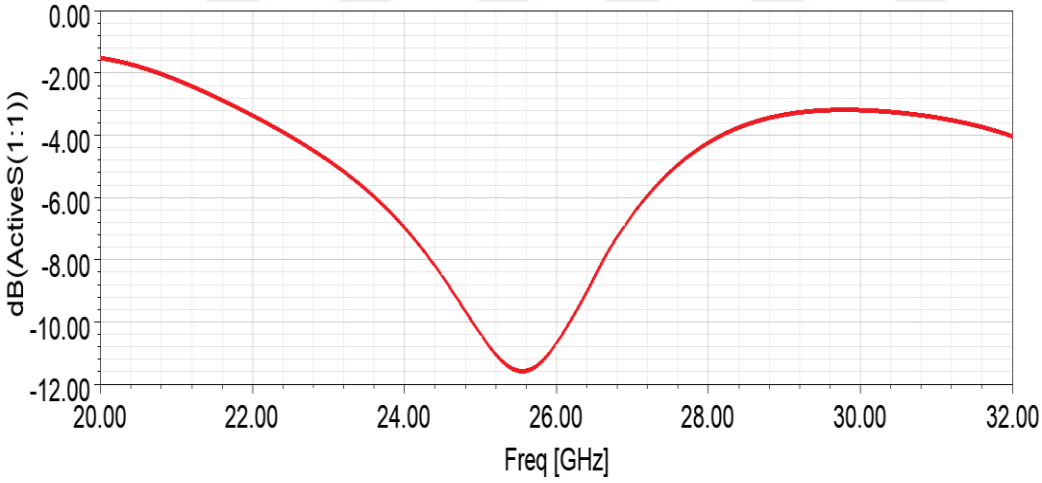

Figure 3.10: Active return loss graph for out-of-phase feeding

3.2 Increasing Pattern Diversity of the Antenna

The designed antenna provides the conical beam when two ports are excited in phase, whereas it provides broadside radiation for out-of-phase feeding. With the aim of obtaining asymmetric radiation patterns, slots are opened on the patch antenna, as shown in Figure 3.11, and the effects of these slots on the radiation pattern are observed.

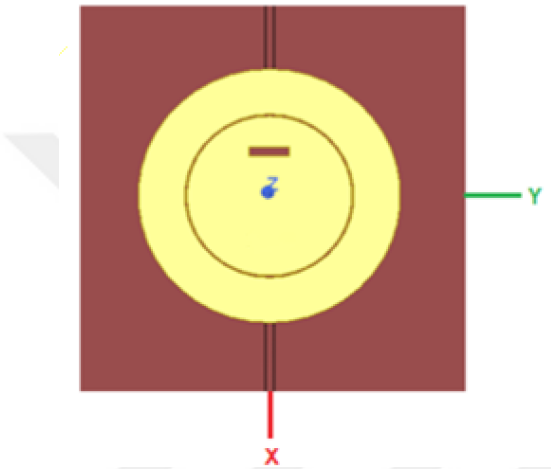

(a) Rectangle shape slot perpendicular to the feedlines

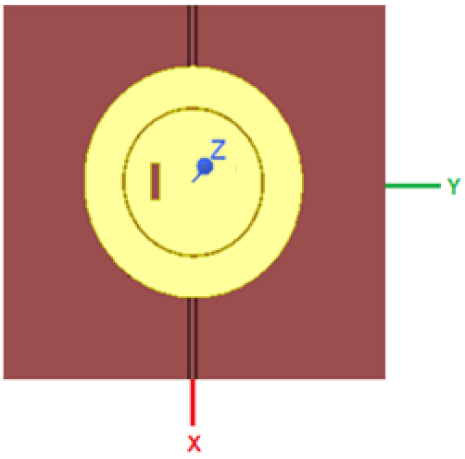

(b) Rectangle shape slot parallel to the feedlines

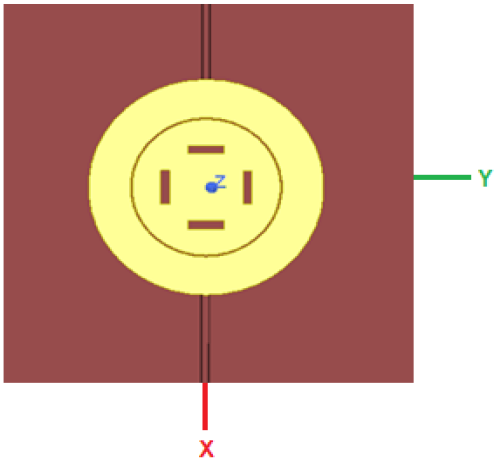

(c) Slots at four sides of the patch

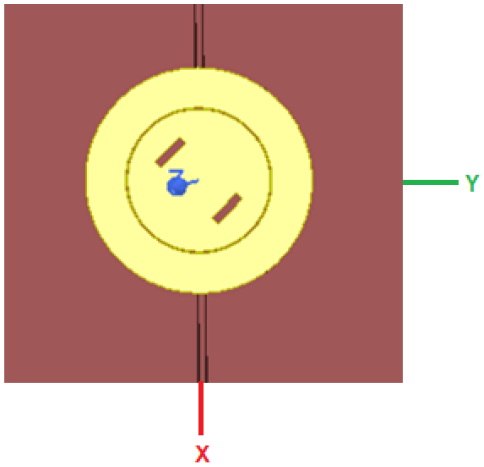

(d) Slots at 45˚ on the patch

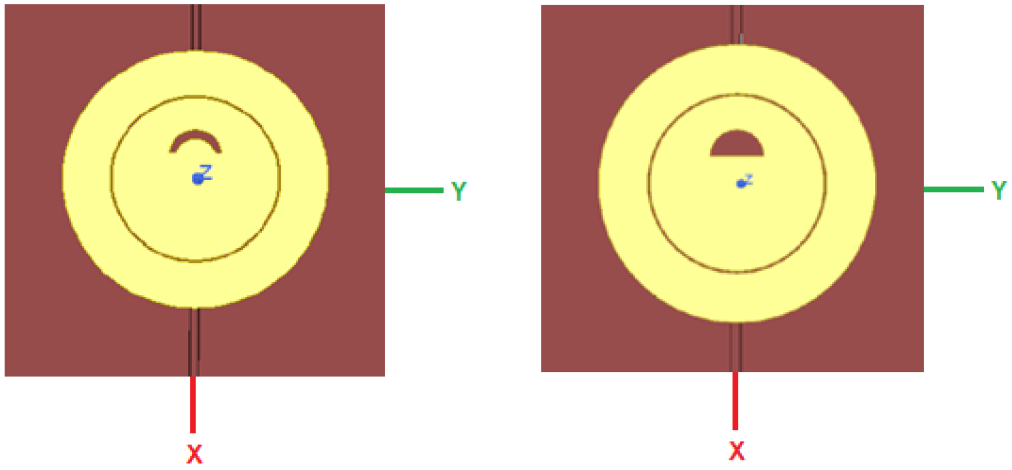

e) Arc shape slot on the patch f) Half circle slot on the patch

Figure 3.11: Antenna structures which different slots are opened on the patch

Simulations are made by changing the width, length, and positions of all slots opened on the antenna shown in Figure 3.11; however, no significant change in the radiation patterns are observed in any geometry. In addition, the resonant frequency shifts due to the slots opened on the patch. Since the radiation characteristics of the antenna can not be changed with the slots opened on the patch, the idea of opening a slot in a different part of the structure came to mind. First, a slot is opened in the ground plane as shown in Figure 3.12 to observe its effects on the radiation characteristics of the antenna. The aim is to obtain an asymmetric radiation pattern for in-phase excitation and steer the main radiation direction for out-of-phase feeding. The slot size and position are optimized to meet this objective, and the slot size is found to be 0.6 mm x 2 mm placed at 0.4 mm from the center of the circular patch.

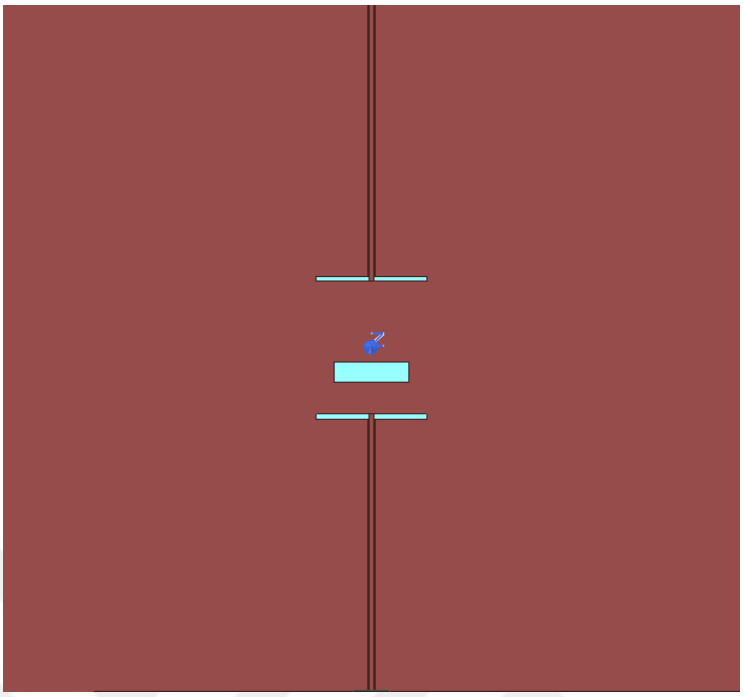

Figure 3.12: Antenna structure which a slot is opened on the ground plane

The designed antenna is modeled in ANSYS HFSS, and simulation results are obtained. The S_{11} and S_{12} are presented in Figure 3.13.

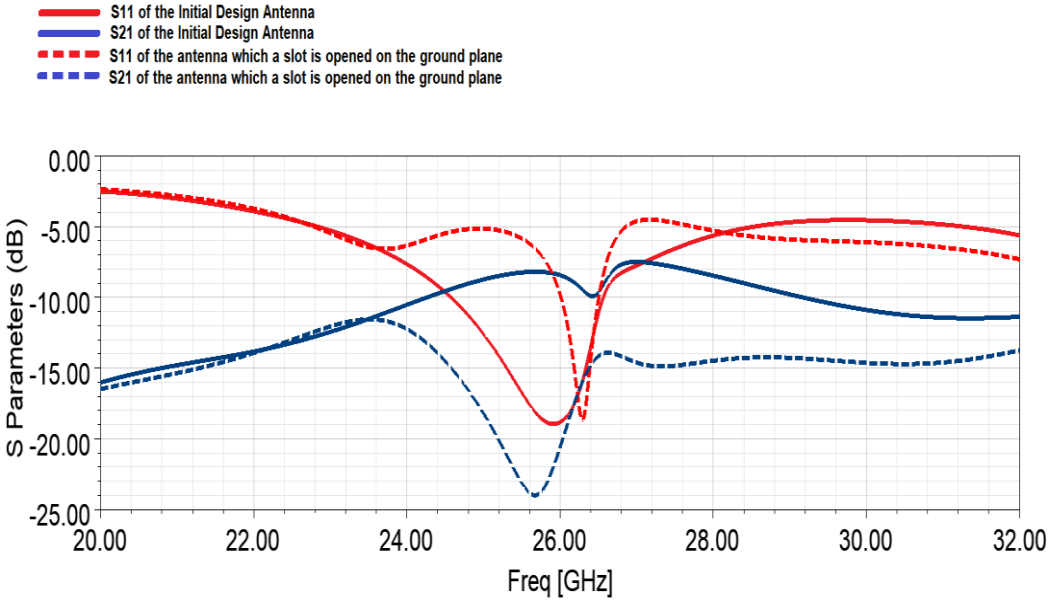

Figure 3.13: Input retrun loss, and isolation between two ports of ringed circular patch antenna

As shown in Figure 3.13, the resonance frequency shifts slightly upward when a slot is opened in the ground plane of the antenna. However, since it is still within 10 dB bandwidth, it can radiate effectively. The isolation between the antenna ports, on the other hand, showed a significant improvement in the case of slot is opened in the ground plane. These results show that the ring circular patch antenna can operate effectively at 26 GHz, even though a slot is placed on the ground plane of the antenna. Radiation pattern results normalized in the ϕ=0˚ plane for in-phase and out-of-phase excitations are presented in Figure 3.14 and Figure 3.15, respectively.

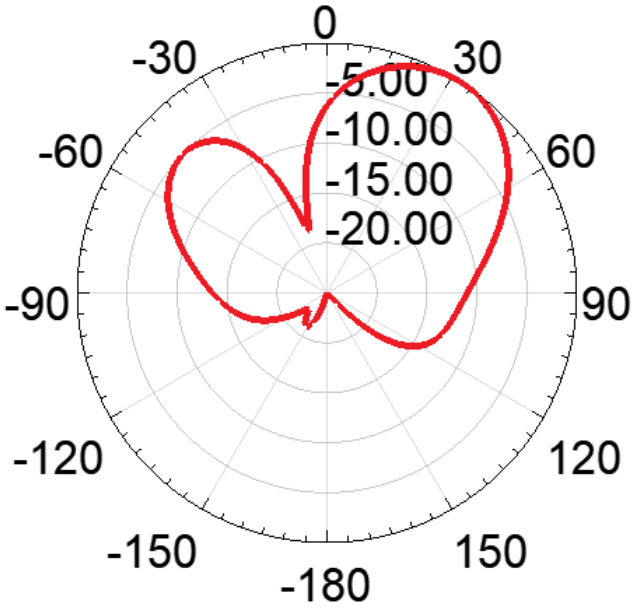

Figure 3.14: Normalized radiation pattern obtained when 0˚ phase differences are applied between two ports

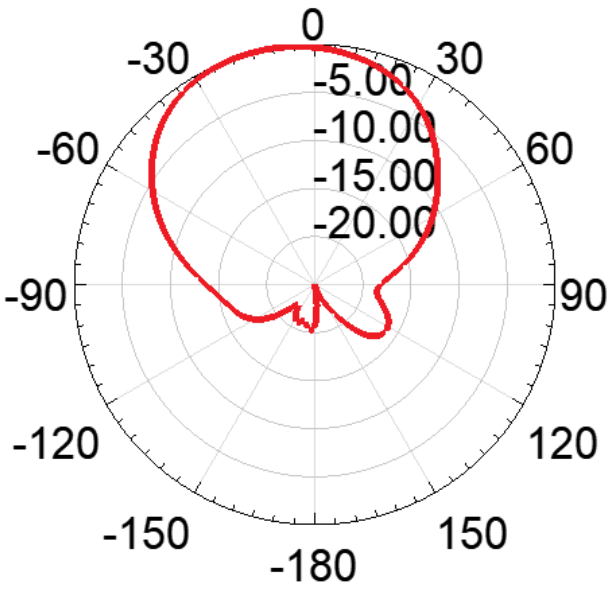

Figure 3.15: Normalized radiation pattern obtained when 180˚ phase differences are applied between two ports

Maximum gains of antenna are given in Table 3.4 and Table 3.5.

Table 3.4: Maximum gain of antenna for in-phase feeding

Feeding Type	Radiation Type	Angle at which maximum gain is seen (degrees)	Maximum Gain (dB)
In-Phase	Asymmetric Conical	30	0.69

Table 3.5: Maximum gain of antenna for out-of-phase feeding

Feeding Type	Radiation Type	Angle of rotation from broadside (degrees)	Maximum Gain (dB)
Out-of-Phase	Off-Broadside	20	5.30

As can be seen from Figure 3.14 and Table 3.4, the one-sided slot in the ground plane of the antenna suppressed the left side of the initially conical radiation pattern and

enhanced the right side when ports are fed in-phase. As can be seen from Figure 3.15 and Table 3.5, the one-sided slot in the ground plane of the antenna has rotated the direction of the main beam 20 degrees from the broadside when the ports are fed out-of-phase.

After it has been seen that the radiation pattern can be reconfigured by a one-sided slot opened in the ground plane, it will be examined whether the slot can be short-circuited by using switches in the slot. The presence and absence of slots will be controlled by OFF and ON states of RF-MEMS switches, respectively. During the simulations, 0.15 mm wide and 0.6 mm long conducting strips are used to imitate the ON state of switches. The number of switches is also optimized, and four switches are found to be adequate. The antenna structure is shown in Figure 3.16.

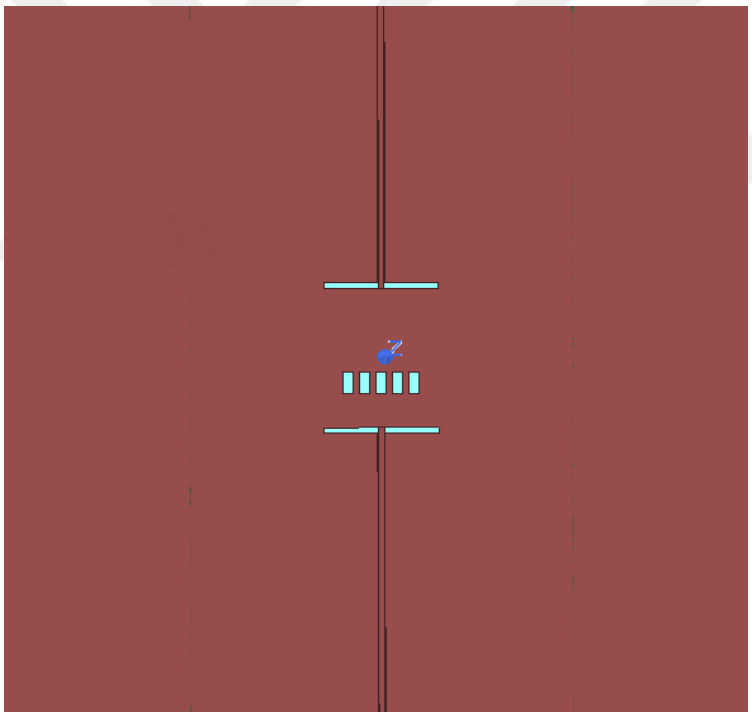

Figure 3.16: Antenna structure which a slot is opened on the ground plane and switches placed on it

The designed antenna is modeled in ANSYS HFSS, and simulation results are obtained. The S_{11} and S_{12} are presented in Figure 3.17.

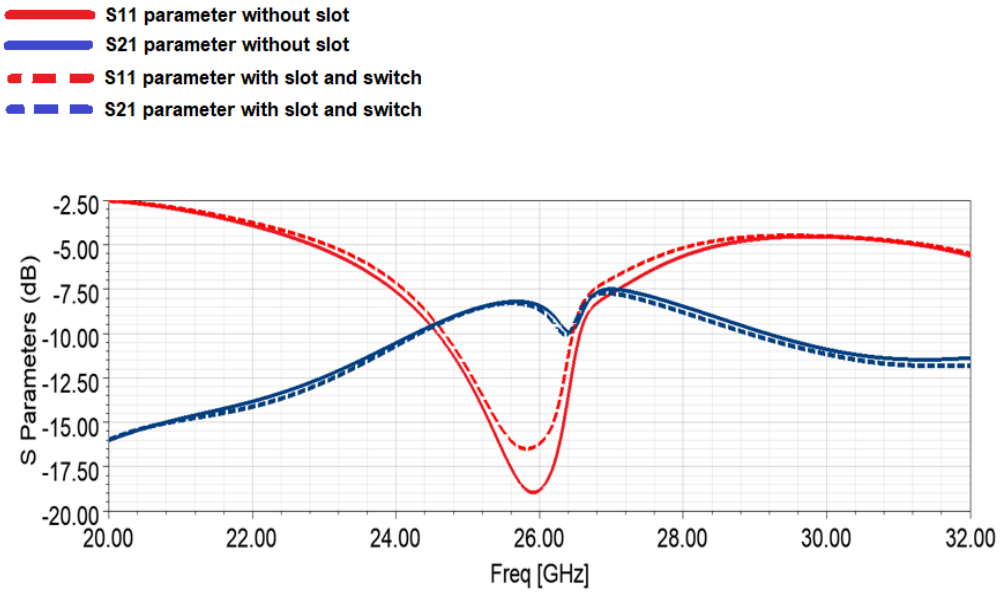

Figure 3.17: Input retrun loss, and isolation between two ports of ringed circular patch antenna

As seen in Figure 3.17, the results of the S parameter of the antenna with RF-MEMS switches placed in the slots in the ground plane, and the antenna without slots in the ground plane are similar. The normalized radiation pattern results at ϕ=0˚ plane for in-phase and out-of-phase excitations are presented in Figure 3.18 and Figure 3.19, respectively.

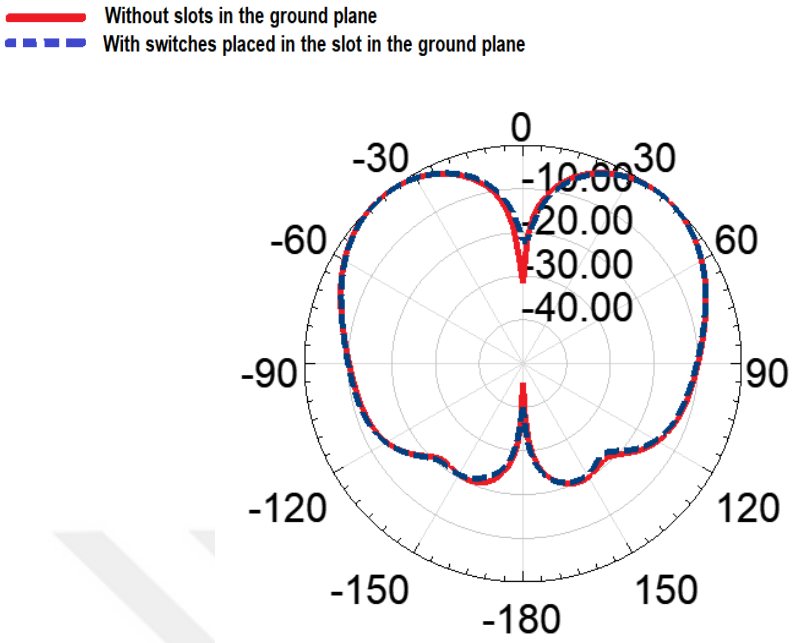

Figure 3.18: Normalized radiation patterns obtained when 0˚ phase differences are applied between two ports

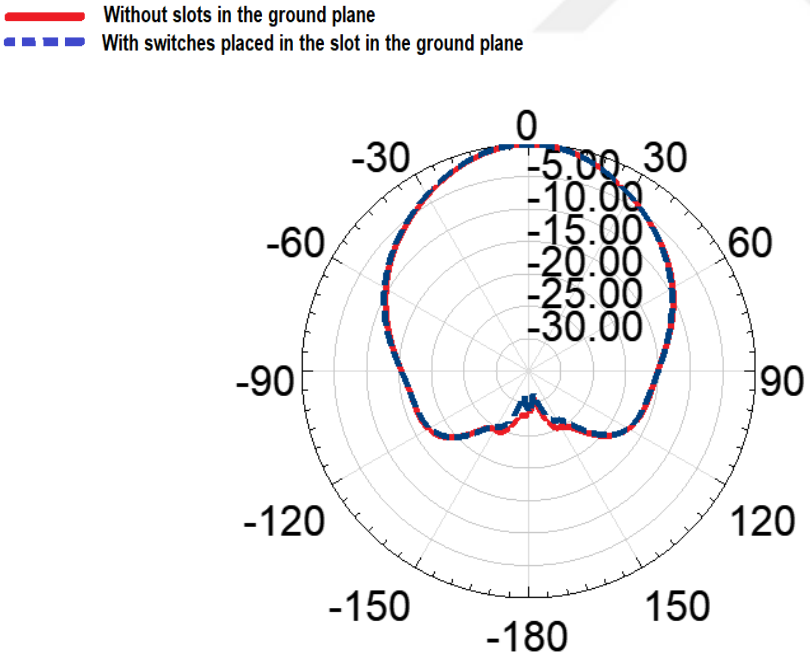

Figure 3.19: Normalized radiation patterns obtained when 180˚ phase differences are applied between two ports

Maximum gains of antenna are given in Table 3.6 and Table 3.7.

Table 3.6: Maximum gain of antenna for in-phase feeding

Feeding Type	Radiation Type	Angle at which maximum gain is seen (degrees)	Maximum Gain (dB)
In-Phase	Asymmetric Conical	±40	-1.53

Table 3.7: Maximum gain of antenna for out-of-phase feeding

Feeding Type	Radiation Type	Angle at which maximum gain is seen (degrees)	Gain (dB)
Out-of-Phase	Broadside	0	7.18

As can be seen in Figure 3.18 and Table 3.6, the slot opened to the ground plane can be short-circuited by the metal strips placed inside slot. Thus, the slot opened in the ground plane is as if it had never been opened. Consequently, the initial conical radiation pattern is achieved for in-phase feeding. As can be seen in Figure 3.19 and Table 3.7, the initial broadside radiation pattern is achieved for out-of-phase feeding.

Then, two equal-sized slots are opened on the ground plane parallel to the inductive slots to observe their effects on the radiation characteristics of the antenna. The antenna structure is given in Figure 3.20.

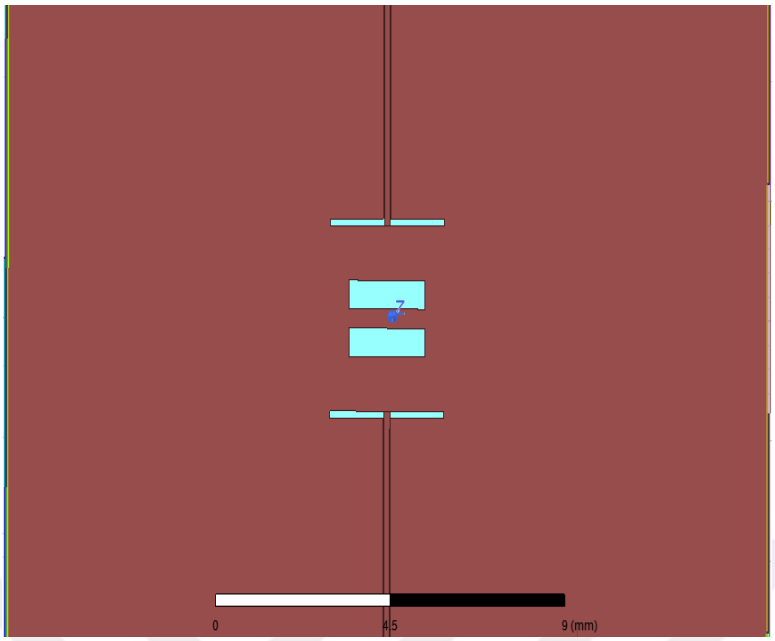

Figure 3.20: Antenna structure which two equal-sized slots are opened on the ground plane

The pattern reconfiguration property of the designed antenna is examined for three states. As shown in Figure 3.21, only the right slot exists in State 1, only the left slot exits in State 2, and in State 3, all switches are ON to short circuit both slots.

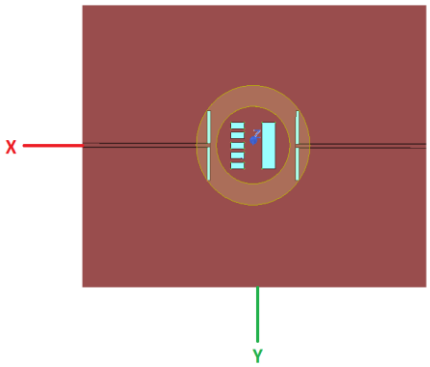

(a) State 1: Switches on the left slot are ON, on the right slot are OFF

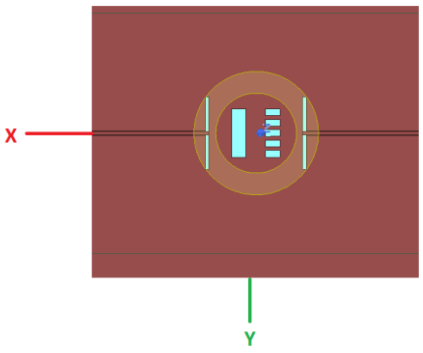

(b) State 2: Switches on the left slot are OFF, on the right slot are ON

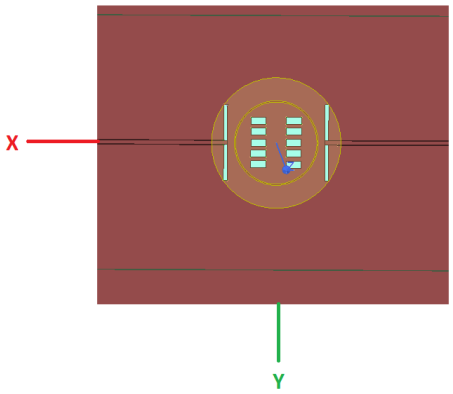

(c) State 3: Switches on the left slot are ON, on the right slot are ON

Figure 3.21: Three states of the pattern reconfiguration property of the designed antenna

The designed antenna is modeled in ANSYS HFSS, and simulation results are obtained. S_{11} graphs for three states are presented in Figure 3.22.

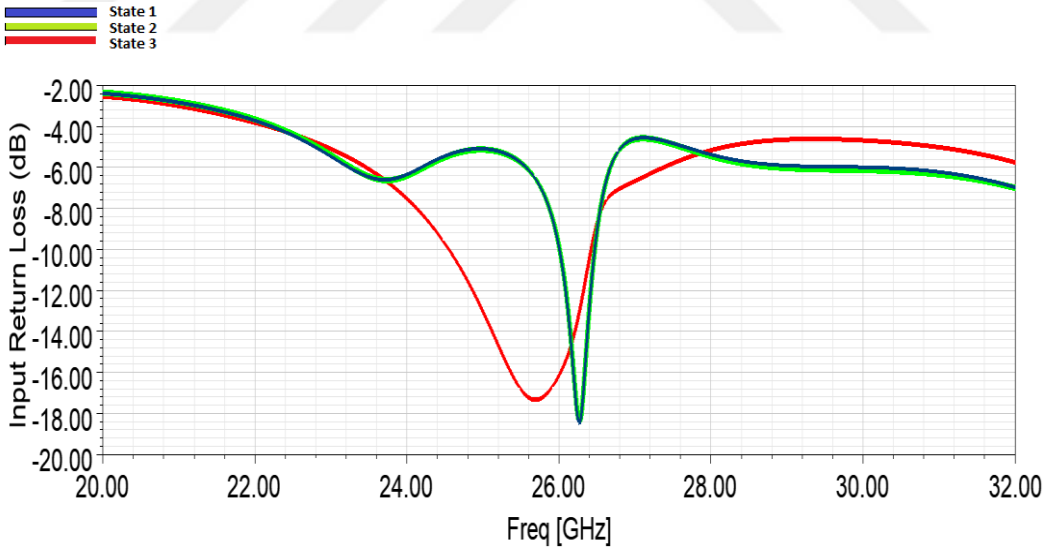

Figure 3.22: Input return loss graphs for three states

The radiation pattern results at $\phi=0^{\circ}$ plane for all states for in-phase and out-of-phase excitations are presented in Figure 3.23 and Figure 3.24, respectively.

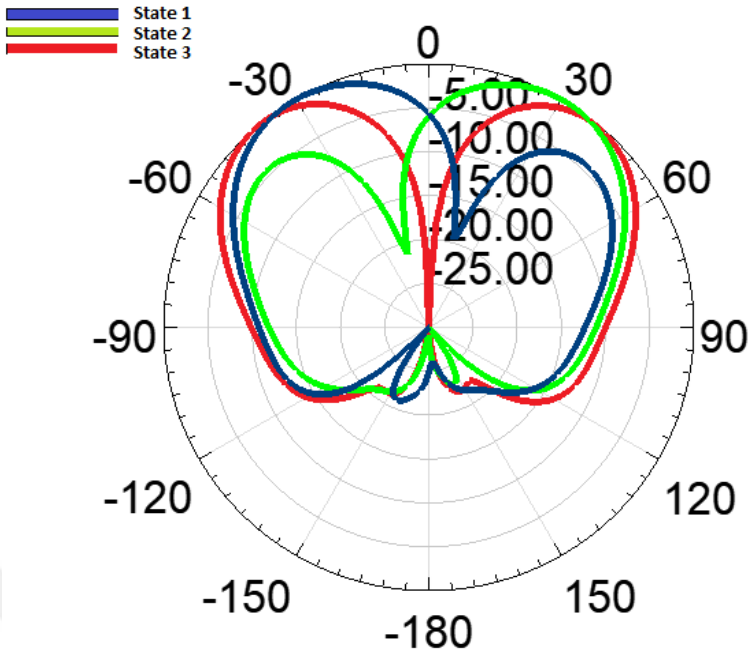

Figure 3.23: Simulated normalized radiation patterns for three states for in-phase feeding

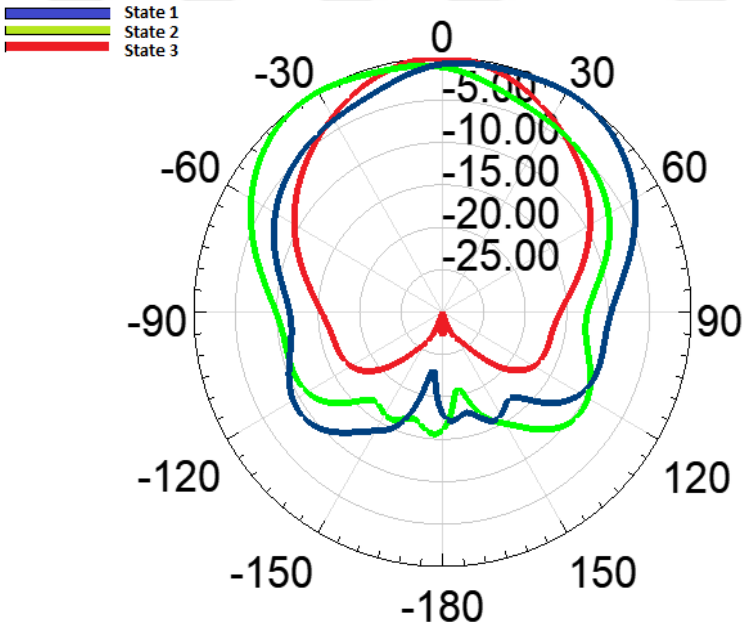

Figure 3.24: Simulated normalized radiation patterns for three states for out-of-phase feeding

Maximum gains for in-phase feeding and out-of-phase feeding are given in Table 3.8 and Table 3.9, respectively.

Table 3.8: Maximum gains for in-phase feeding

	Radiation Type	Angle at which maximum gain is seen (degrees)	Gain (dB)
State 1	Asymmetric Conical	-30	0.43
State 2	Asymmetric Conical	30	0.37
State 3	Conical	±40	-1.63

Table 3.9: Maximum gains for out-of-phase feeding

	Radiation Type	Angle of rotation from broadside (degrees)	Gain (dB)
State 1	Off-Broadside	18	5.11
State 2	Off-Broadside	-18	5.14
State 3	Broadside	0	7.14

As can be seen from Figure 3.23 and Table 3.8, state 1 of the antenna enhanced the left side of the initially conical radiation pattern and, suppressed the right side for in-phase feeding. State 2 of the antenna suppressed the left side of the initially conical radiation pattern and enhanced the right side for in-phase feeding. The last state, state 3, provided the initial conical beam. Due to suppression of the beam on one side, gain value increases compared to conical radiation pattern.

As can be seen from Figure 3.24 and Table 3.9, state 1 of the antenna rotated the direction of the main beam 18 degrees from the broadside as a result of out-of-phase feeding. State 2 of the antenna rotated the direction of the main beam -18 degrees from the broadside. The last state, state 3, provided initial broadside radiation.

In another graduate research, there were studies to reduce the coupling between the ports of the antenna. During that research, it is realized when a slot is opened in the ring as shown in Figure 3.25, the radiation modes of the antenna changes for certain slot widths. Radiation mode change means that conical beam is obtained for out of phase feeding and broadside beam is obtained for in-phase feeding. Consequently, by feeding both ports in-phase, the radiation mode can be controlled by introducing a slot into the ring. As a result, the need for 180^0 phase shift for reconfiguration can be avoided. Inspired by that research, slots were opened to investigate if the same concept could be applied to our antenna. Two equal-sized slots are opened on the ring in the same direction as the slots opened in the ground plane to observe their effects on the radiation characteristics of the antenna. The size and the position of the slots are optimized, and the slot size is found to be 0.4 mm x 0.907 mm. The current distributions for only in-phase feeding are shown in Figure 3.26.

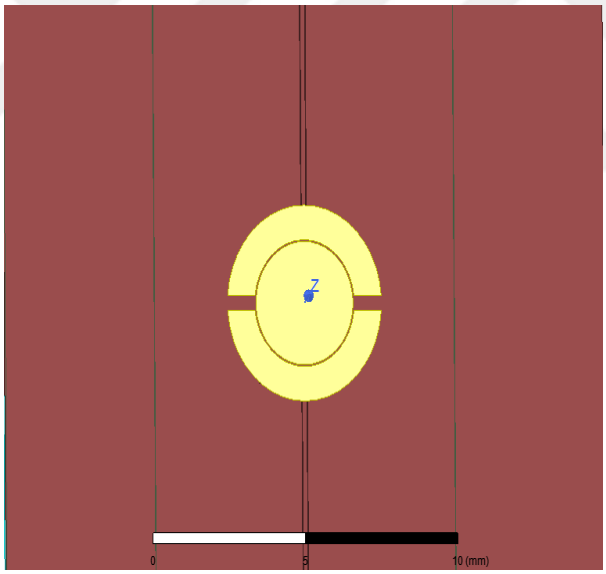

Figure 3.25: Antenna structure which two equal-sized slots are opened on the ring

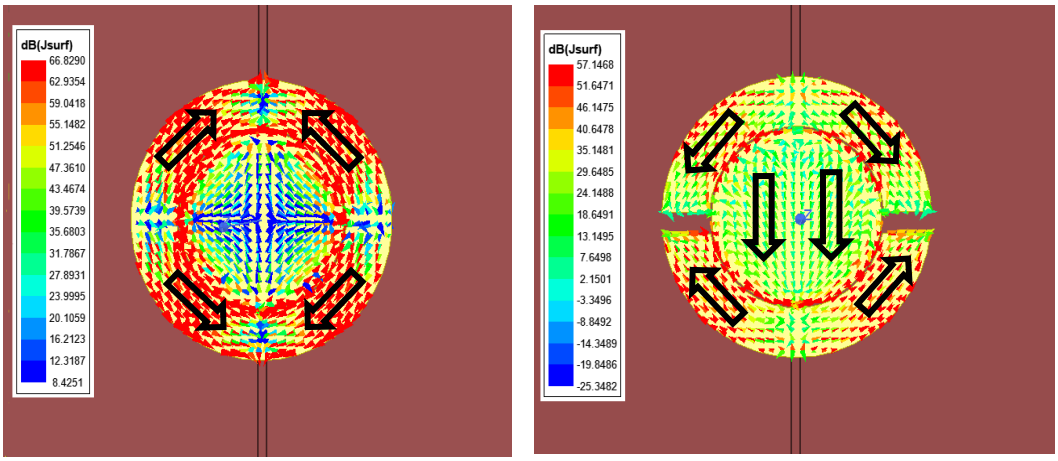

(a) Current distribution without slots on the ring

b) Current distribution with slots on the ring

Figure 3.26: Current distribution for only in-phase feeding (a) without slots on the ring (b) with slots on the ring

As can be seen from Figure 3.26, the slots opened on the outer ring have changed the current distribution on the central patch. Similarly, to short circuit the slots and control the existence and absence of the slot, switches are placed inside the slot. During the simulations, 0.15 mm wide and 0.4 mm long conducting strips are used to imitate the ON state of switches. The number of switches is also optimized, and three switches are found to be adequate.

At this stage, three sets of switches were determined, and these sets are as follows.

1) Switches on the circular ring

2) Switches in the left slot on the ground plane

3) Switches in the right slot on the ground plane

There should be eight states depending on whether these switch sets are ON or OFF; however, the switches in the slot on the ground plane will not be simultaneously OFF. Therefore, there are six states in total. These can be expressed as binary. In the

binary representation here, “0” represents the switch OFF state and “1” represents the switch ON state. The writing order of the binary representation that creates the states is in the same order as the three sets of switches defined above.

State 1 : 111 State 4 : 011

State 2 : 110 State 5 : 010

State 3 : 101 State 6 : 001

As shown in Figure 3.27, all switches are ON to short circuit entire slots in State 1. In State 2 and State 3, all switches are ON to short circuit the slots on the ring, while only the right slot exists on the ground plane for State 2 and only the left slot exits in the ground plane in State 3. In State 4, State 5 and State 6 slots on the ring exists with no slots on the ground plane for State 4. Only the right slot exits in the ground plane in State 5, and only the left slot exits in the ground plane in State 6.

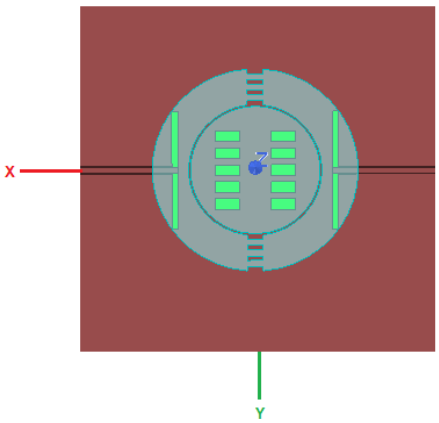

(a) State 1

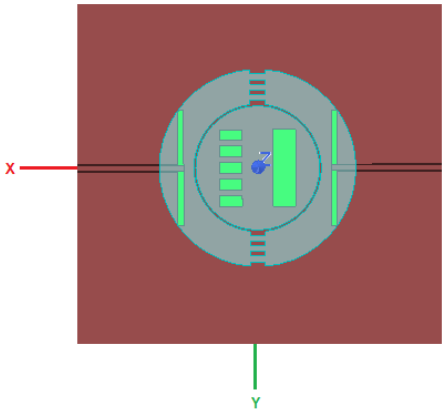

(b) State 2

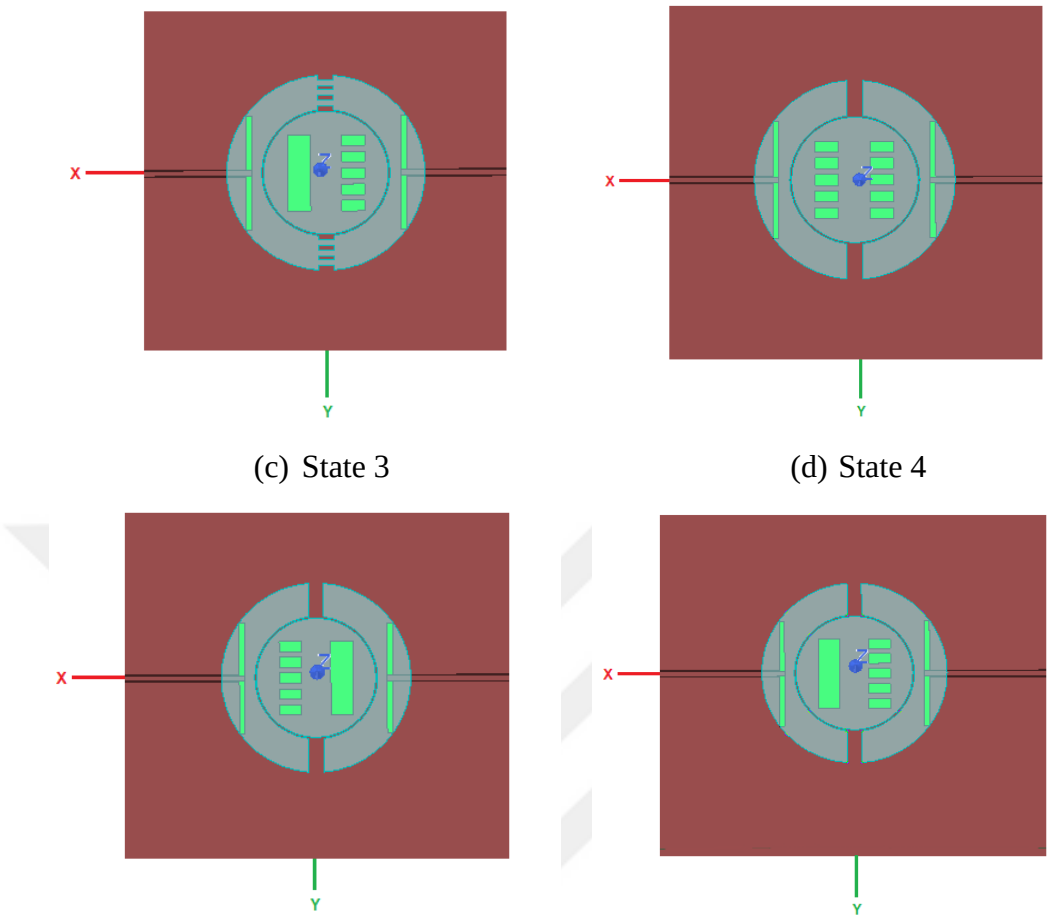

(c) State 3 (d) State 4

(e) State 5 (f) State 6

Figure 3.27: Six states of the pattern reconfiguration property of the designed antenna

The designed antenna is modeled in ANSYS HFSS, and simulation results are obtained. Since the slots on the ring result in a radiation mode change in the antenna, the first three cases shown in Figure 3.27 are examined as a particular group and the last three cases as a different group. S_{11} graphs for states 1, 2, 3 and, states 4, 5, 6 are presented in Figure 3.28 and Figure 3.29, respectively.

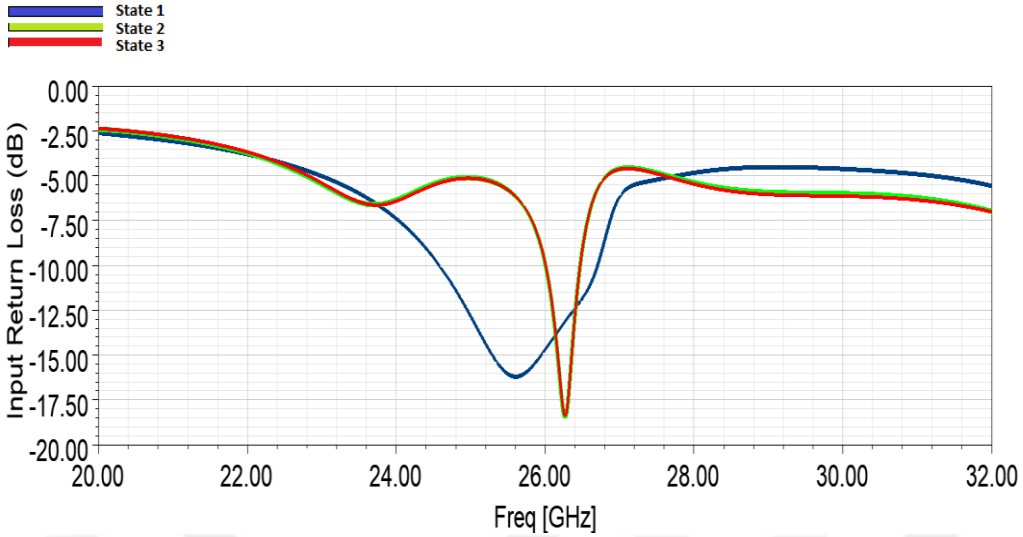

Figure 3.28: Input return loss graphs for in-phase feeding for state 1, state 2 and state 3

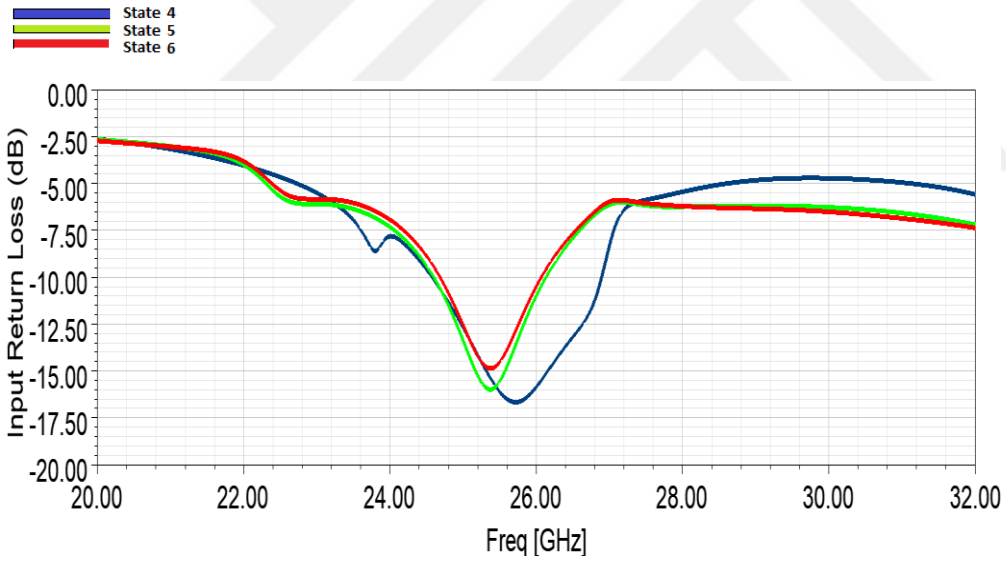

Figure 3.29: Input return loss graphs for in-phase feeding for state 4, state 5 and state 6

The radiation pattern results at $\phi=0^{\circ}$ plane for only in-phase excitation for the states 1, 2, 3 and states 4, 5, 6 are presented in Figure 3.30 and Figure 3.31, respectively.

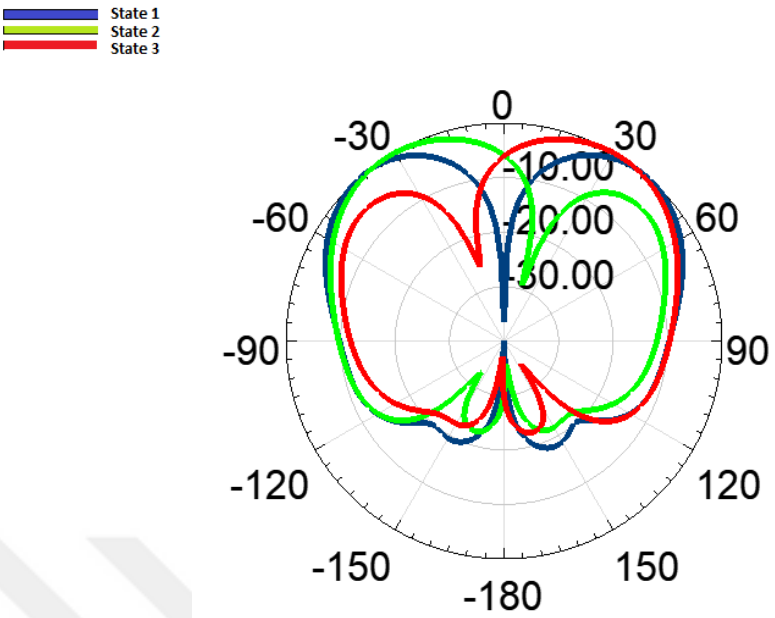

Figure 3.30: Simulated normalized radiation patterns for for state 1, state 2 and state 3

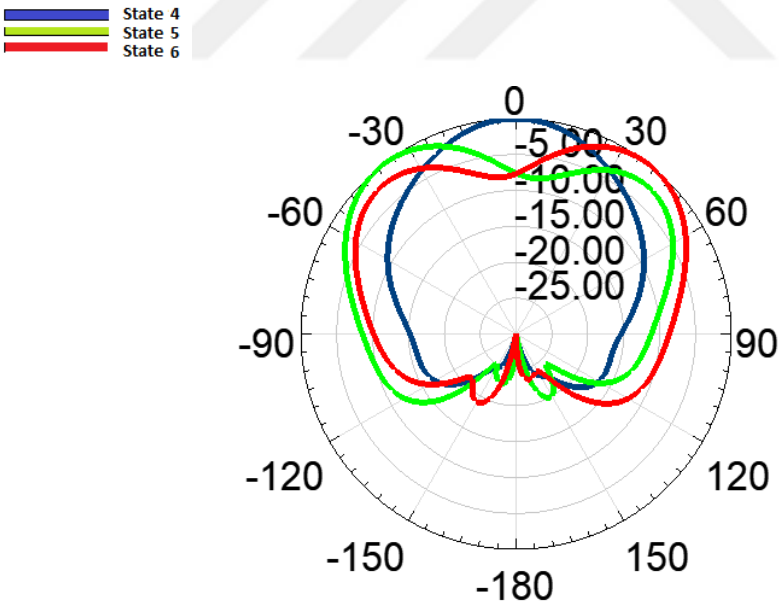

Figure 3.31: Simulated normalized radiation patterns for state 4, state 5 and state 6

Maximum gains of antenna are given in Table 3.10 and Table 3.11.

Table 3.10: Maximum gains of antenna

States	Radiation Type	Angle at which maximum gain is seen (degrees)	Maximum Gain (dB)
State 1	Conical	±40	-1.88
State 2	Asymmetric Conical	-32	0.41
State 3	Asymmetric Conical	32	0.39

Table 3.11: Maximum gains of antenna

States	Radiation Type	Angle of rotation from broadside (degrees)	Maximum Gain (dB)
State 4	Broadside	0	7.18
State 5	Off-Broadside	-36	4.97
State 6	Off-Broadside	36	4.92

As can be seen from Figure 3.30 and Table 3.10, state 1 of the antenna provided the initial conical beam. State 2 of the antenna suppressed the right side of the initially conical radiation pattern and enhanced the left side for in-phase feeding. The last state, state 3, enhanced the right side of the initially conical radiation pattern, and suppressed the left side for. Due to suppression of the beam on one side, gain value increases compared to conical radiation pattern.

As can be seen from Figure 3.31 and Table 3.11, state 4 of the antenna provided initial broadside radiation. The state 5 of the antenna rotated the direction of the main beam -36 degrees from the broadside as a result of out-of-phase feeding. The last state, state 6, of the antenna rotated the direction of the main beam 36 degrees from the broadside.

The radiation patterns in Figure 3.30 are similar to the radiation patterns in Figure 3.23. When the radiation patterns in Figure 3.31 are examined, it is observed that the beam is wider compared to the radiation patterns obtained in Figure 3.24, where radiation mode change was done by out of phase excitation of the ports. Therefore, the radiation mode changing approach by opening slot in the ring should be preferred if only the application could tolerate this wider beam.

CHAPTER 4

DESIGN AND ANALYSIS OF RINGED CIRCULAR PATCH ANTENNA AT SUB-6 GHz

It was agreed with METU MEMS Center for the production of the ringed circular patch antenna designed at 26 GHz. However, this antenna could not be produced due to some production problems. Based on this development, antenna design studies have been carried out in the sub-6 GHz band, which is another 5G frequency band.

3.3 GHz is chosen as the antenna operating frequency. Since the antenna size increases at low frequency, it is planned to control the slots in the ground plane of the antenna with PIN diode switches for pattern reconfiguration. The antenna is constructed by placing a circular ring around a circular microstrip patch antenna and excited by the aperture coupling technique using two feeds. A microstrip transmission line is chosen as the feeding structure. ROGERS4003 with a thickness of 0.508 mm, a dielectric constant (ε_r) of 3.55, and a loss tangent (tan δ) of 0.0027 is chosen as the substrate of the feed line, and ROGERS4003 with a thickness of 1.524 mm, is chosen as the substrate of the antenna. The ground plane on which slots will be opened to control the radiation pattern is placed between these two substrates. The side view of the antenna is shown in Figure 4.1. The top views of the antenna layer and ground layer together with microstrip feed lines are shown in Figures 4.2(a) and 4.2(b), respectively.

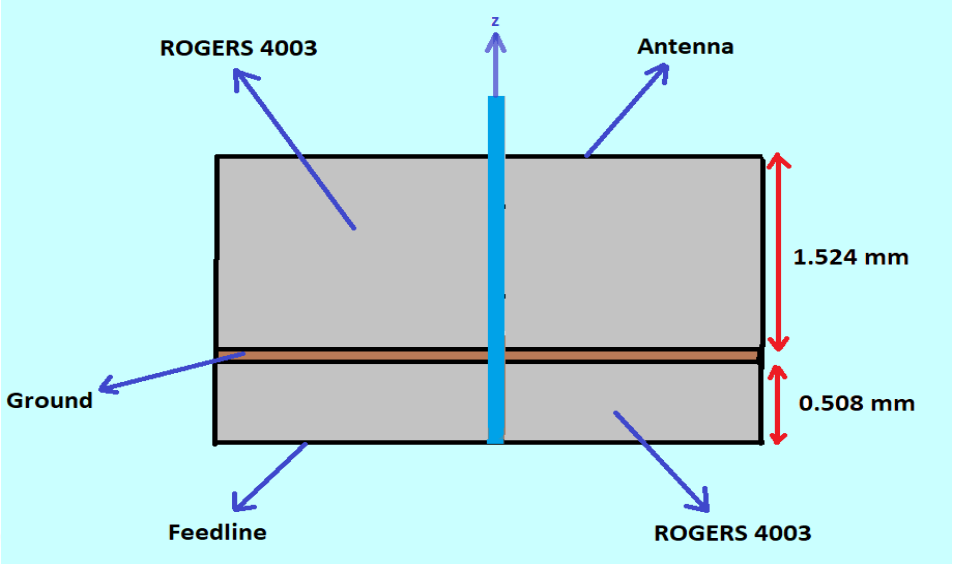

Figure 4.1: Side view of proposed antenna

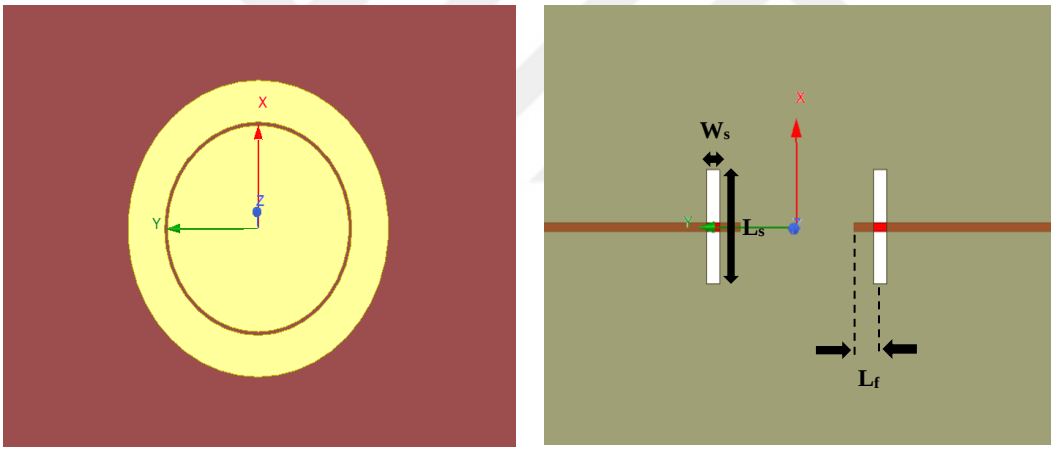

(a) (b)

Figure 4.2: Top views of (a) antenna layer and (b) ground layer with microstip feed lines

When the antenna analysis is performed, the front-to-back ratio of the antenna becomes 7.5 dB. For the suppression of the back lobe, it is considered to place a PEC plate behind the antenna substrate, on which the feed lines are located. The new structure is shown in Figure 4.3. The plate distance is set to $\lambda_0/10$ at 3.3 GHz.

Consequently, the plate distance is about 9.09 mm. The PEC plate size is also chosen to be $2\lambda_0$ x $2\lambda_0$.

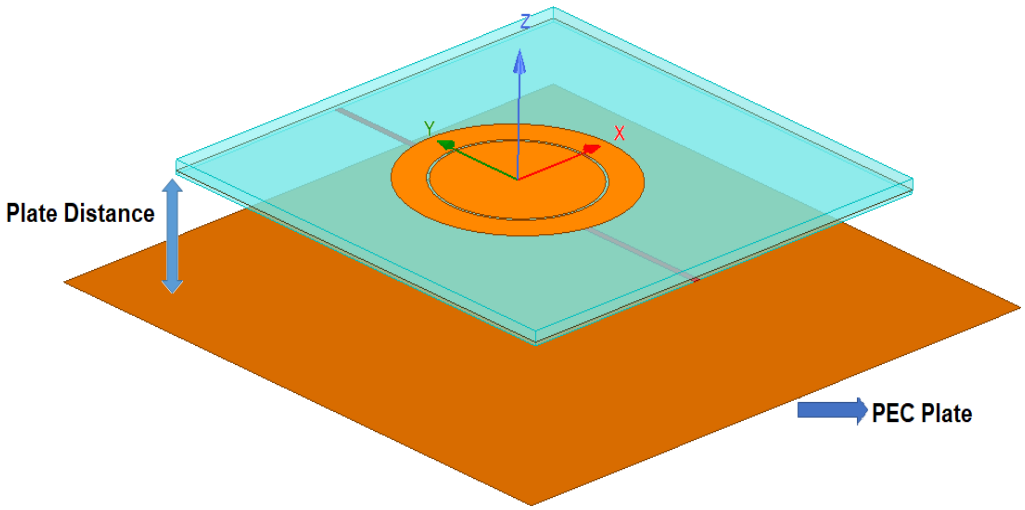

Figure 4.3: Antenna Structure with PEC Plate

During the design of the antenna at 26 GHz, input return loss values of one of the ports of the antenna are considered during the optimization process of antenna parameters. However, it is realized that the isolation between the ports should also be considered since the antenna will always be excited through both of its ports and high coupling between the ports reduces the gain especially for in-phase feeding. In the light of this observation, the optimization process of the antenna parameters for the antenna that will operate at 3.3 GHz, is performed by considering active s-parameters for both in-phase and out of phase feeding. Because S_{12} parameter directly appears in the active s-parameter expressions and as the port isolation is improved, the active s-parameter values for in-phase and out of phase feeding approach to each other. The parameters of the optimized antenna are listed in Table 4.1. Active input return loss of ringed circular patch antenna for in-phase and out of phase feeding are presented in Figure 4.4 and Figure 4.5, respectively.

Table 4.1: Optimized parameters of ringed circular patch antenna

Parameters	Values
Radius of the circular patch	13.55 mm
Inner radius of the ring	14.05 mm
Outer radius of the ring	19.50 mm
50Ω signal line width	1.17 mm
Aperture Length (L_s)	15.5 mm
Aperture Width (W_s)	2 mm
Stub length (L_f)	4 mm

The largest dimension of the designed antenna is 2x19.5=39 mm. At 3.3 GHz, the wavelength is 90.9 mm. The antenna size is 0.43 wavelength.

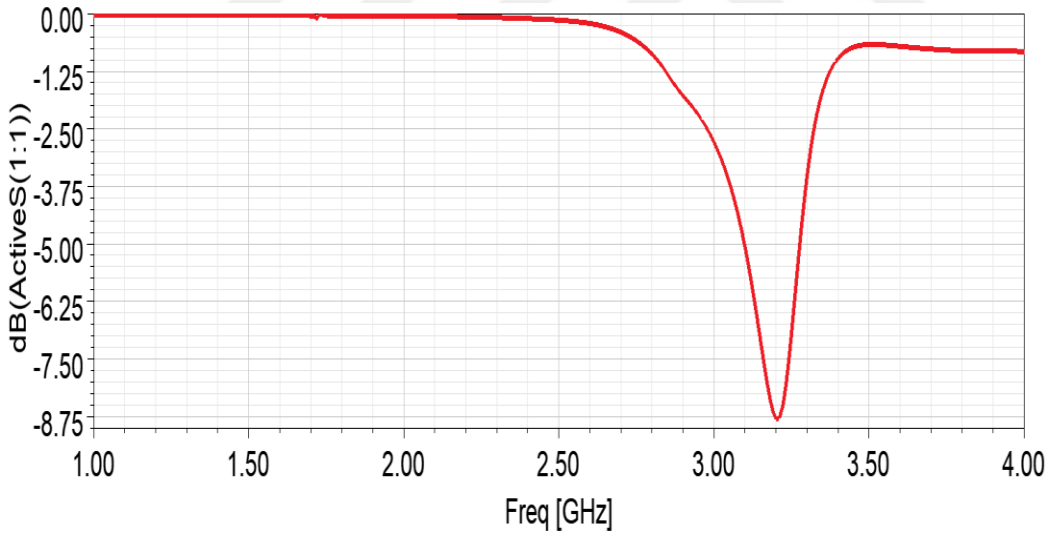

Figure 4.4: Active input return loss of ringed circular patch antenna for in-phase feeding

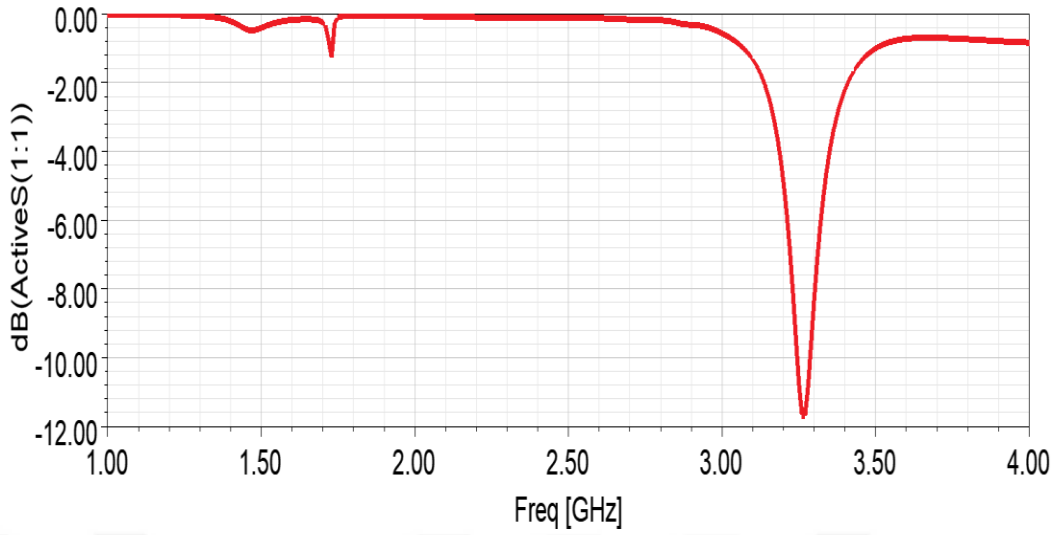

Figure 4.5: Active input reflection loss of ringed circular patch antenna for out-of-phase feeding

As can be seen from Figure 4.4 and Figure 4.5, the minimum value of active return losses for the in-phase and out-of-phase excitations occur approximately at the same frequencies. In the antenna designed at 26 GHz, on the other hand, since the optimization was made according to a single port, the minimum values of active return losses appeared at different frequencies for in-phase and out-of-phase excitations. The S_{11} and, S_{12} parameters of the antenna are presented in Figure 4.6.

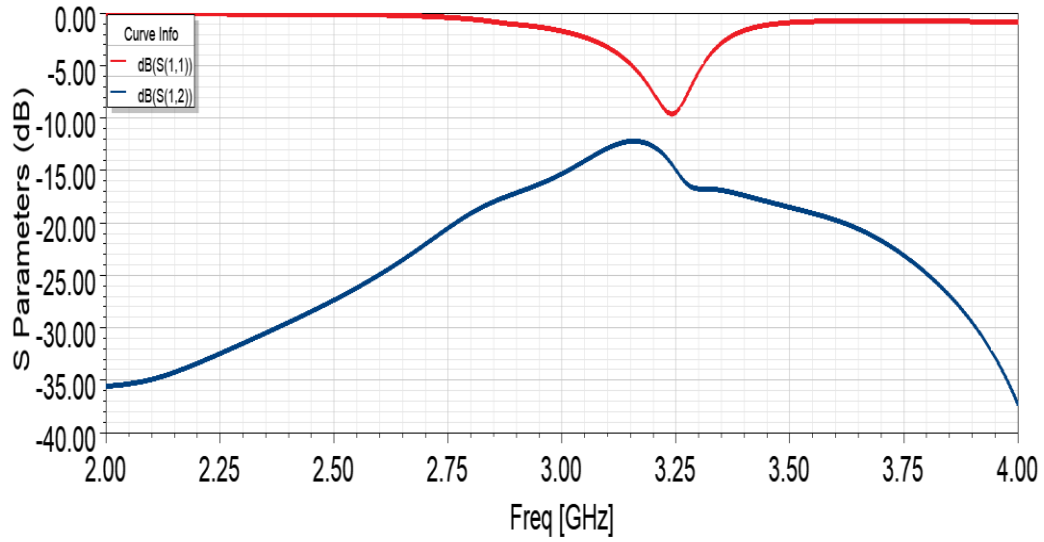

Figure 4.6: S_{11} and S_{12} parameters of ringed circular patch antenna

As expected from active s-parameter results, the isolation between the two ports is good (around -16 dB at 3.3 GHz), and it is much more better than the isolation (-8.15dB) of the antenna designed at 26 GHz. The current distributions for in-phase and out-of-phase feeding are shown in Figure 4.7 and Figure 4.8, respectively.

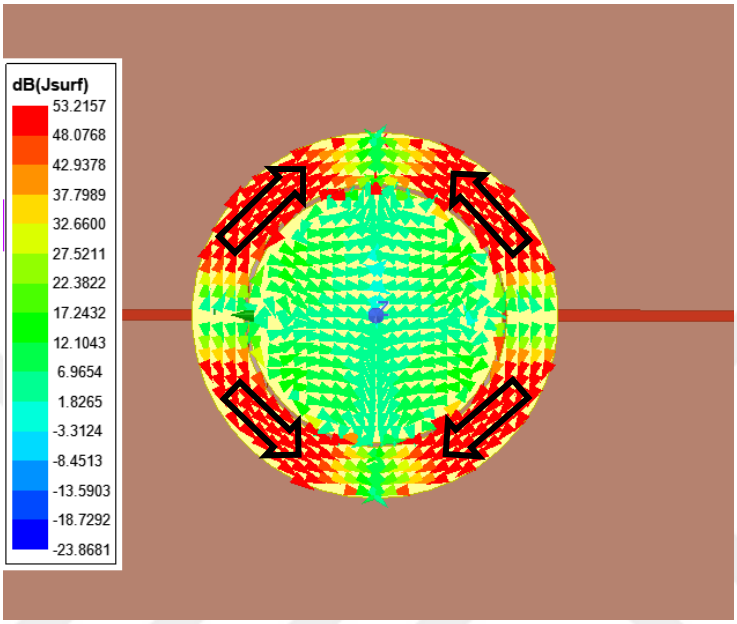

Figure 4.7: Current distribution for in-phase feeding

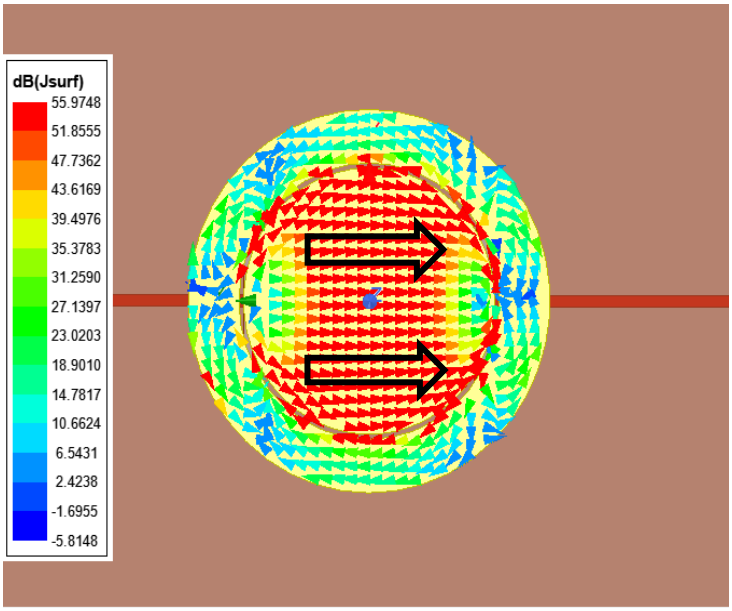

Figure 4.8: Current distribution for out-of-phase feeding

The normalized radiation pattern results at ϕ=90 plane for cases where two ports are fed with 0˚ (in-phase) and 180˚ (out-of-phase) are presented in Figure 4.9.

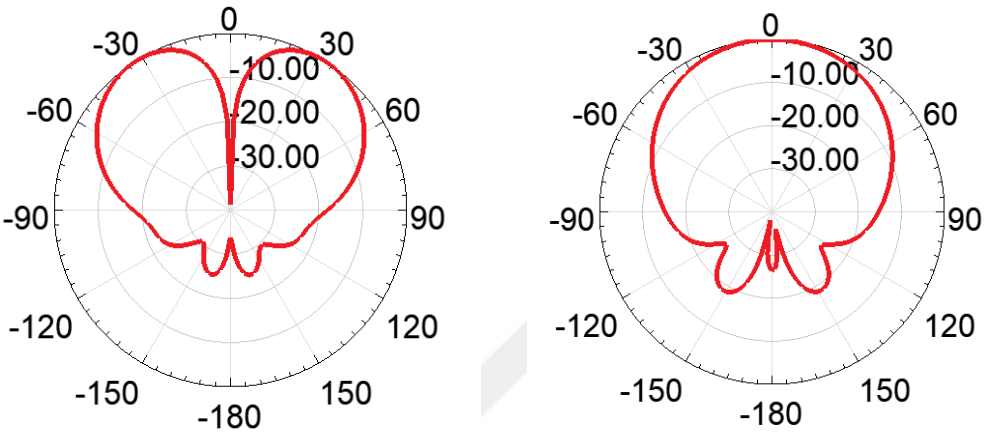

(a) (b)

Figure 4.9: Radiation patterns obtained when different phases are applied between two ports (a) 0˚ phase differences (b) 180˚ phase differences

As seen from Figure 4.9, in-phase and out-of-phase excitation of the two feeds provided conical beam and broadside radiation, respectively. These results are also consistent with the current distributions in Figure 4.7 and Figure 4.8.

Maximum gains of antenna are given in Table 4.2 and Table 4.3.

Table 4.2: Maximum gain of antenna for in-phase feeding

Feeding Type	Radiation Type	Angle at which maximum gain is seen (degrees)	Maximum Gain (dB)
In-Phase	Asymmetric Conical	±32	9.40

Table 4.3: Maximum gain of antenna for out-of-phase feeding

Feeding Type	Radiation Type	Angle at which maximum gain is seen (degrees)	Maximum Gain (dB)
Out-of-Phase	Broadside	0	7.52

As seen from Table 4.2, in this antenna, the gain value of the in-phase feeding is not decrease since the optimization is made according to the active s parameters.

4.1 Improving Pattern Diversity of the Antenna

As shown in Figure 4.10, a slot is opened in the ground plane in front of the rectangular aperture on the left side of the antenna, to observe its effects on the radiation characteristics of the antenna. The slot size and position are optimized to achieve maximum variation in the radiation pattern, and the slot size is found to be 5 mm x 11 mm placed at 6 mm from the center of the circular patch. Meanwhile the length of the rectangular aperture also needed to be adjusted to obtain a resonance at the same frequency as the antenna without a slot opening. The best aperture length that provides resonance at the same frequency (3.24 GHz) for both in-phase and out of phase excitation is found to be 9.5 mm. Active return loss graphs for in-phase and out-of-phase feeding are presented in Figure 4.11 and Figure 4.12, respectively.

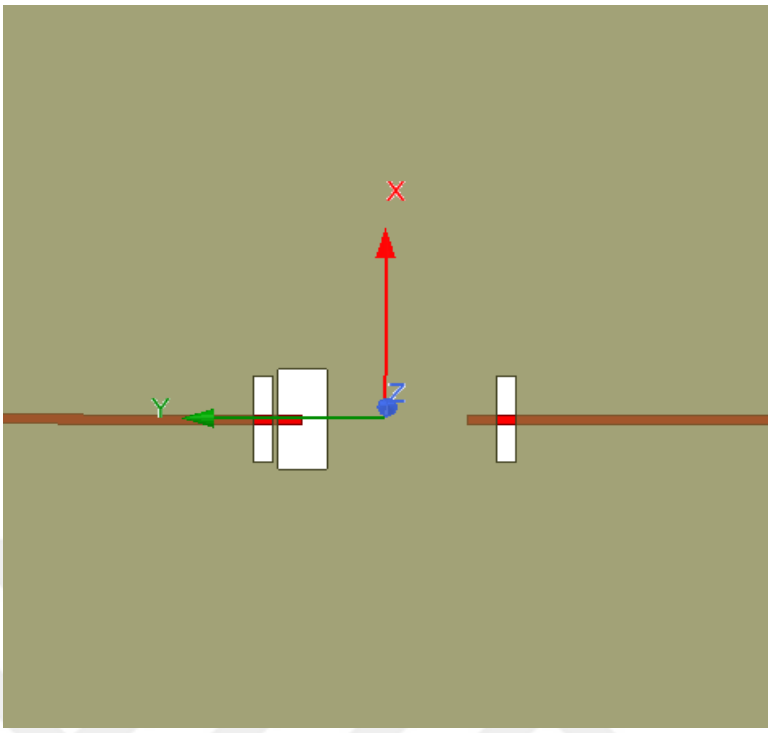

Figure 4.10: Antenna structure which a slot is opened on the ground plane

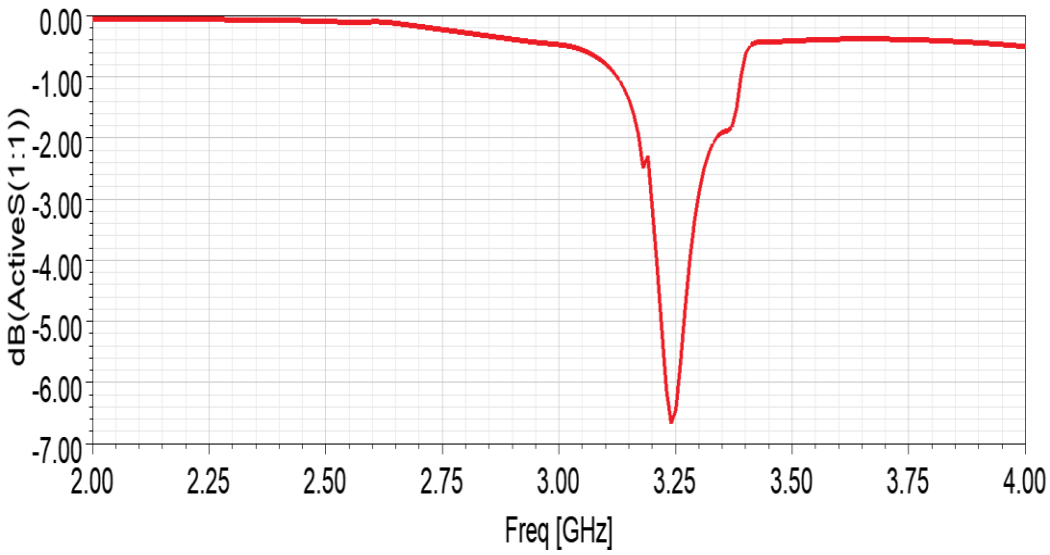

Figure 4.11: Active return loss graph for in-phase feeding

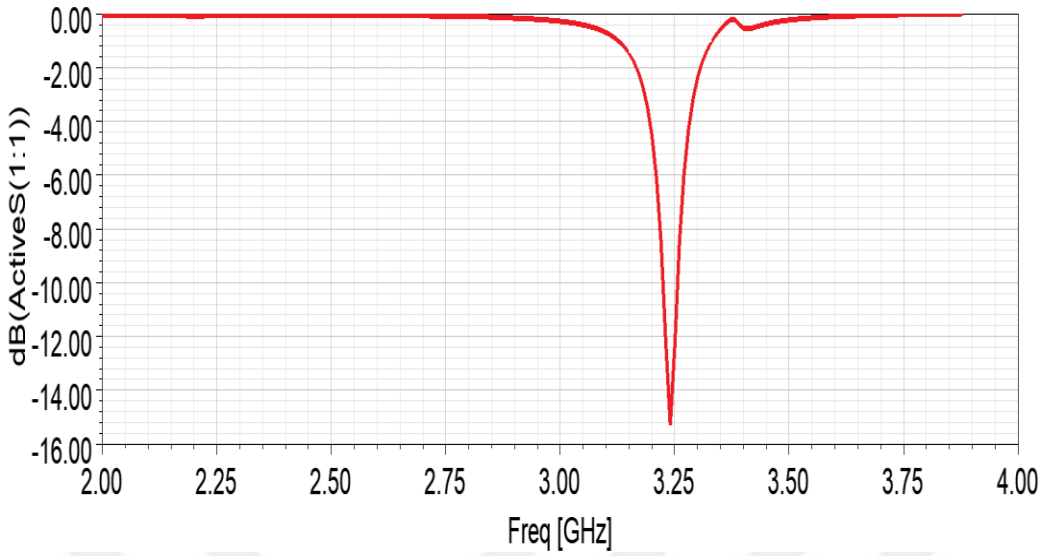

Figure 4.12: Active return loss graph for out-of-phase feeding

The normalized radiation pattern results at ϕ=90˚ plane for in-phase and out-of-phase excitations are presented in Figure 4.13.

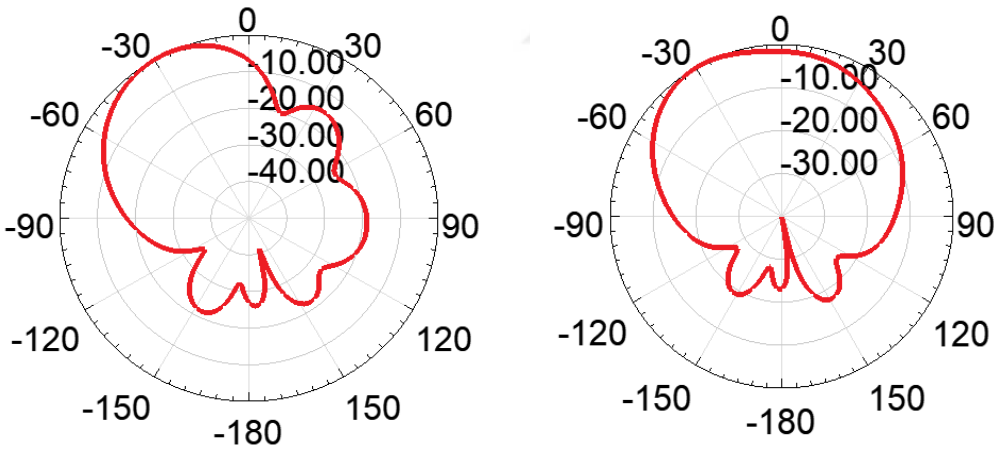

(a) (b)

Figure 4.13: Simulated normalized radiation patterns obtained when different phases are applied between two ports (a) 0˚ phase differences (b) 180˚ phase differences

Maximum gains of antenna are given in Table 4.4 and Table 4.5.

Table 4.4: Maximum gain of antenna for in-phase feeding

Feeding Type	Radiation Type	Angle at which maximum gain is seen (degrees)	Maximum Gain (dB)
In-Phase	Asymmetric Conical	-28	10.92

Table 4.5: Maximum gain of antenna for out-of-phase feeding

Feeding Type	Radiation Type	Angle at which maximum gain is seen (degrees)	Maximum Gain (dB)
Out-of-Phase	Broadside	-28	7.97

As can be seen from Figure 4.13 and Table 4.4, the one-sided slot in the ground plane of the antenna enhanced the left side of the initially conical radiation pattern and suppressed the right side for in phase feeding. In addition, As can be seen from Figure 4.13 and Table 4.5, the one-sided slot in the ground plane of the antenna has rotated the direction of the main beam -28 degrees from broadside for out-of-phase feeding.

After it is seen that the radiation pattern reconfiguration capability of the antenna can be improved by opening slots in the ground plane of the antenna, two equal-sized slots are opened on the ground plane parallel to the aperture to observe their effects on the radiation characteristics of the antenna. The antenna structure is given in Figure 4.14. The size and the position of the slots are optimized to meet this objective, and the slot size is found to be 5 mm x 11 mm placed at 6 mm from the center of the circular patch.

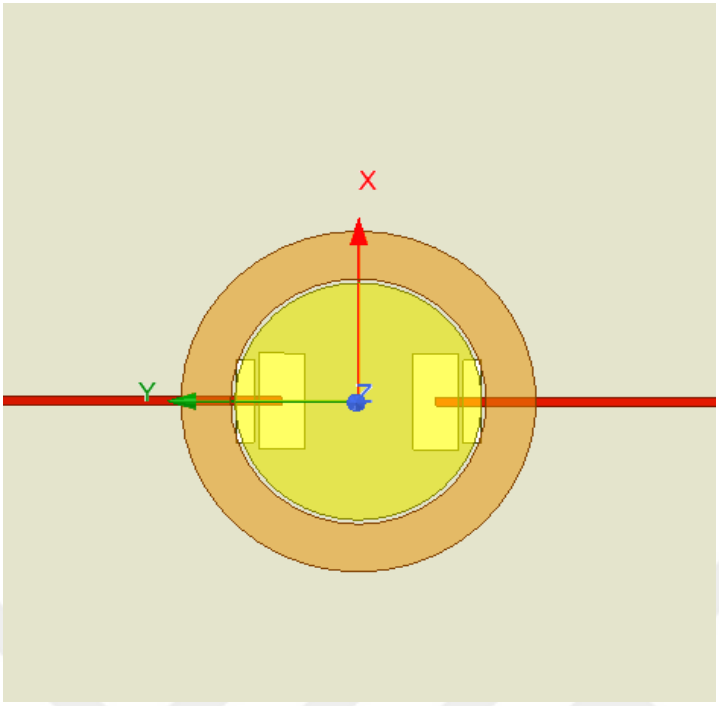

Figure 4.14: Antenna structure which two equal-sized slots are opened on the ground plane

Recall that the length of the aperture to obtain resonance at the same frequency was 15.5 mm when there is not any additional slot in the ground plane and it was 9.5 mm when the slot was open. However, these two length values should be same for the proper operation of the reconfigurable antenna. Thereupon, aperture lengths are optimized, and it is found that the aperture length providing the same resonance in all cases is 14 mm. Moreover, the slot length has also been optimized, and it has been found that 9 mm slot length is resulting in the best return loss and gain values.

The pattern reconfiguration property of the designed antenna is examined for three states. The presence and absence of slots will be controlled by OFF and ON states of PIN diode switches, respectively. During the simulations, 1.17 mm wide and 5 mm long conducting strips are used to imitate the ON state of switches. The number of switches is also optimized, and three switches are found to be adequate. As shown in Figure 4.15, only the right slot exists in State 1, only the left slot exits in State 2, and in State 3, all switches are ON to short circuit both slots. Note that eventhough

the circular patch exists in the simulation model, it is made transparent in the following figures to increase the visibility of the coupling aperture and slots in the ground plane.

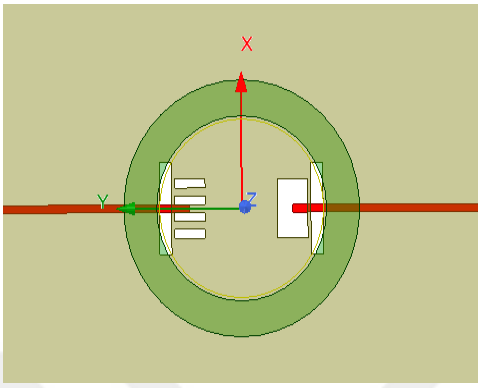

(a) State 1: Switches on the left slot are ON, on the right slot are OFF

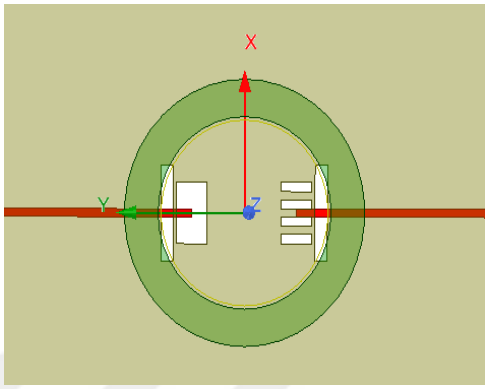

(b) State 2: Switches on the left slot are OFF, on the right slot are ON

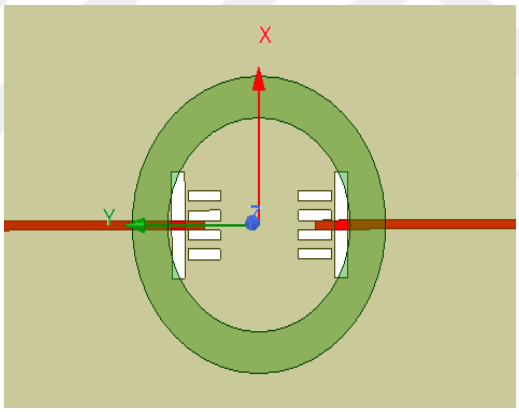

(c) State 3: Switches on the left slot are ON, on the right slot are ON

Figure 4.15: Three states of the pattern reconfiguration property of the designed antenna

Active return loss graphs for in-phase and out-of-phase feeding for three states are presented in Figure 4.16 and Figure 4.17, respectively.

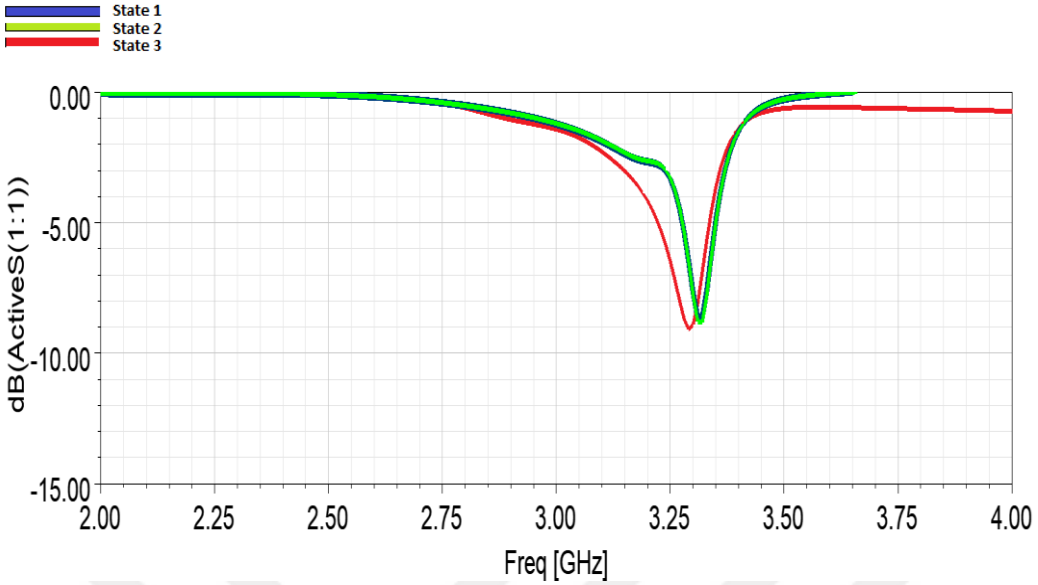

Figure 4.16: Active return loss graphs for in-phase feeding for three states

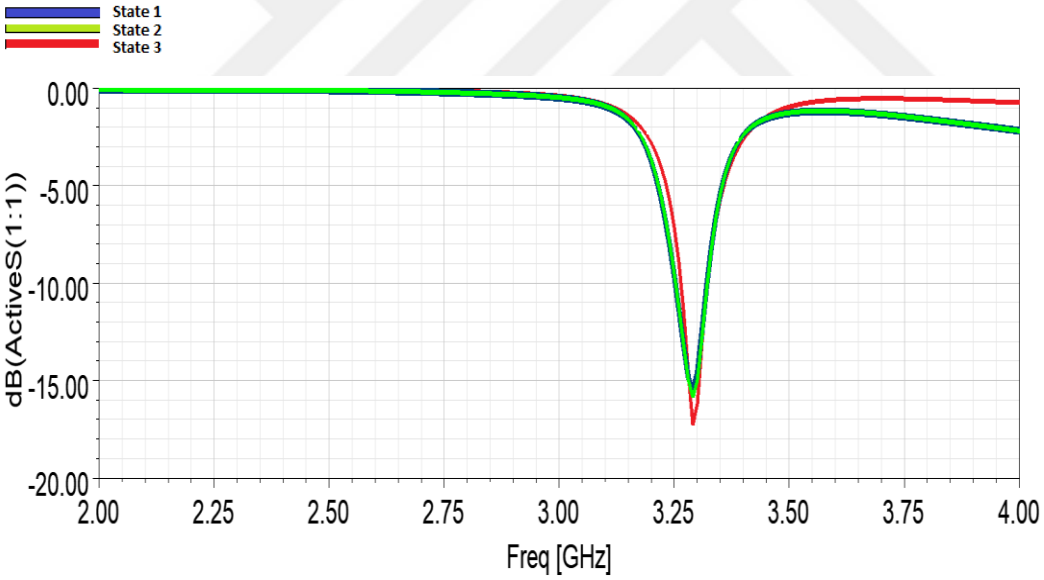

Figure 4.17: Active return loss graphs for out-of-phase feeding for three states

The radiation pattern results at ϕ=90˚ plane and at 3.3 GHz for all states for in-phase and out-of-phase excitations are presented in Figure 4.18 and Figure 4.19, respectively.

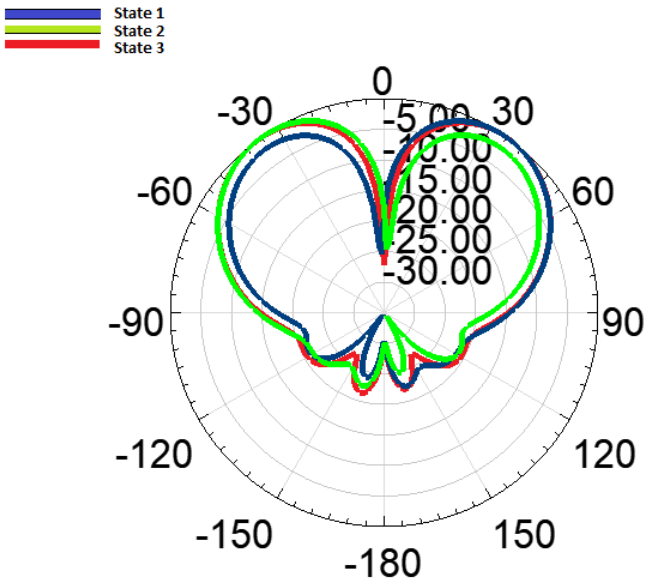

Figure 4.18: Simulated normalized radiation patterns for three states for in-phase feeding

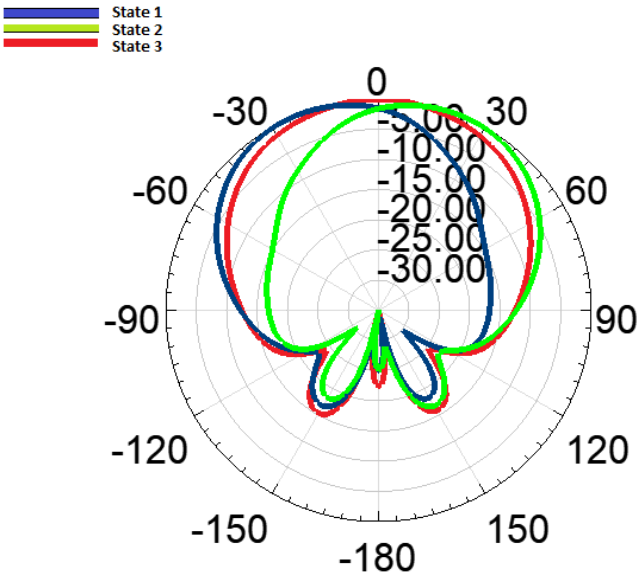

Figure 4.19: Simulated normalized radiation patterns for three states for out-of-phase feeding

When the antenna is fed in-phase, radiation asymmetry is obtained in state 1, and, the radiation pattern maximum is observed at 34˚. In state 2, radiation asymmetry is obtained, and, the radiation pattern is observed at -34˚. If the switches on the left and right sides are closed simultaneously, then in state 3, the initial radiation pattern symmetry is obtained again. Note that the level of asymmetry in the radiation pattern is not as high as the one obtained for GCPW fed antenna operating at 26 GHz. It is observed that the level of the asymmetry can be improved by changing the slot length and position. However, for that case the amount of beam tilt from broadside decreases when the antenna is fed out of phase. Therefore, among these two alternative designs, the amount of beam tilt is favored and it is decided to continue with the current design.

When the antenna is fed out-of-phase, in state 1, the radiation pattern is rotated from broadside to -24˚, and the maximum gain of the antenna is 8.06 dB. In state 2, the radiation pattern is rotated from broadside to +24˚, and the maximum gain of the antenna is 8.08 dB. If the switches on the left and the right sides are off simultaneously, in state 3, the radiation pattern is obtained in broadside, and the maximum gain of the antenna is 6.81 dB.

Summaries of radiaiton for in-phase feeding and out-of-phase feeding are given in Table 4.6 and Table 4.7, respectively.

Table 4.6: Summary of radiaiton for in-phase feeding

	Radiation Type	Angle at which maximum gain is seen (degrees)	Maximum Gain (dB)
State 1	Asymmetric Conical	34	9.72
State 2	Asymmetric Conical	-34	9.73
State 3	Conical	±34	8.86

Table 4.7: Summary of radiaiton for out-of-phase feeding

	Radiation Type	Angle of rotation from broadside (degrees)	Maximum Gain (dB)
State 1	Off-Broadside	-24	8.06
State 2	Off-Broadside	24	8.08
State 3	Broadside	0	6.81

After creating asymmetry in the radiation pattern, two equal-sized slots are opened on the ring in the same direction as the slots are opened in the ground plane as shown in Figure 4.20 to investigate whether it is possible to reconfigure the antenna without the need of 180^0 phase shifter as discussed in the previous chapter.

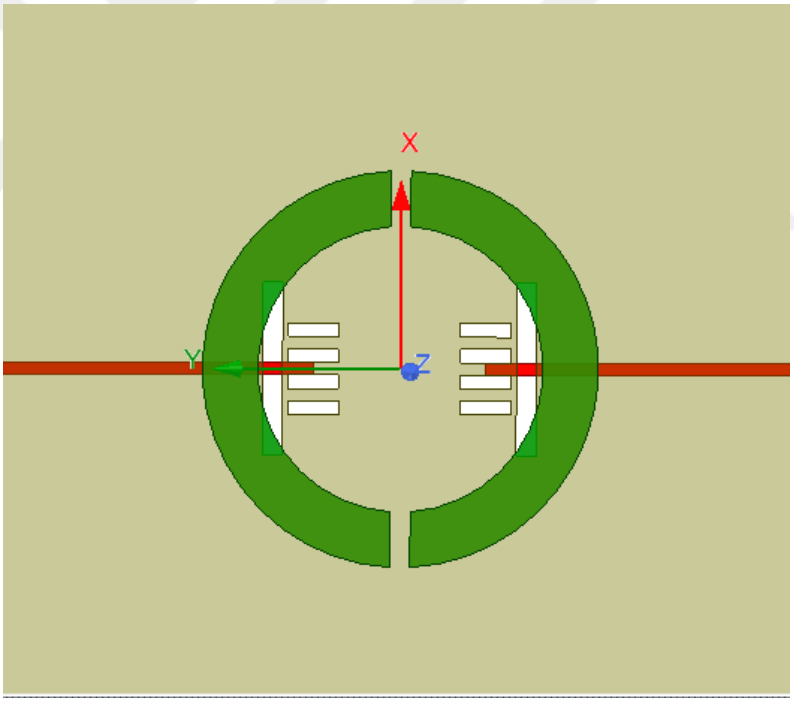

Figure 4.20: Antenna structure which two equal-sized slots are opened on the ring

For the optimization of slot size on the ring, parametric studies are made. The slot width has been increased from 1 mm to 8 mm in 1 mm increments. However, as it

can be observed from active return loss results obtained for different slots (Figure 4.21) and radiation pattern results given in Figure 4.22, the antenna radiates conical beam for all slot sizes and no change in the radiation mode is observed for any slot size.

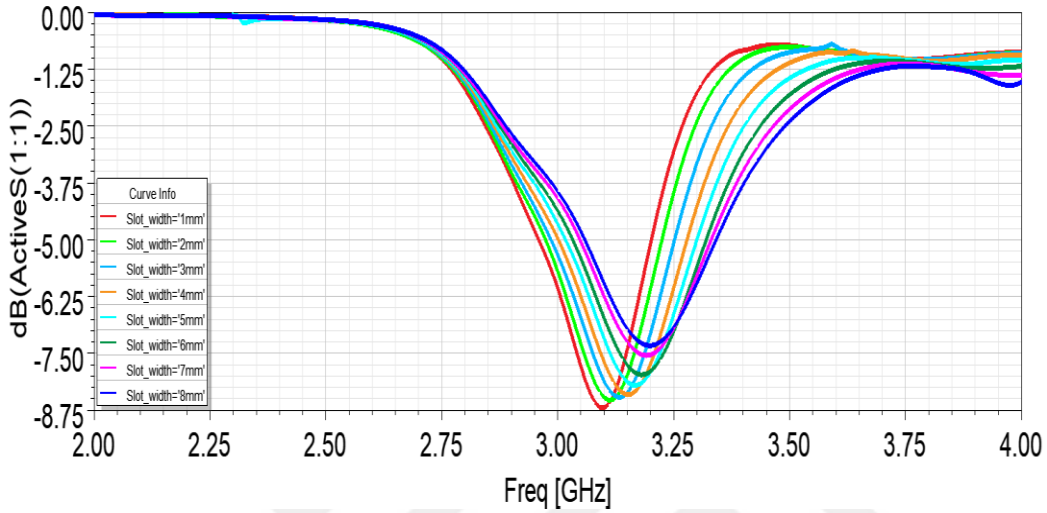

Figure 4.21: Active scattering parameters (S_{11}) with respect to frequency for different slot widths

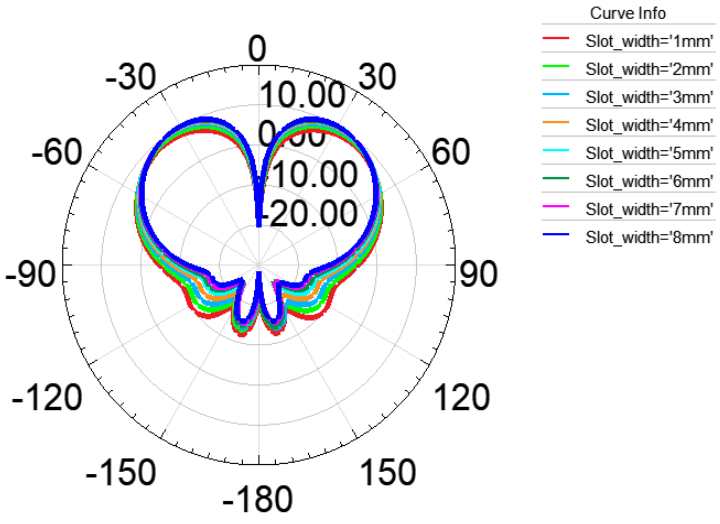

Figure 4.22: Simulated radiation patterns at ϕ=90˚ plane for different slot widths

After it is observed that the slots opened on the ring in the same direction as the slots opened on the ground plane did not change the radiation pattern, slots are opened on the ring and on the patch in different positions and geometries to investigate whether a radiation mode change can be observed with a different topology. The studied antenna structures are given in Figure 4.23.

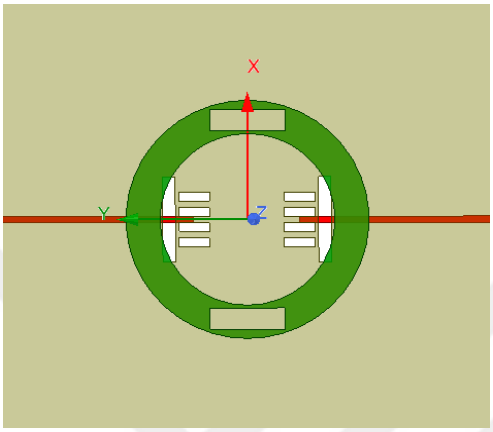

(a) Vertical slots on the ring

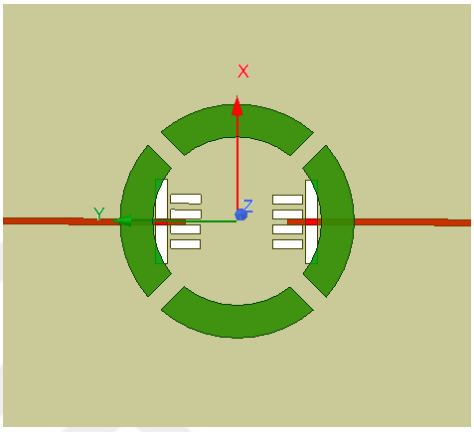

(b) Slots at 45˚ on the ring

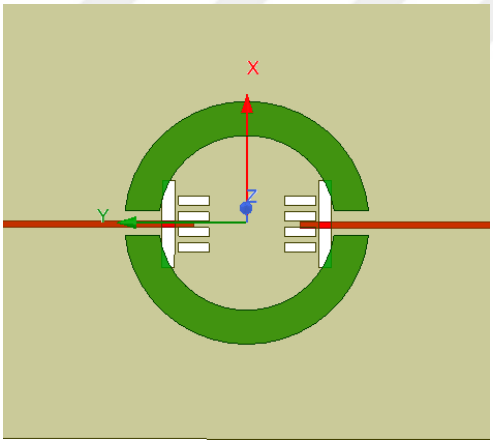

(c) Y-axis slots on the ring

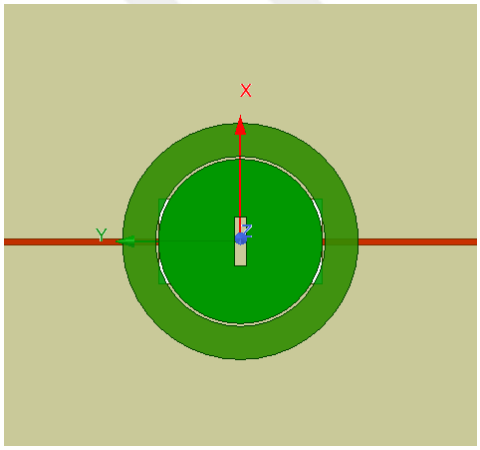

(d) Slot in the middle circle

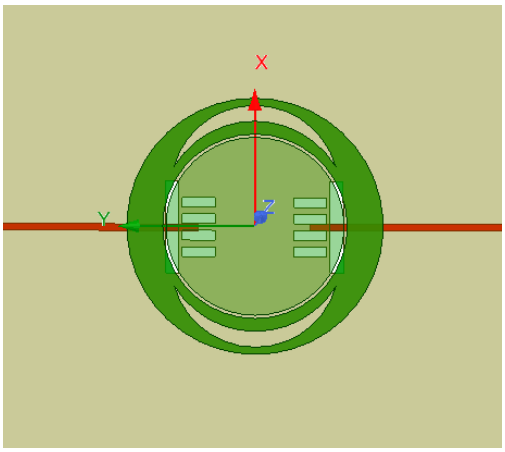

(e) Arc-shaped slots on the ring

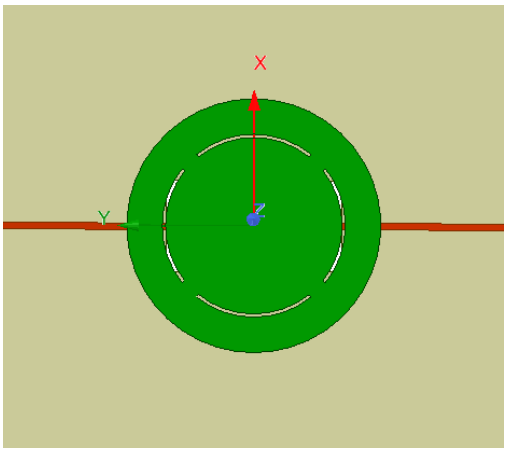

(f) Short circuiting between the patch and the ring at ±45˚ and ±135˚

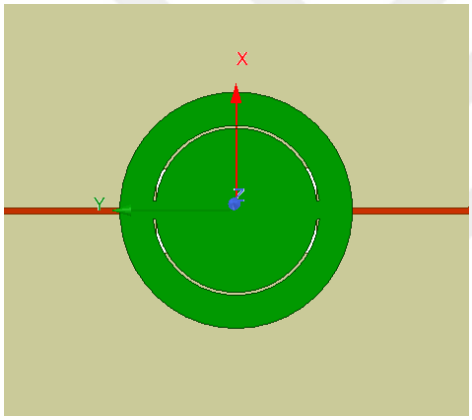

(g) Short circuiting between the patch and the ring at ±90˚

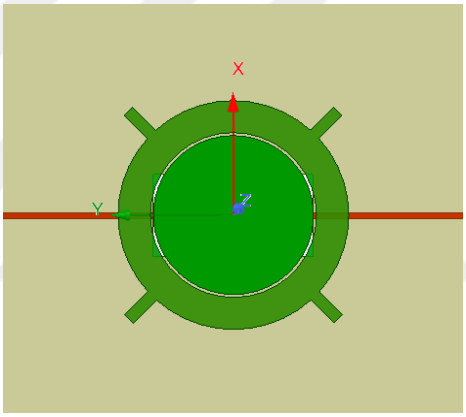

(h) Adding stub to ±45 degrees and ±135 degrees on the ring

Figure 4.23: Antenna structures which different slots are opened on the ring and on the patch

Simulations have been made with all the antenna geometries shown in Figure 4.23, however, no mode change of the antenna has been observed in any geometry. But a mode change was observed in the antenna designed at 26 GHz by simply inserting a slot in the ring. The reason why such a behaviour is not observed for this antenna is explored. The first difference noticed between two antennas is the level of isolation

between two ports of the antenna. Since the previous antenna was designed by considering only the return loss value of one of the ports, the isolation between the ports were poor (about -8 dB at 26 GHz), whereas the isolation between the ports of this antenna is good (around -18 dB) since it is optimized by considering the active return loss values for both types of excitations (in-phase and out of phase). It is thought that this might be the reason why there is a mode change in the antenna operating at 26 GHz when the slots are opened on the ring, and there is no mode change in the antenna operating at 3.3 GHz. In order to test this claim, it is planned to increase the coupling between the two feeds. To achieve this, a parametric study is carried out with the aperture length. Isolation graphs for different aperture lengths are given in Figure 4.24. Active return loss graphs for in-phase and out-of-phase feeding for different aperture lengths are presented in Figure 4.25 and Figure 4.26, respectively.

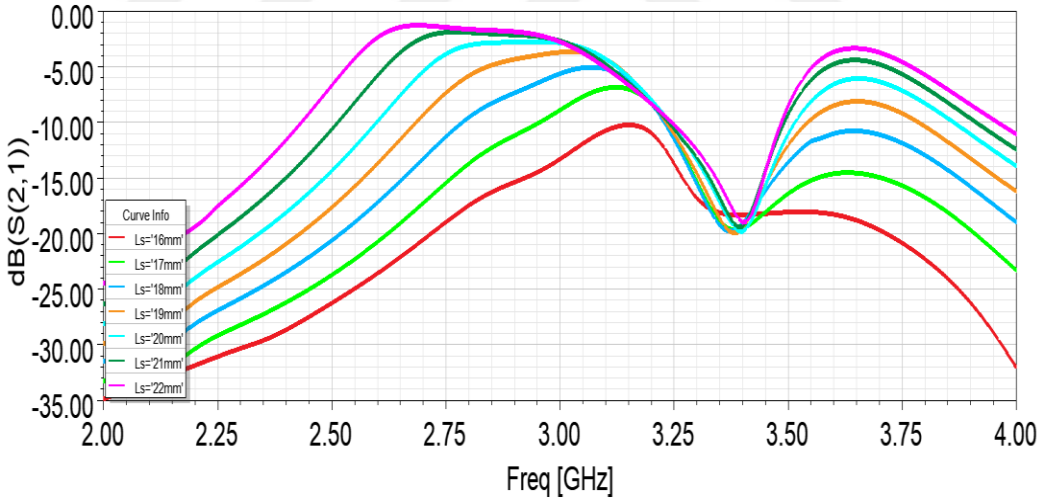

Figure 4.24: Isolation (S_{21}) with respect to frequency for different aperture lengths

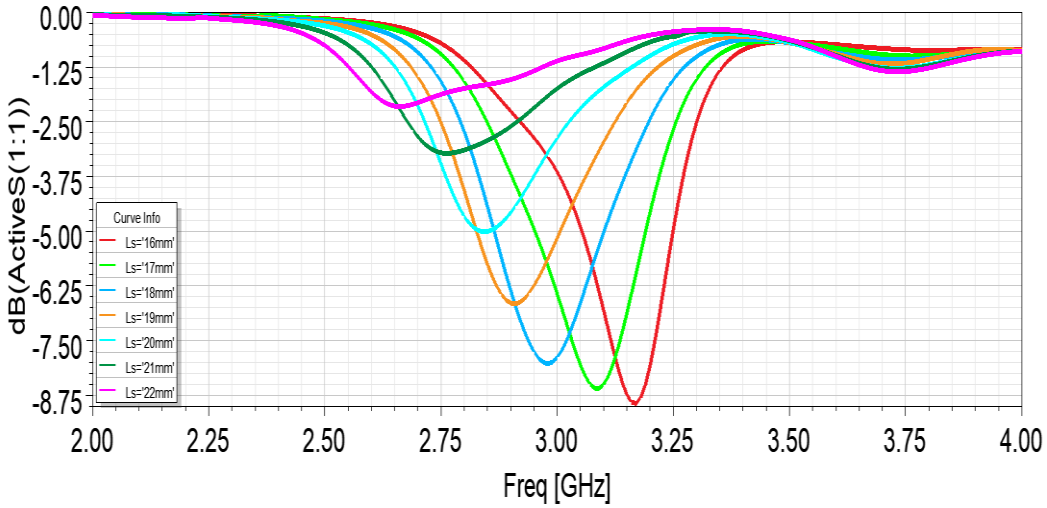

Figure 4.25: Active scattering parameters (S_{11}) with respect to frequency for different aperture lengths for in-phase feeding

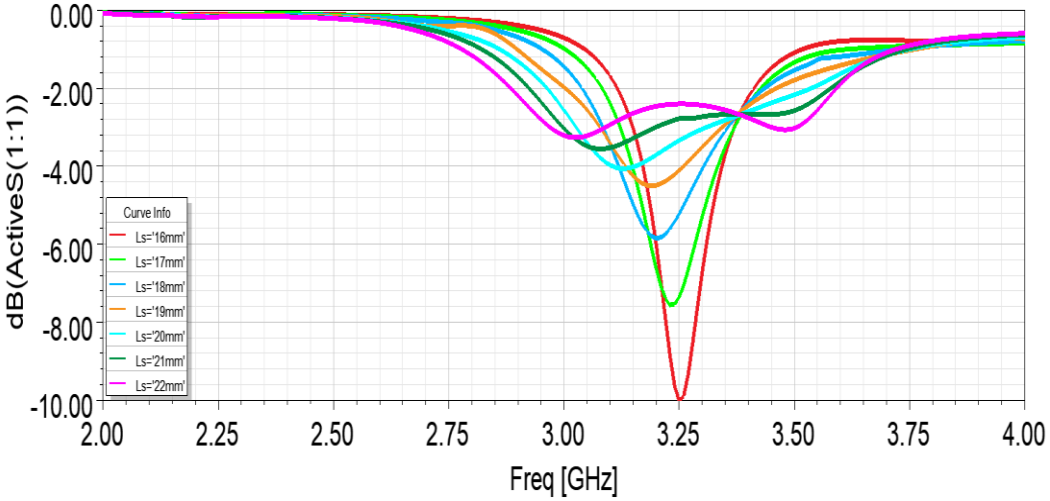

Figure 4.26: Active scattering parameters (S_{11}) with respect to frequency for different aperture lengths for out-of-phase feeding

As seen in Figure 4.24, the coupling between the two feeds increases as the aperture length increases. However, as can be seen in Figure 4.25 and Figure 4.26, as the aperture length increases, the frequency shift between the resonance frequencies of in-phase and out-of-phase excitations becomes larger as expected. The length of the aperture is increased to 18 mm to incease the coupling between ports and a slot is

opened in the ring to investigate whether a radiation mode change can be observed for this antenna with poor isolation between ports. For different values of the width of the slot, simulations are performed with in-phase excitation but the radiation pattern remained as conical beam and no mode change is observed. As a result the pattern reconfiguration technique applied for the antenna designed at 26 GHz is not found to be applicable to this antenna. Hence the antenna needs to be excitated both in-phase and out of phase for pattern reconfiguration. To meet this need a rat-race coupler is designed. The design steps will be presented in the next section.

4.2 Design Considerations of Rat-Race Coupler

The illustration of a rat-race coupler is shown in Figure 4.27. Rat-race coupler is a 4-port device, 2 of them are the input ports and 2 of them are the output ports. It is also known as 180˚ hybrid coupler.

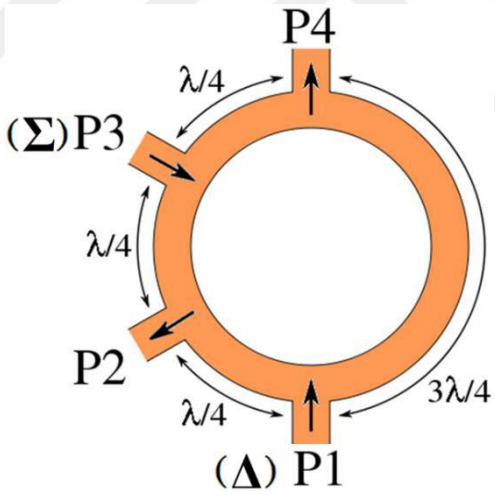

Figure 4.27: Sum and difference ports of a rat-race coupler [25]

In case the 1^{st} port is fed as the source, the power is divided equally between the 2^{nd} and 4^{th} ports with 180˚ phase difference between them. This situation is only valid when port 3 is terminated with the matched load. In the case where the 3^{rd} port is fed as the source, the power is divided equally between the 2^{nd} and 4^{nd} ports, and

there is no phase difference between them so that in-phase feeding occurs. This situation is only valid when port 1 is terminated with the matched load.

The rat race structure presented in [12] is evaluated to be feasible considering the antenna geometry and the layer where the feedline is located. In the study proposed in [12] and shown in Figure 4.28, a rectangular rat-race structure is designed. The structure fed from port 1 created a 180 degree phase difference between ports 3 and 4. On the other hand, the structure fed from Port 2 did not create a phase difference between ports 3 and 4.

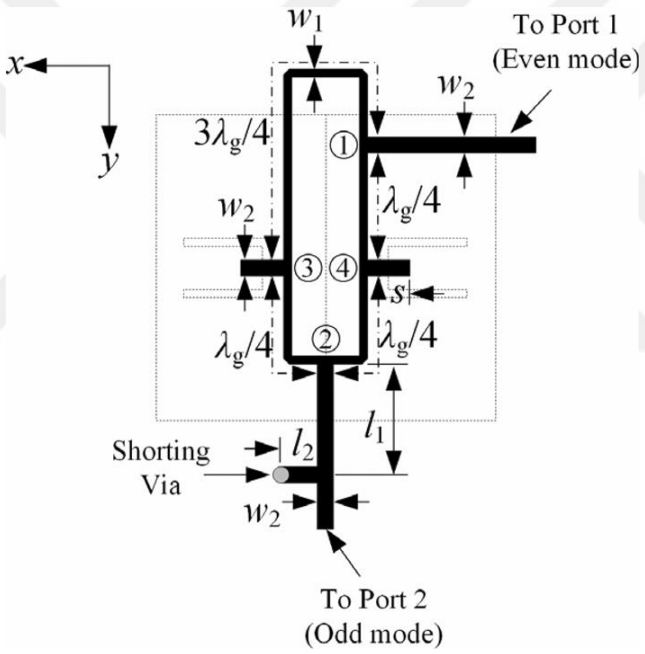

Figure 4.28: Geometry of a rat-race feeding network [12]

When starting the rat-race design, first of all, the widths of the microstrip lines with a characteristic impedance of 50 Ω (w_2) and with a characteristic impedance of about 70 Ω (w_1) should be found.

For 0.508 mm thick ROGERS4003 they are found as w_2 =1.17 mm and w_1 = 0.62 mm. Then the guided wavelength, λ_g, need to be found. Bu simulating microstrip line with 70 Ω characteristic impedance, the guided wavelength is found as 54.52 mm. Using these line width values and guided wavelength value, the rat-race structure shown in Figure 4.29 is simulated.

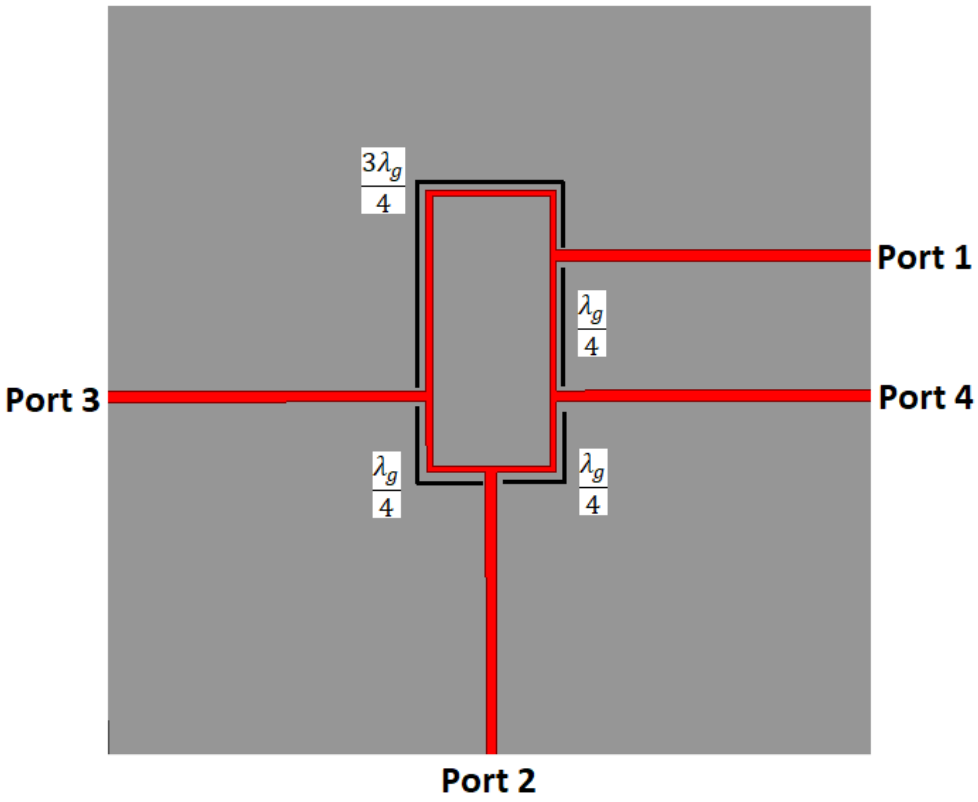

Figure 4.29: Rat-rate structure

Return loss graphs for every port, phase graphs for S_{13} and S_{14} and phase graphs for S_{23} and S_{24} are presented in Figure 4.30, Figure 4.31, and Figure 4.32, respectively.

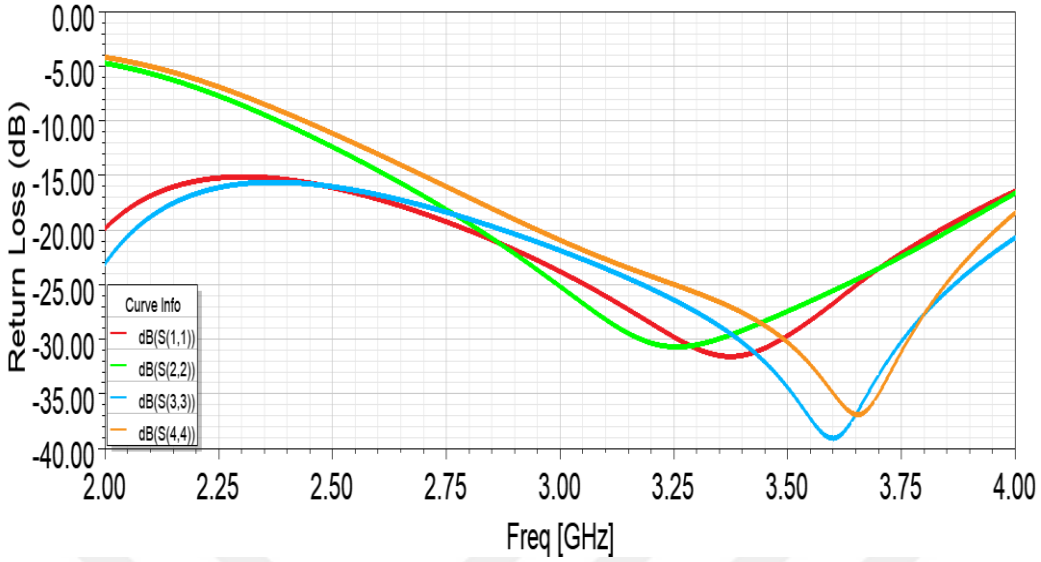

Figure 4.30: Return loss graph

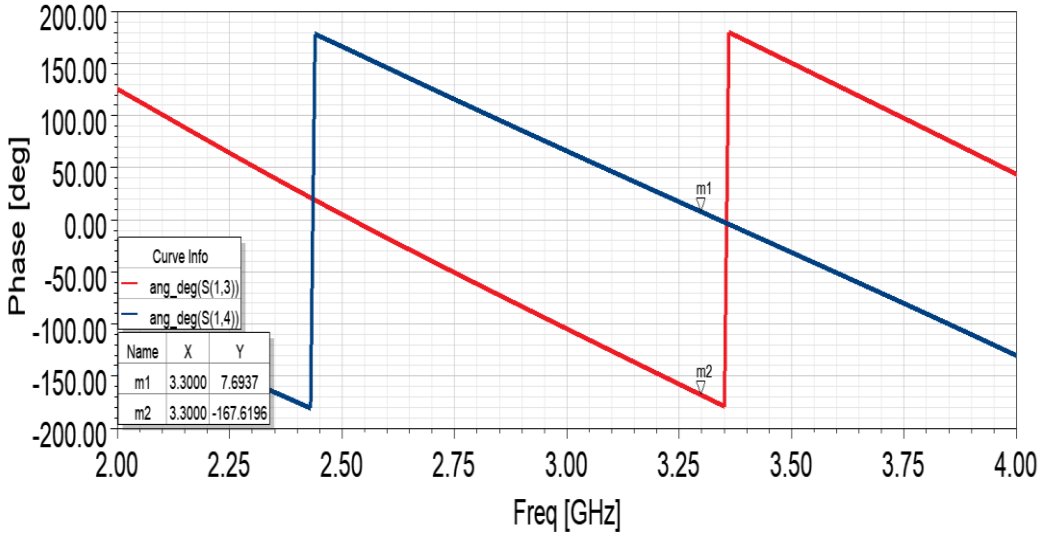

Figure 4.31: Phase Graph for S_{13} and S_{14}

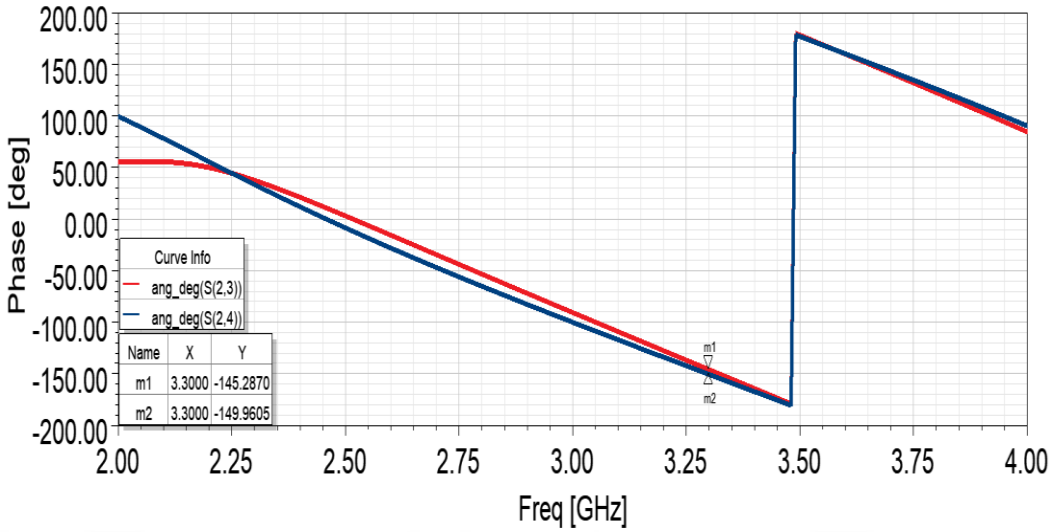

Figure 4.32: Phase Graph for S_{23} and S_{24}

As can be seen in Figure 4.30, the return loss for each port is about -30 dB for 3.3 GHz. As can be seen from Figure 4.31, although there should be 180˚ phase difference between S_{13} and S_{14} parameters, 175˚ phase difference is observed. Also, as can be seen from Figure 4.32, although there should be 0˚ phase difference between the S_{23} and S_{24} parameters, 4˚ phase difference is observed. Thereupon, the λ_g value will be tuned, and the phase differences of 180˚ and 0˚ will be tried to be achieved. The λ_g value is set to 56 mm, and the phase graphs of the parameters S_{13} and S_{14} are drawn. Phase graphs of parameters S_{13} and S_{14} are shown in Figure 4.33.

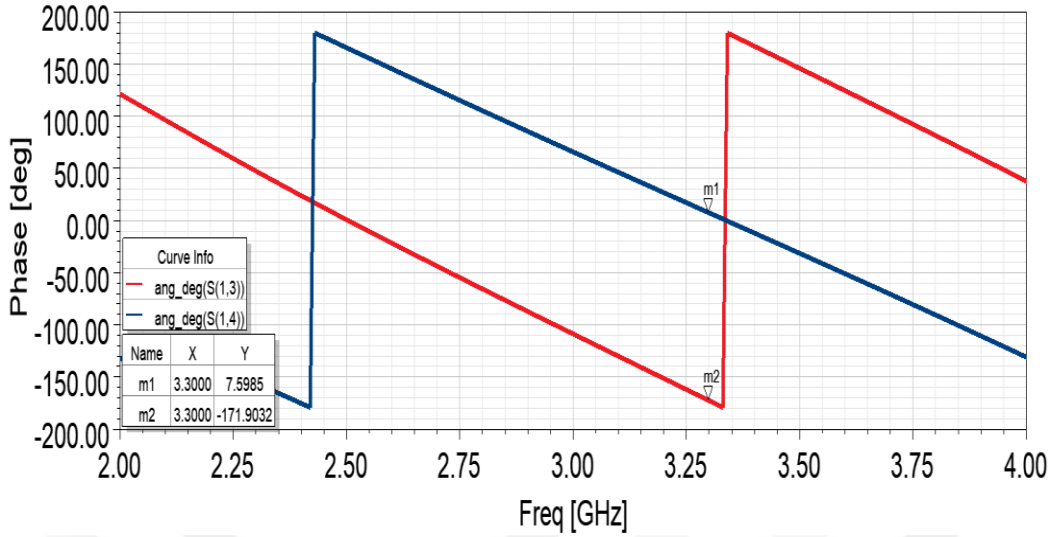

Figure 4.33: Phase Graph for S_{13} and S_{14} for $\lambda_g = 56\ mm$

As can be seen in Figure 4.33, the phase difference between the parameters S_{13} and S_{14} is observed as almost 180˚ at 3.3 GHz. Phase graphs of parameters S_{23} and S_{24} are shown in Figure 4.34.

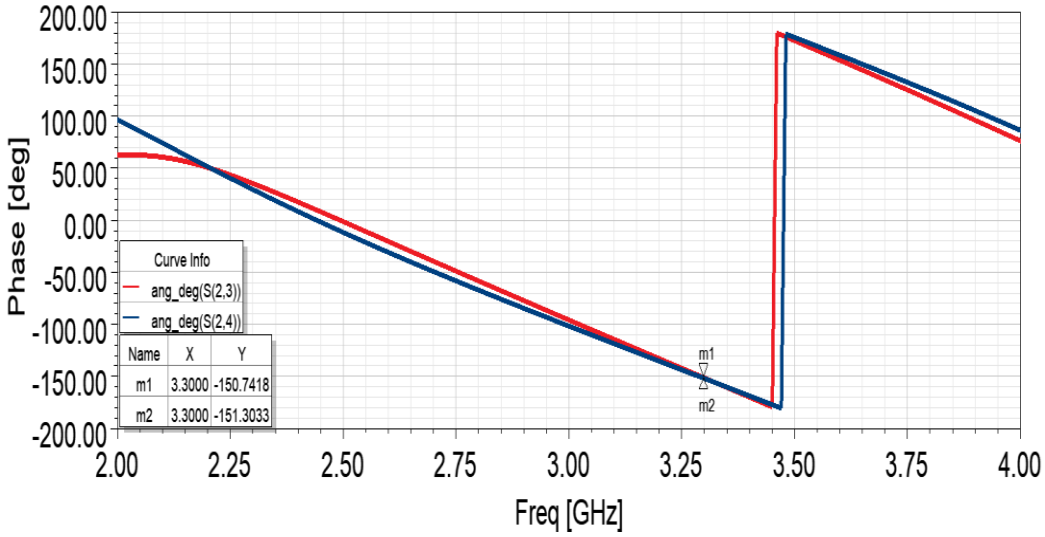

Figure 4.34: Phase Graph for S_{23} and S_{24} for λ_g=56 mm

As can be seen in Figure 4.34, the phase difference between the parameters S_{23} and S_{24} is observed as almost 0˚ at 3.3 GHz. The power splitting from Port 1 (common port) and Port 2 (differential port) to the branches is shown in Figure 4.35 and Figure 4.36, respectively.

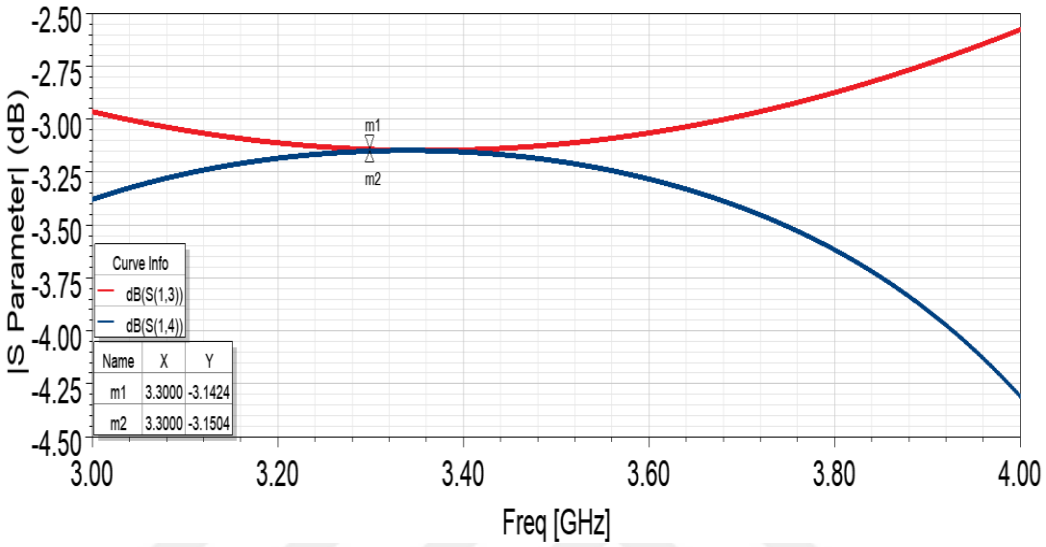

Figure 4.35: Power splitting graph to the branches from the differential port

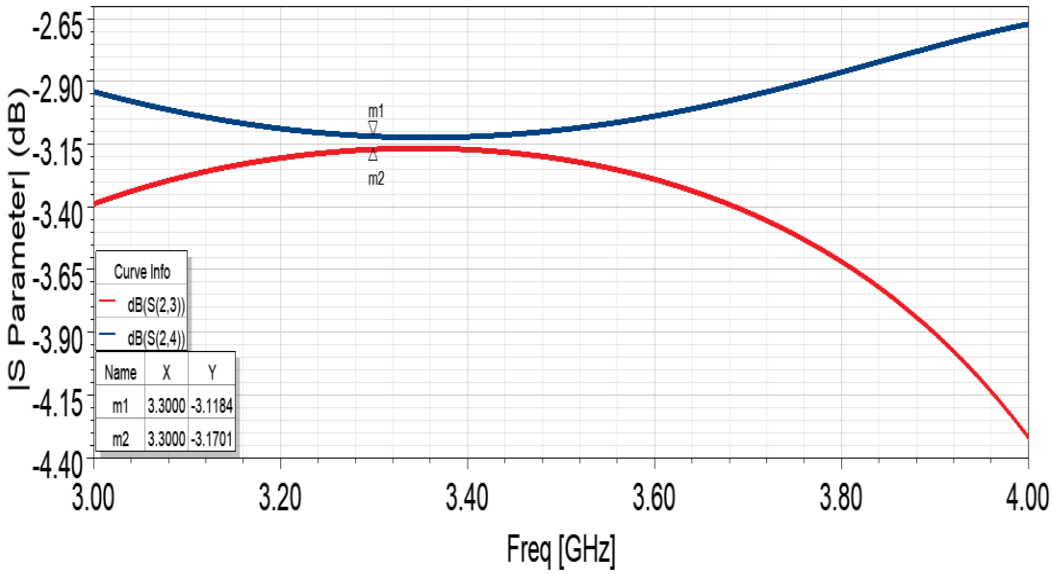

Figure 4.36: Power splitting graph to the branches from the common port

As can be seen from Figure 4.35 and Figure 4.36, the amount of power going to the branches from differential port and common port are approximately equal to each other (-3 dB). With these simulation results, it has been shown that the rat-race structure works properly.

4.3 Integration of Antenna and Rat-Race Coupler

After the rat-race coupler was shown to work properly, it started to be combined with the designed antenna. The pattern reconfiguration property of the designed antenna is examined for three states. As shown in Figure 4.37, only the right slot exists in State 1, only the left slot exits in State 2, and in State 3, all switches are ON to short circuit both slots.

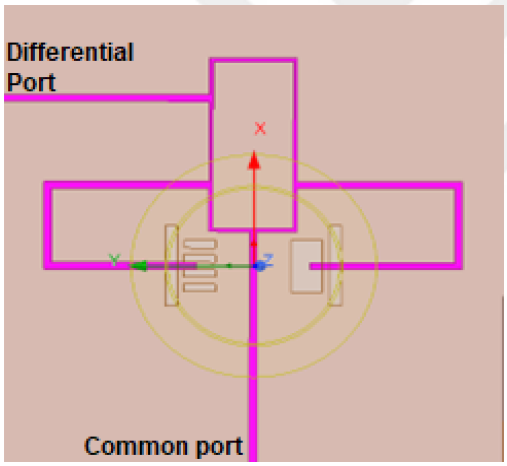

(a) State 1: Switches on the left slot are ON, on the right slot are OFF

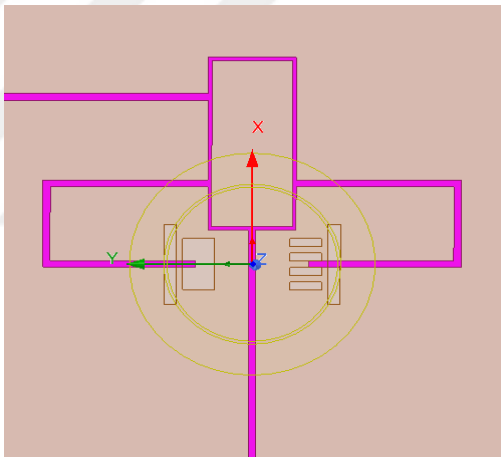

(b) State 2: Switches on the left slot are OFF, on the right slot are ON

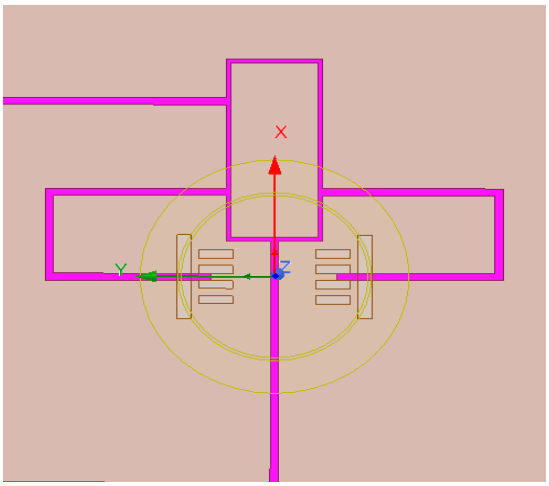

(c) State 3: Switches on the left slot are ON, on the right slot are ON

Figure 4.37: Three states of the pattern reconfiguration property of the designed antenna

Return loss graphs for three states when the antenna is excited from common port and differential port are presented in Figure 4.38 and Figure 4.39, respectively.

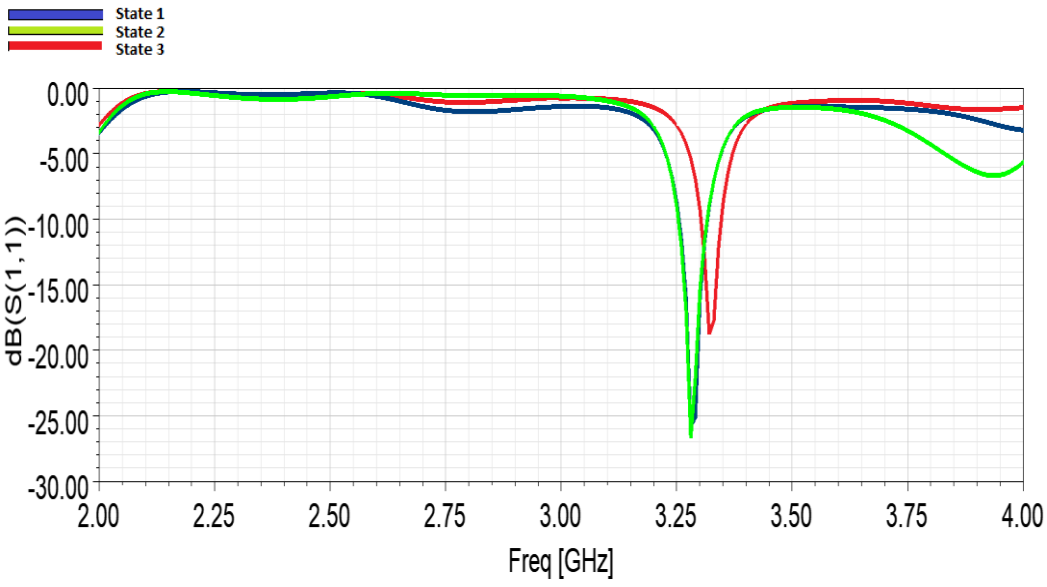

Figure 4.38: Return loss graphs for three states when differential port is excited

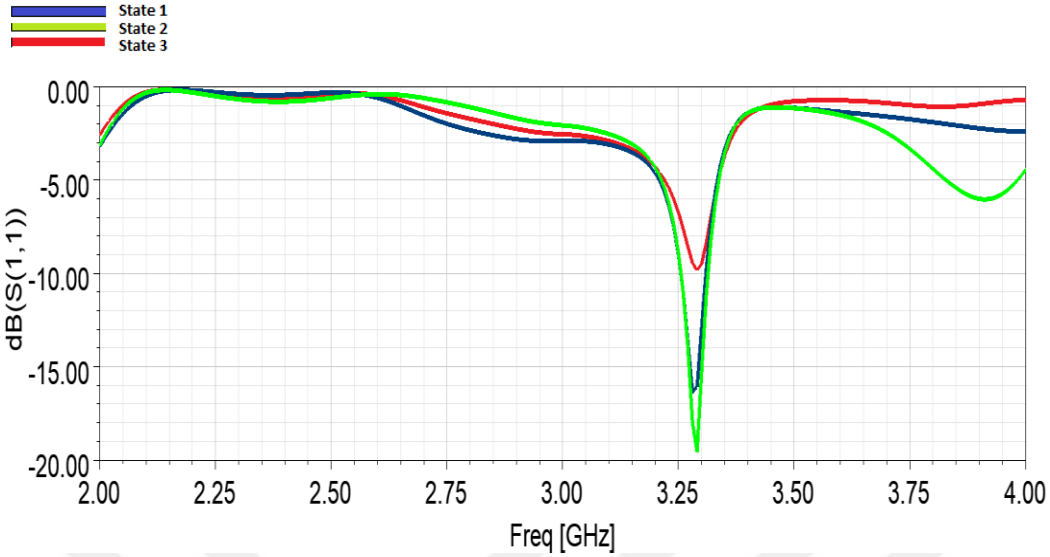

Figure 4.39: Return loss graphs for three states when common port is excited

As can be seen from Figure 4.38 and 4.39, there is resonance at the 3.3 GHz frequency for all three cases.

The current distributions for common mode and differential mode are shown in Figure 4.40, Figure 4.41, Figure 4.42 and Figure 4.43.

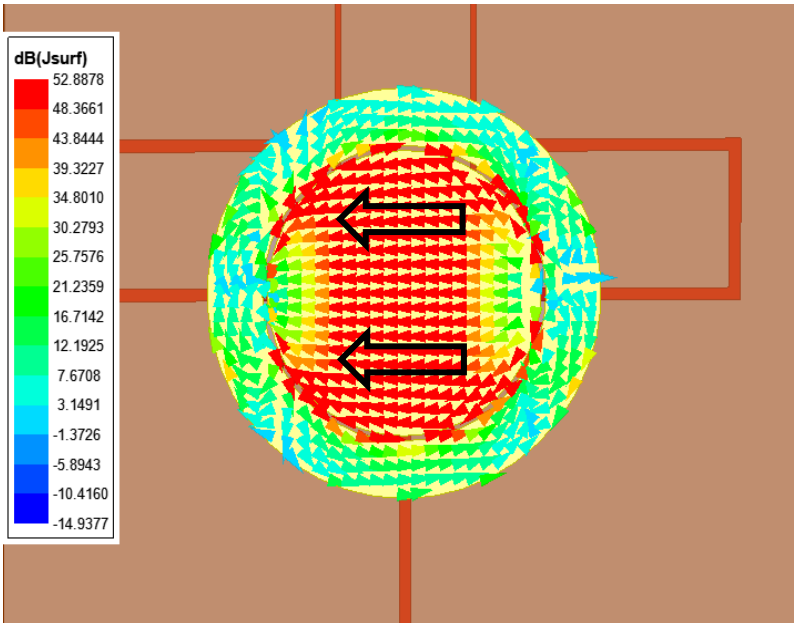

Figure 4.40: Current distribution for differential mode (ON-ON State)

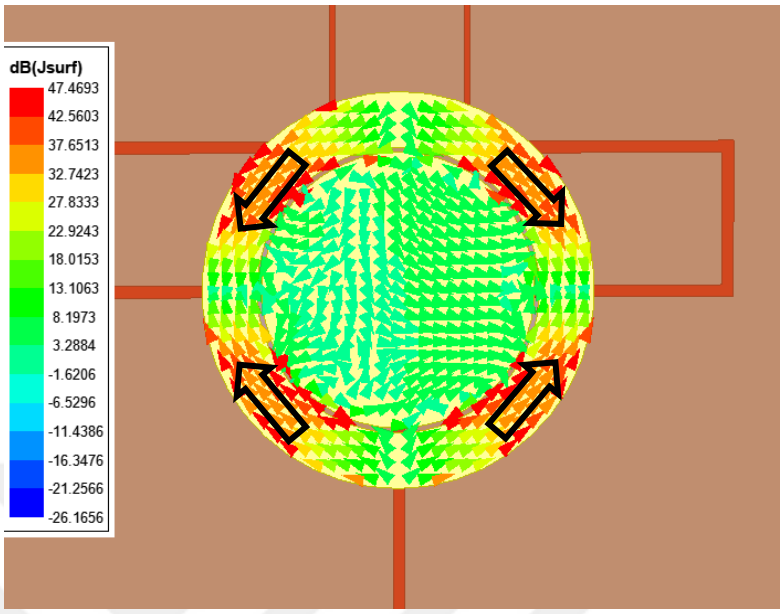

Figure 4.41: Current distribution for common mode (ON-ON State)

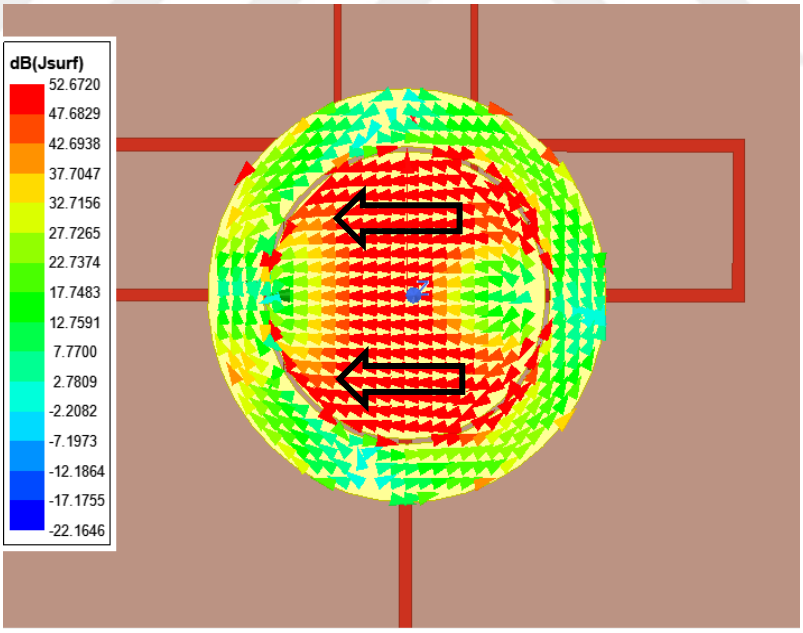

Figure 4.42: Current distribution for differential mode (OFF-ON State)

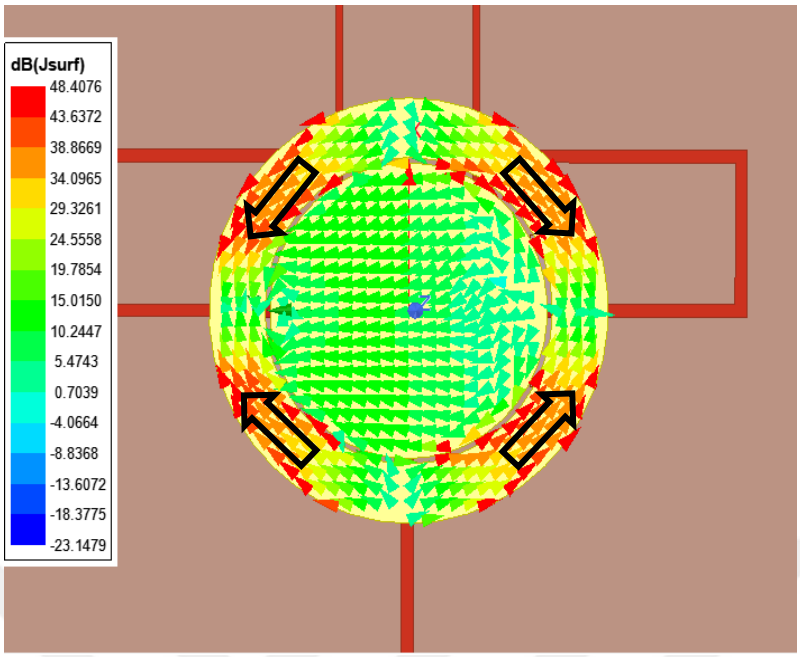

Figure 4.43: Current distribution for common mode (OFF-ON State)

The radiation pattern results at ϕ=90˚ plane and at 3.3 GHz for all states for differential and common port excitations are presented in Figure 4.44 and Figure 4.45, respectively.

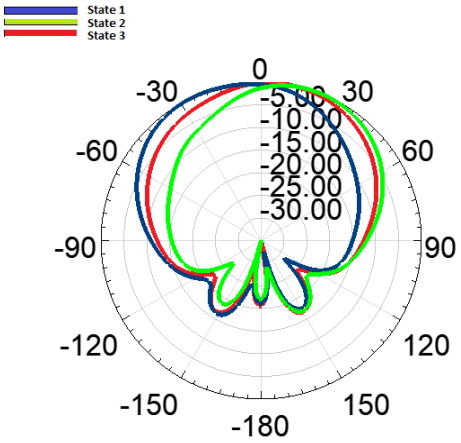

(a) Antenna patterns when its integrated rat-race coupler

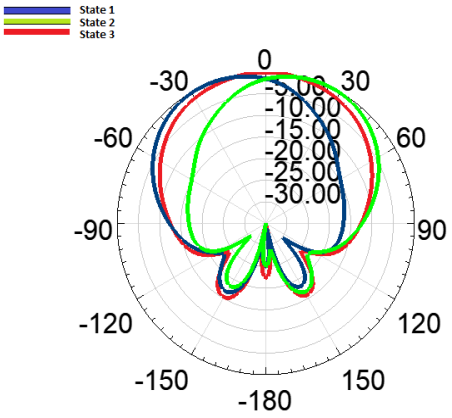

(b) Antenna patterns when it is fed out-of-phase

Figure 4.44: Radition pattern results (a) when its integrated rat-race coupler (b) when it is fed out-of-phase

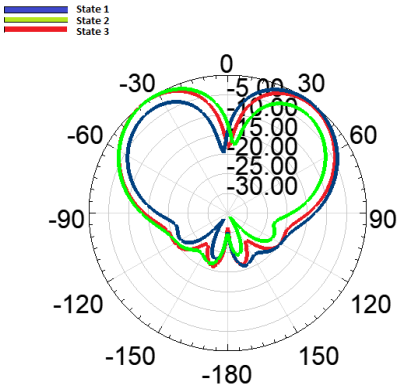

(c) Antenna patterns when its integrated rat-race coupler

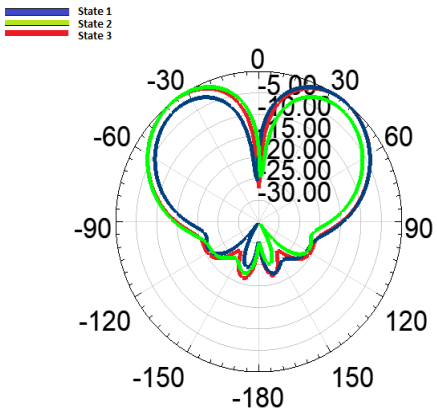

(d) Antenna patterns when it is fed in-phase

Figure 4.45: Radition pattern results (a) when its integrated rat-race coupler (b) when it is fed in-phase

As seen in Figure 4.44, when the antenna is fed from differential port and common port is terminated with 50 Ω, it behaves like an out-of-phase feed and realizes broadside radiation. In state 1, the radiation pattern is rotated from broadside to -24 degrees, and the maximum gain of the antenna is 7.45 dB. In state 2, the radiation pattern is rotated from broadside to 18 degrees, and the maximum gain of the antenna is 7.30 dB. If both switches are ON simultaneously, in state 3, the radiation pattern is obtained in broadside, and the maximum gain of the antenna is 7.16 dB. In addition, the radiation patterns of the antenna with integrated rat-race coupler and the antenna fed out-of-phase are similar.

As seen in Figure 4.45, when the antenna is fed from common port, and the differential port is terminated with 50 Ohm, it behaves like an in-phase feed and realizes the conical beam. State 1 enhanced the right side of the initially conical radiation pattern and, suppressed the left side. State 2, enhanced the left side of the initially conical radiation patter, and suppressed the right side. If the switches on the left side and the right side are closed simultaneously, then in state 3, the initial radiation pattern symmetry is obtained again. Additionaly, the radiation patterns of the antenna with integrated rat-race coupler and the antenna fed in-phase are similar.

Summaries of radiation, when the antenna is fed from common port and from differential port, are given in Table 4.8 and Table 4.9, respectively.

Table 4.8: Summary of radiation when the antenna is fed from common port

	Radiation Type	Angle at which maximum gain is seen (degrees)	Maximum Gain (dB)
State 1	Asymmetric Conical	36	9.43
State 2	Asymmetric Conical	-36	9.65
State 3	Conical	±36	8.81

Table 4.9: Summary of radiaiton when the antenna is fed from differential port

	Radiation Type	Angle of rotation from broadside (degrees)	Maximum Gain (dB)
State 1	Off-Broadside	-24	7.45
State 2	Off-Broadside	18	7.30
State 3	Broadside	0	7.16

CHAPTER 5

FABRICATION AND MEASUREMENT RESULTS OF RINGED CIRCULAR PATCH ANTENNA

5.1 Fabrication of the Antenna

The designed antenna is produced and measured using the facilities of ASELSAN Inc. The designed antenna and rat-race coupler are fabricated by the LPKF Protolaser S milling machine shown in Figure 5.1. ROGERS 4003 is used as the antenna and rat-race coupler material, and FR4 is used as back radiation blocking ground. The produced components and the final antenna formed by combining these components are given in Figure 5.2 and Figure 5.3, respectively. SMA connectors are used to feed the structure and soldered to the layer with the rat-race coupler.

Figure 5.1: Fabrication of the designed antenna

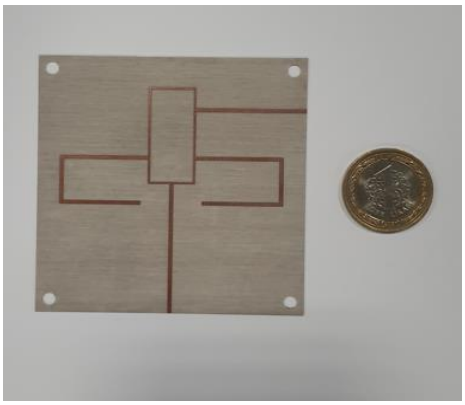

(a) Rat-race coupler

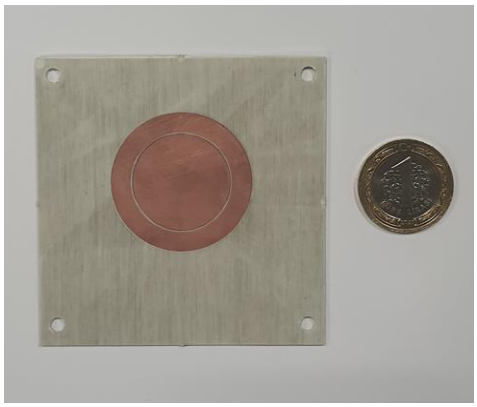

(b) Ringed circular patch antenna

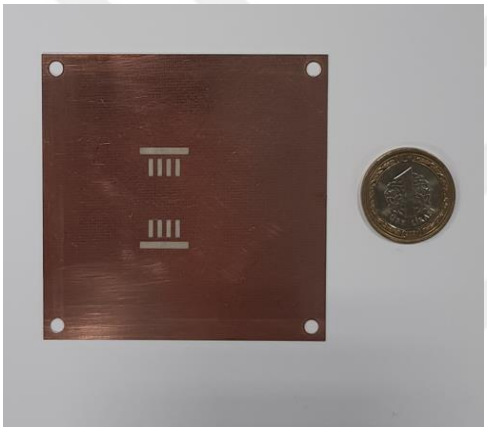

(c) Ground plane #1 (ON-ON state)

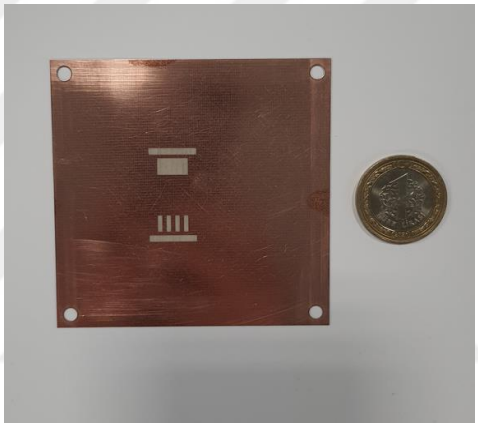

(d) Ground Plane #2 (OFF-ON state)

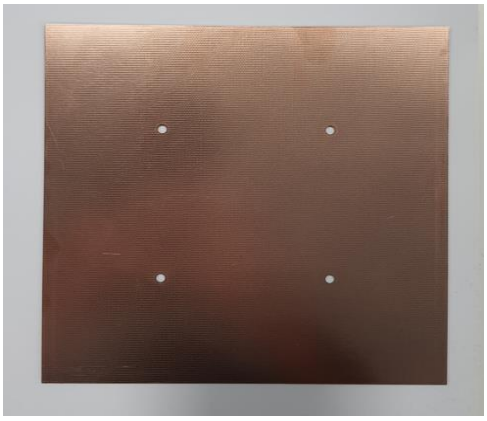

(e) Back radiation blocking ground

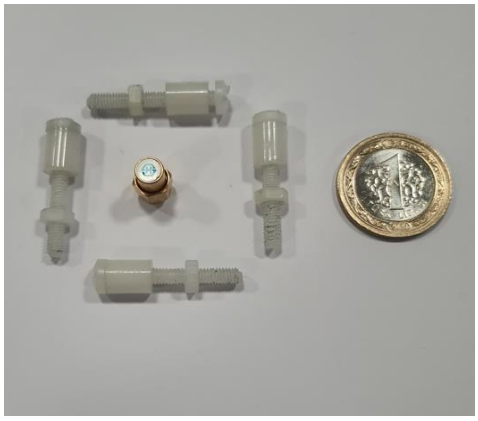

(f) Plastic screws and 50 Ω matched load

Figure 5.2: Fabricated components of the designed antenna

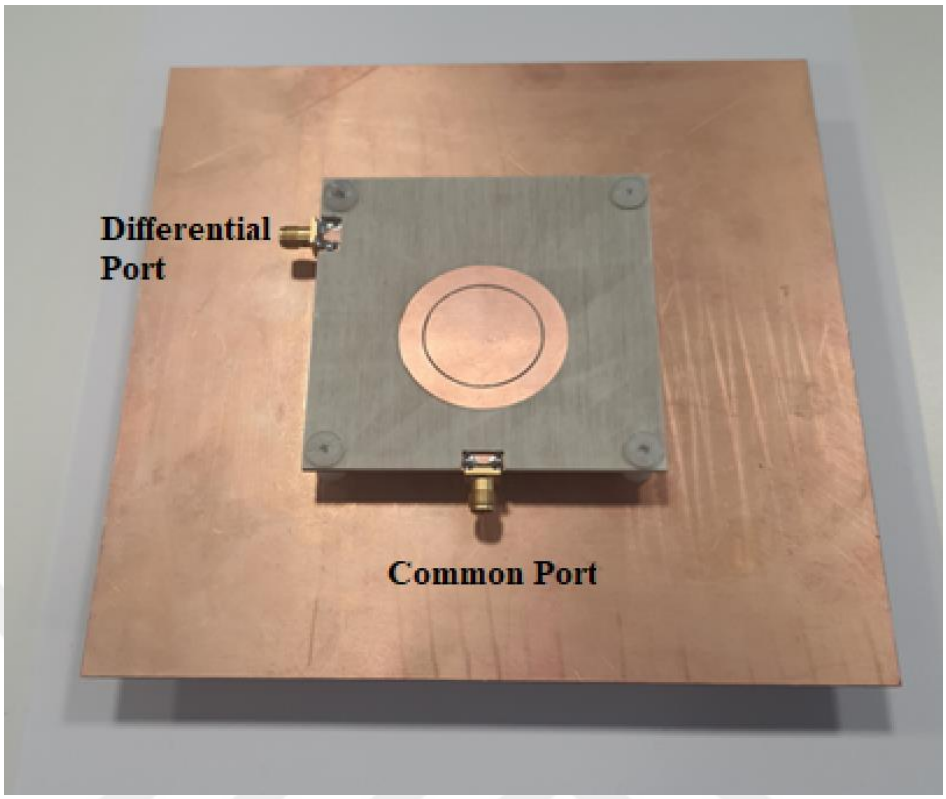

Figure 5.3: Final form of the fabricated antenna

5.2 S-parameter and Radiation Pattern Measurements

Keysight Agilent E8364B Vector Network Analyzer (VNA) is used to measure the return loss of the antenna. The measurement setup is given in Figure 5.4. Separate measurements are taken for different slot configurations given in Figure 5.2(c) (ON-ON state) and Figure 5.2(d) (OFF-ON state). Measurement and simulation results are compared in Figure 5.5 and Figure 5.6 for ON-ON state and OFF-ON state, respectively.

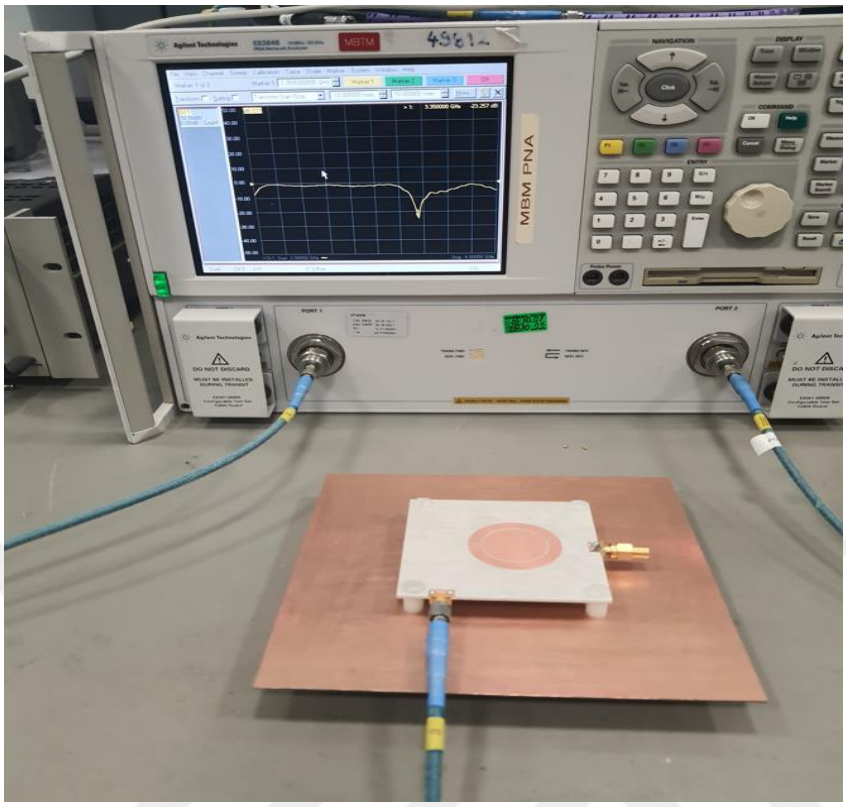

Figure 5.4: The measurement setup

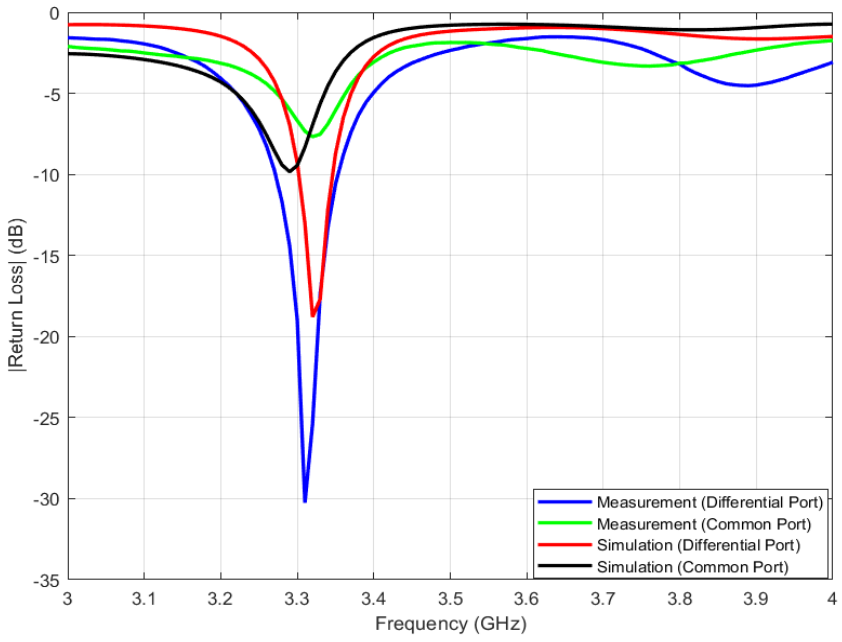

Figure 5.5: Measurement and simulation results of the S_{11} parameter of the antenna for switches on the top slot are ON, on the bottom slot are ON

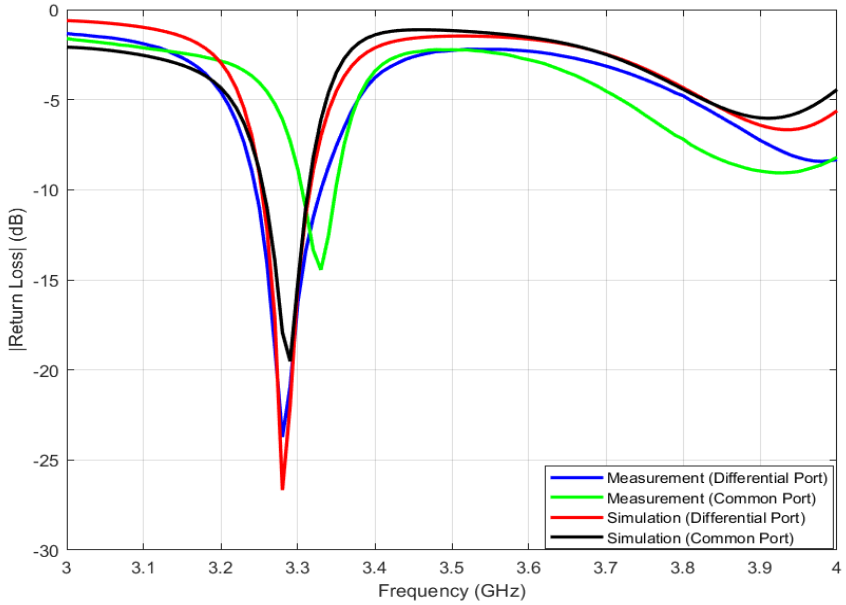

Figure 5.6: Measurement and simulation results of the S_{11} parameter of the antenna for switches on the top slot are OFF, on the bottom slot are ON

As seen in Figure 5.5, the simulation results obtained from the two ports of the antenna and the s parameter measurement results are in good agreement. As a result of the simulation for differential port, the antenna makes its deepest resonance at 3.32 GHz, and the return loss value is -18.79 dB. As a result of the measurement, the antenna makes its deepest resonance at 3.31 GHz, and the return loss value is -30.25 dB. As a result of the simulation for common port, the antenna makes its deepest resonance at 3.29 GHz, and the return loss value is -9.92 dB. As a result of the measurement, the antenna makes its deepest resonance at 3.32 GHz, and the return loss value is -7.67 dB. The measurement results come at a higher frequency than the simulation results because no matter how hard the plastic screws connecting the two-layer structure are tightened, an air gap remains between the two layers. Due to this air gap, the resonance frequency shifts up a little.

As seen in Figure 5.6, the simulation results obtained from the two ports of the antenna and the s parameter measurement results are in good agreement as well when one of the slots is made active. As a result of the simulation for differential port, the antenna makes its deepest resonance at 3.28 GHz, and the return loss value is -26.66 dB. As a result of the measurement, the antenna makes its deepest resonance at 3.28 GHz, and the return loss value is -23.72 dB. As a result of the simulation for common port, the antenna makes its deepest resonance at 3.3 GHz, and the return loss value is -19.02 dB. As a result of the measurement, the antenna makes its deepest resonance at 3.33 GHz, and the return loss value is -14.44 dB.

After measuring the s parameter of the antenna, the radiation pattern measurement phase is started. The far-field radiation pattern of the antenna are measured in the SATIMO Spherical Near-Field Measurement System, shown in Figure 5.7. In this system, automatic transformations are made to obtain the far-field radiation pattern after the radiation pattern is measured in the near field. The SH2000 antenna is used as the standard gain source antenna in the radiation pattern measurement. The source antenna is placed in the system, as shown in Figure 5.8, and the calibration process is performed.

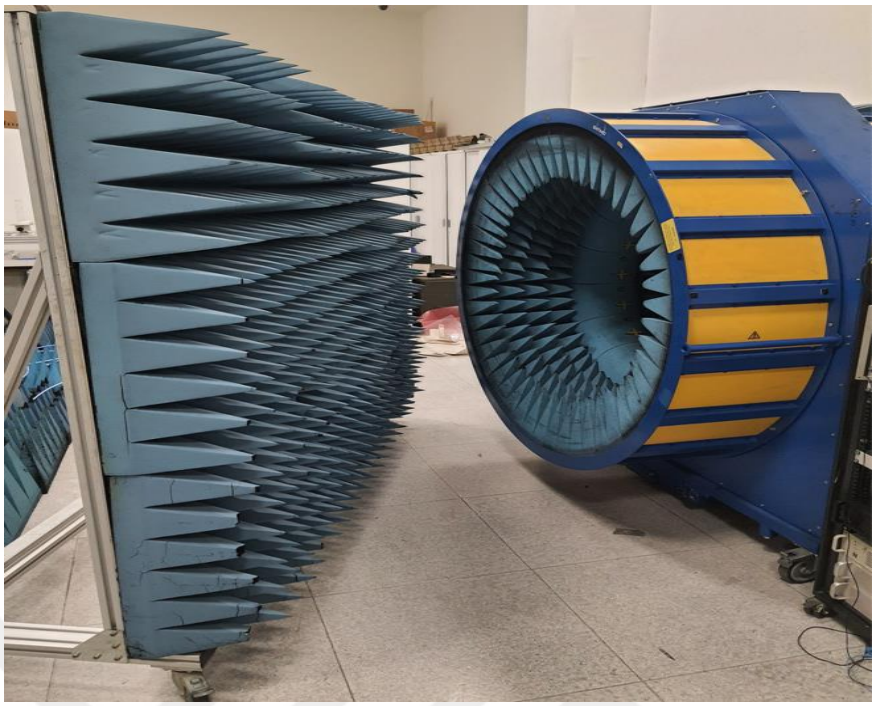

Figure 5.7: SATIMO Spherical Near Field Measurement System

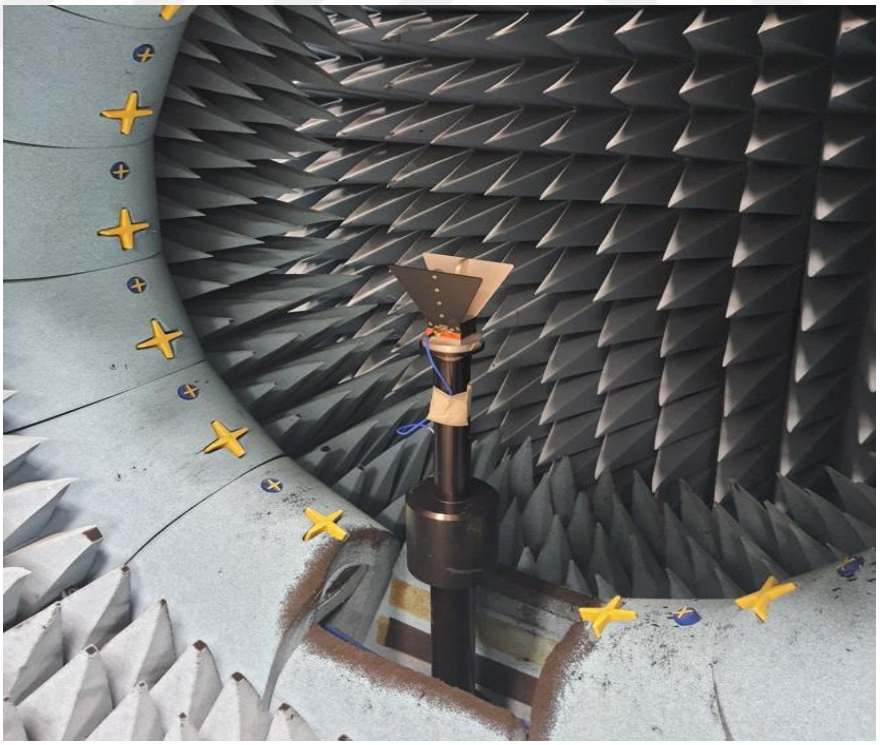

Figure 5.8: SH2000 source antenna

After the gain calibration of the source antenna, the antenna whose radiation pattern and gain will be measured is placed in SATIMO, as shown in Figure 5.9.

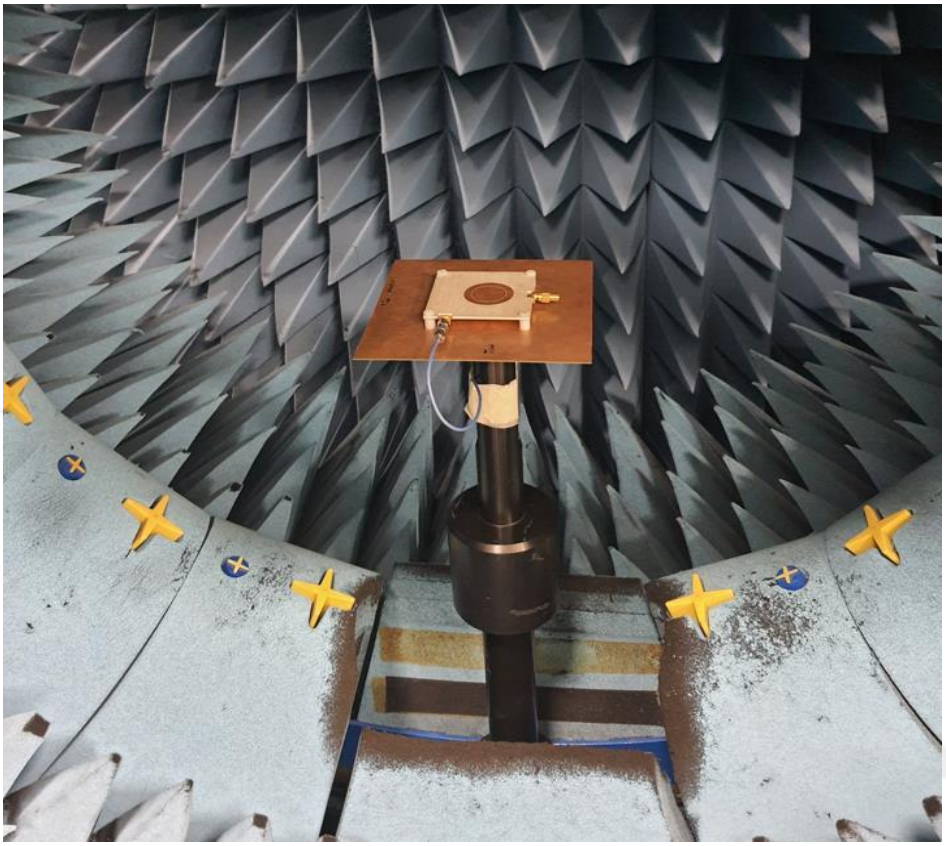

Figure 5.9: Placement of the antenna in SATIMO

Separate measurements have been taken for different slot configurations shown in Figure 5.2(c) and Figure 5.2(d). Measurement results and simulation results for ON-ON state are compared in Figure 5.10 and Figure 5.11, for differential and common ports, and for OFF-ON state in Figure 5.12 and Figure 5.13 for differential and common ports, respectively.

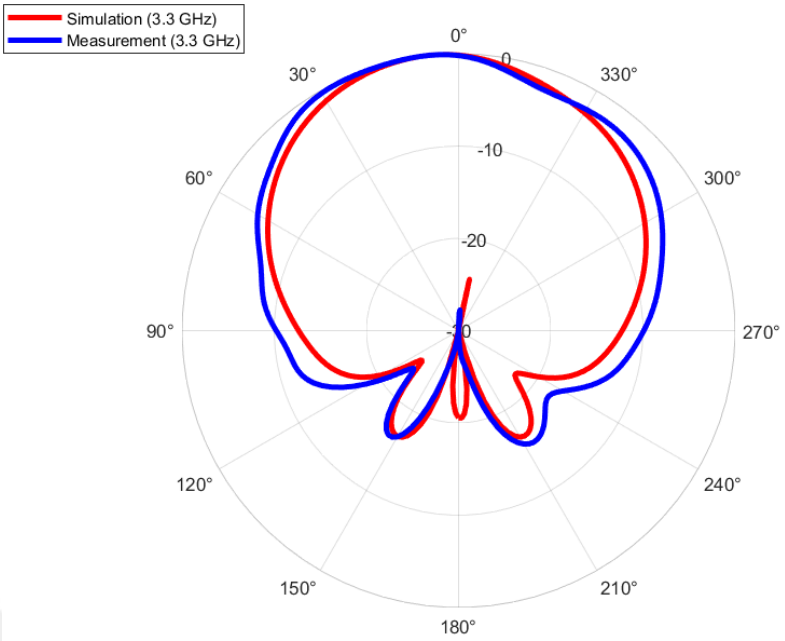

Figure 5.10: Normalized radiation pattern results of the antenna at ϕ=90˚ plane for ON-ON state when the differential port is excited

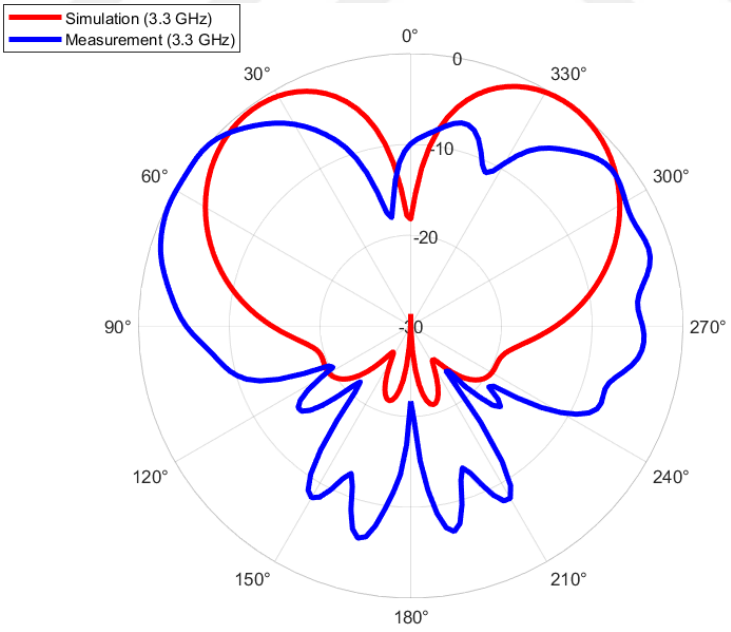

Figure 5.11: Normalized radiation pattern results of the antenna at ϕ=90˚ plane for ON-ON state when the common port is excited

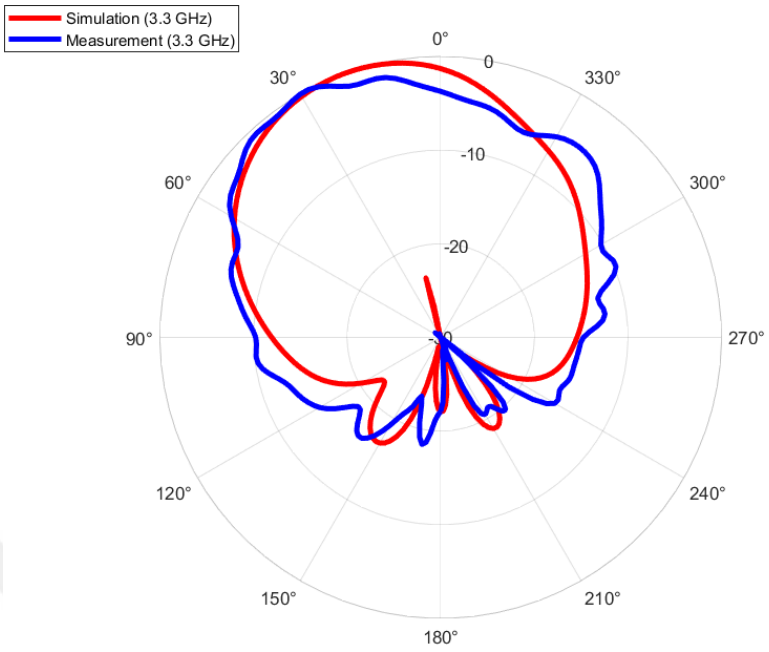

Figure 5.12: Normalized radiation pattern results of the antenna at ϕ=90˚ plane for OFF-ON state when the differential port is excited

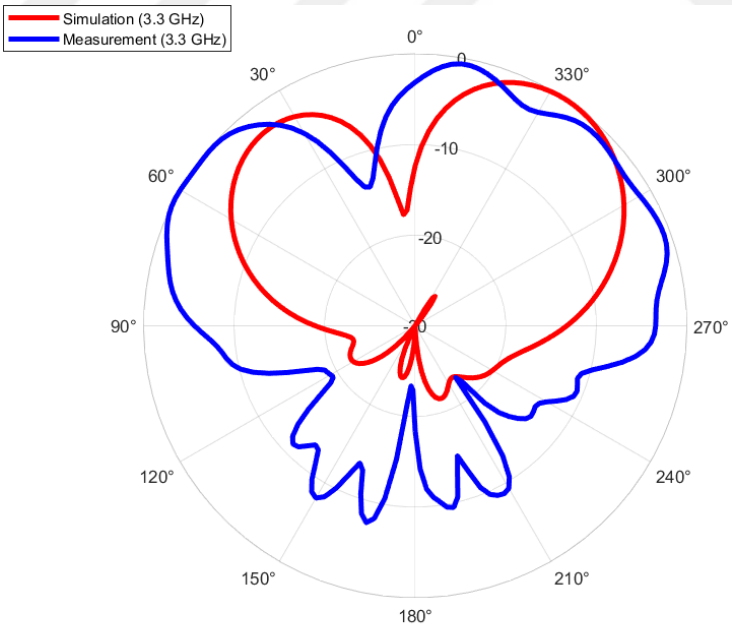

Figure 5.13: Normalized radiation pattern results of the antenna at ϕ=90˚ plane for OFF-ON state when the common port is excited

As can be seen in Figures 5.10, 5.11, 5.12, and 5.13, the radiation pattern of the antenna did not match the simulation results when the rat-race coupler and the antenna were integrated and measured together. Although the differential port feed results are similar to the simulation results, there is a serious mismatch in the common port feed results. In order to understand where the problem originates, the rat-race coupler and microstrip dual-fed antenna will be produced and measured separately in the next step.

5.3 Separate Production and Measurements of Rat-Race Coupler and Two Feed Antenna

The rat-race coupler produced for the measurement and the measurement setup prepared is given in Figure 5.14 and Figure 5.15, respectively. VNA measurement results are given in Figure 5.16, Figure 5.17, Figure 5.18, Figure 5.19, and Figure 5.20, respectively.

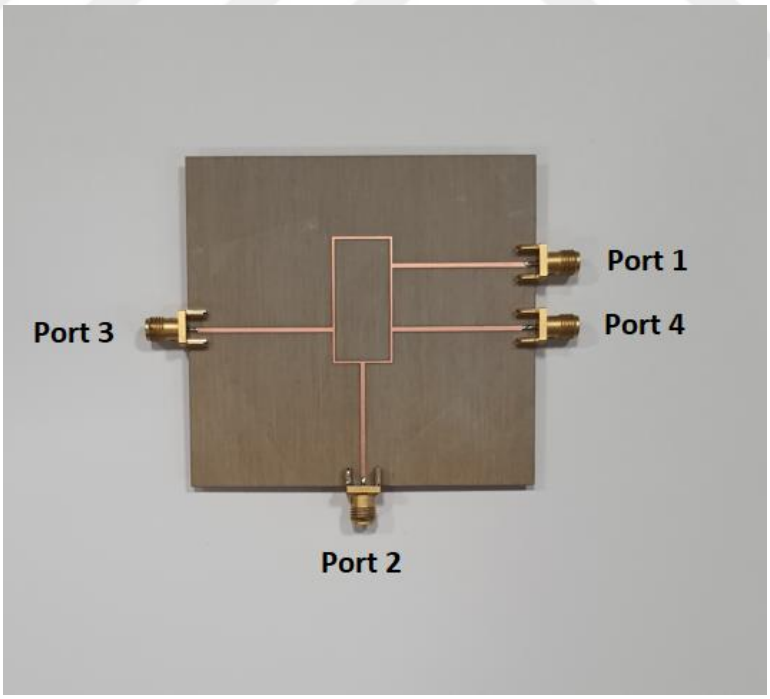

Figure 5.14: Rat-Race Coupler

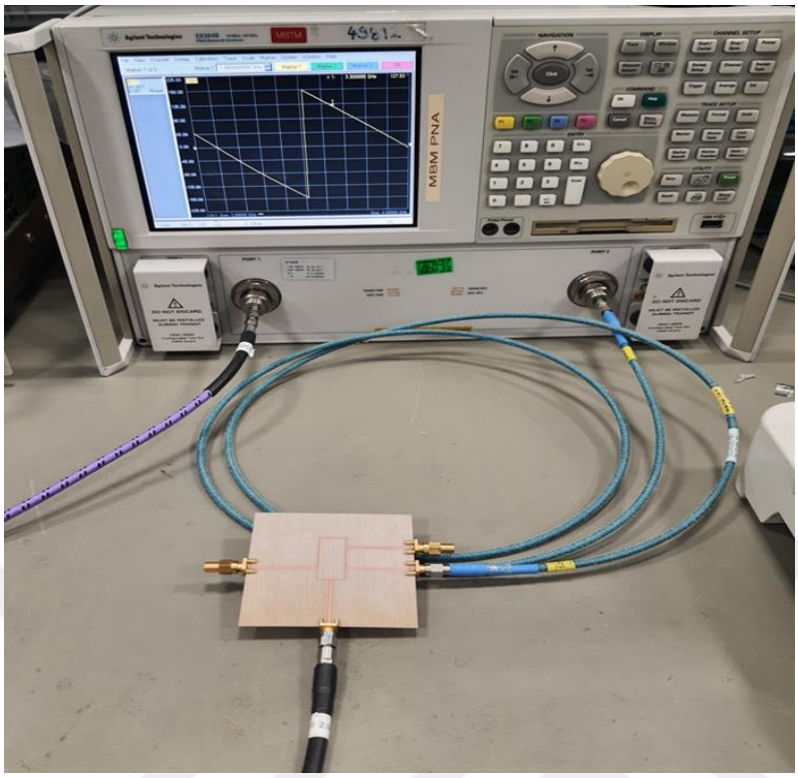

Figure 5.15: The measurement setup of rat-race coupler

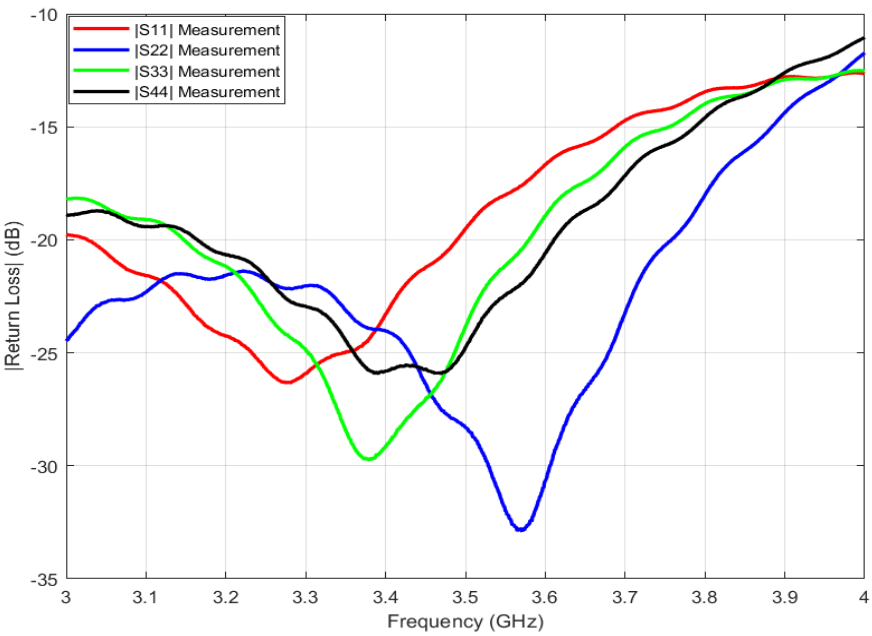

Figure 5.16: Measured return losses of all ports

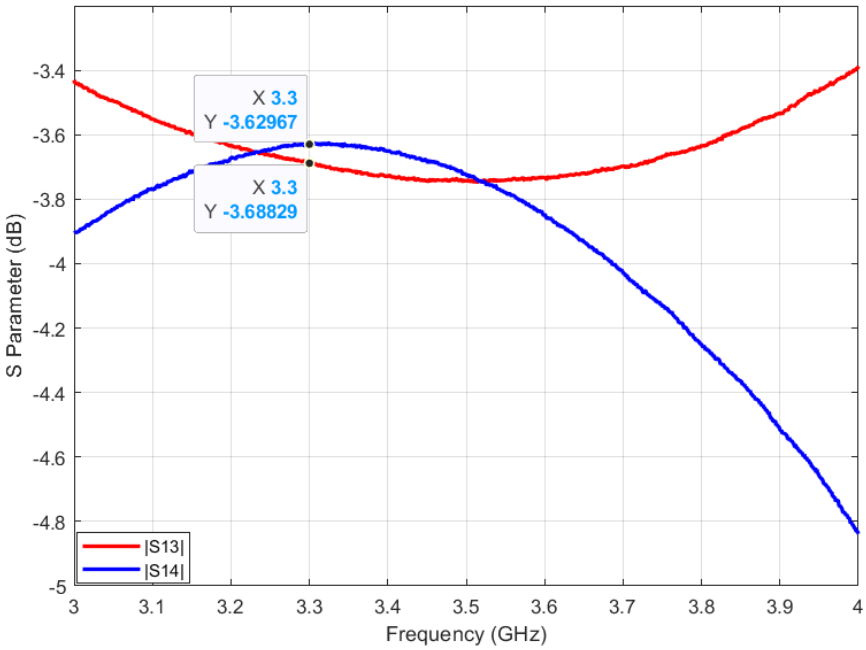

Figure 5.17: Measured magnitudes of S_{13} and S_{14}

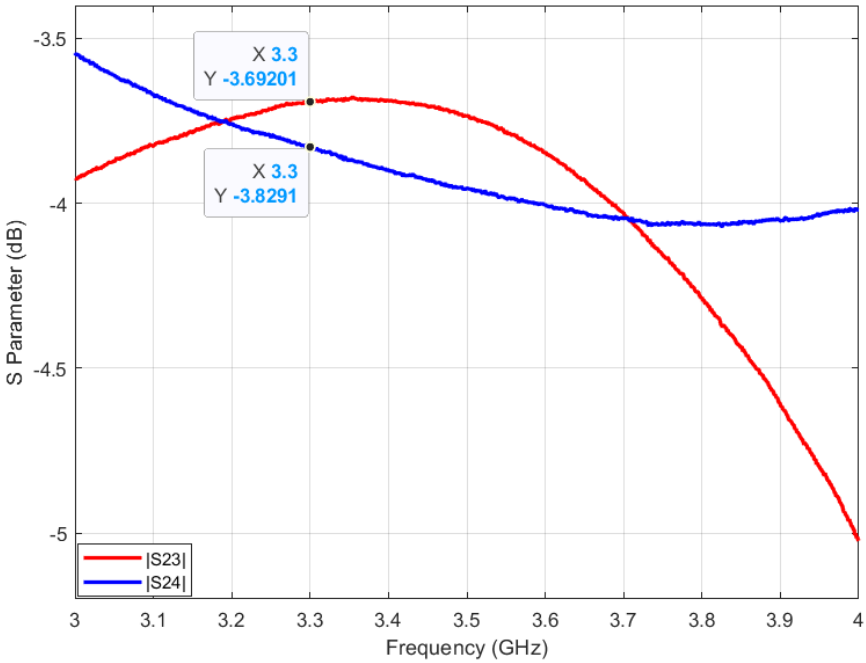

Figure 5.18: Measured magnitudes of S_{23} and S_{24}

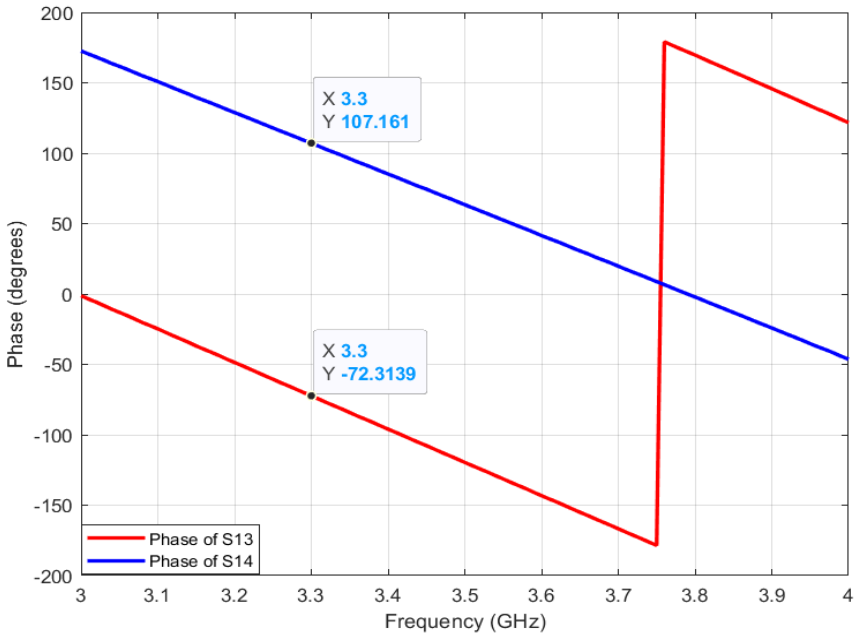

Figure 5.19: Measured phases of S_{13} and S_{14}

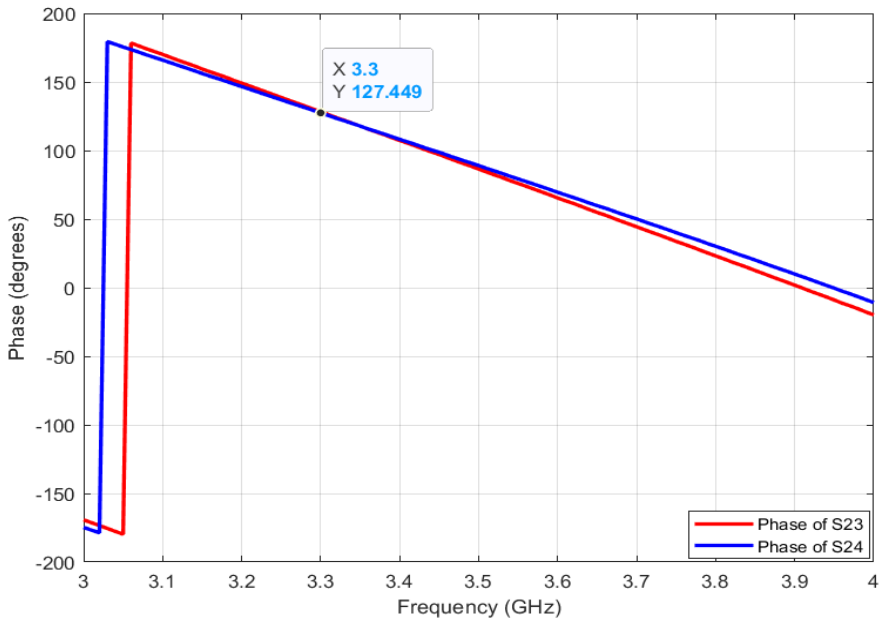

Figure 5.20: Measured phases of S_{23} and S_{24}

As can be seen in Figure 5.16, the return loss for each port is below -22 dB for 3.3 GHz. The frequency at which the return loss of Port 2 is lowest, has shifted to a higher frequency than other ports.

In the case where the rat-race coupler is fed from port 1 (differential port) or port 2 (common port), it is expected that the power would be equally divided into the antenna outgoing ports 3 and 4. As can be seen in Figure 5.17, when the rat-race coupler is fed from differential port, the incoming power is measured as -3.68 dB in 3^{rd} port and -3.63 dB in 4^{th} port at 3.3 GHz resonance frequency. According to this result, as expected, the power is divided into branches equally, with some loss. As can be seen in Figure 5.18, when the rat-race coupler is fed from common port, the incoming power is measured as -3.69 dB in 3^{rd} port and -3.82 dB in 4^{th} port at 3.3 GHz resonance frequency. According to this result, as expected, the power is divided into branches equally, with some loss.

When the rat-race coupler is fed from differential port, a 180˚ difference between the phases of port 3 and port 4 going to the antenna is expected. As can be seen in Figure 5.19, when the antenna is fed from differential port at 3.3 GHz resonant frequency, the phase of port 3 is -72.31˚, and the phase of port 4 is 107.16˚. According to this result, as expected, there is an almost 180˚ phase difference between the branches going to the antenna.

When the rat-race coupler is fed from common port, a 0˚ difference between the phases of port 3 and port 4 going to the antenna is expected. As can be seen in Figure 5.20, when the antenna is fed from common port at 3.3 GHz resonant frequency, the phase of port 3 is 128.28˚, and the phase of port 4 is 127.44˚. According to this result, as expected, there is an almost 0˚ phase difference between the branches going to the antenna.

A comparison of the simulation and measurement results of the power divided into branches from the excitation ports is given in Figure 5.21 and Figure 5.22, respectively.

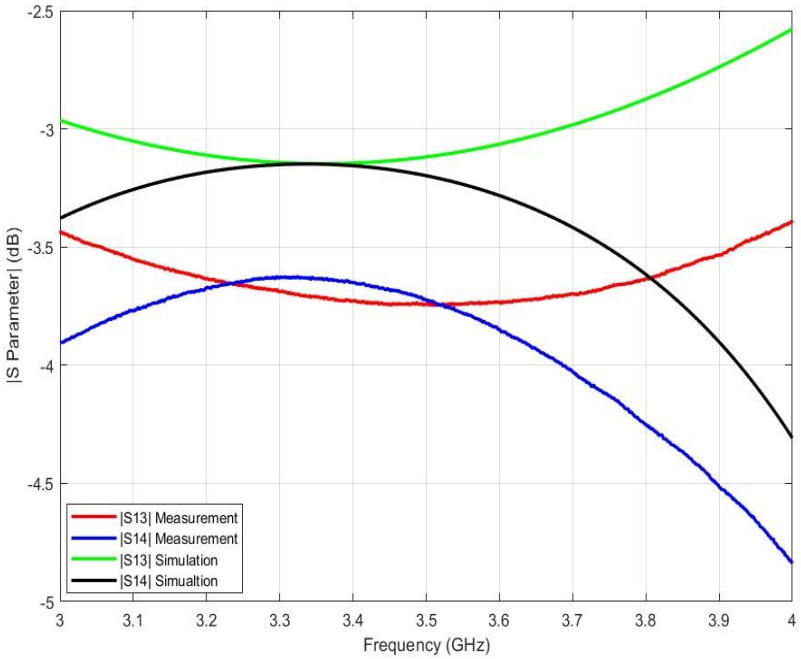

Figure 5.21: Comparison of the simulation and measurement results of the power divided into branches from Port 1

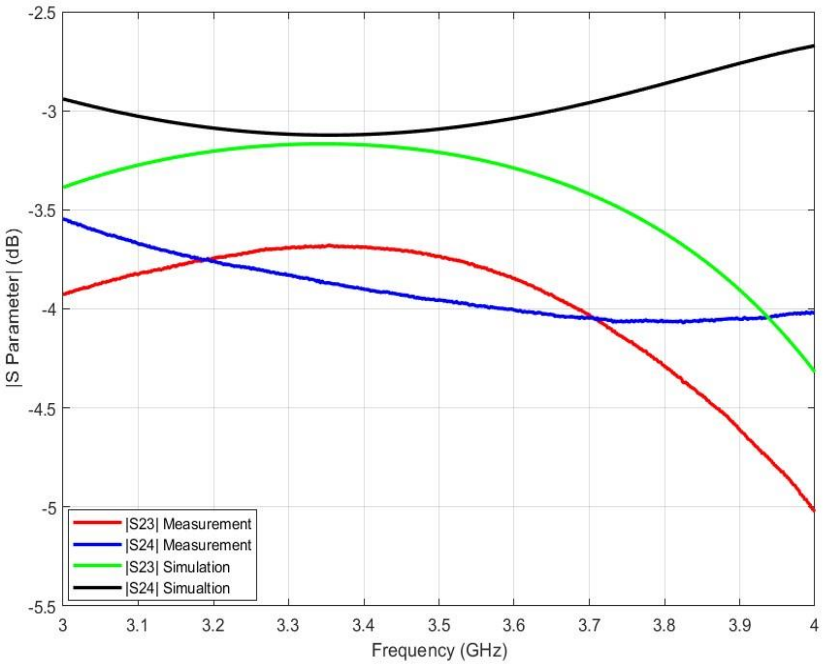

Figure 5.22: Comparison of the simulation and measurement results of the power divided into branches from Port 2

As can be seen from Figure 5.21 and Figure 5.22, the frequency dependent characteristics of the simulation and measurement results are same. The power is evenly divided into branches from the excitation ports. The reason for the loss of about 0.5 dB observed between the simulation and measurement results might be due to SMA connectors and soldering, which are not modeled in simulations.

After it is seen that the rat-race coupler is working properly, the two-port antenna is fabricated and connected to the rat-race coupler by cable. The two-port antenna ground and the cable connection of this antenna to the rat-race coupler are shown in Figure 5.23 and Figure 5.24, respectively.

Figure 5.23: Antenna feeding with two microstrip lines

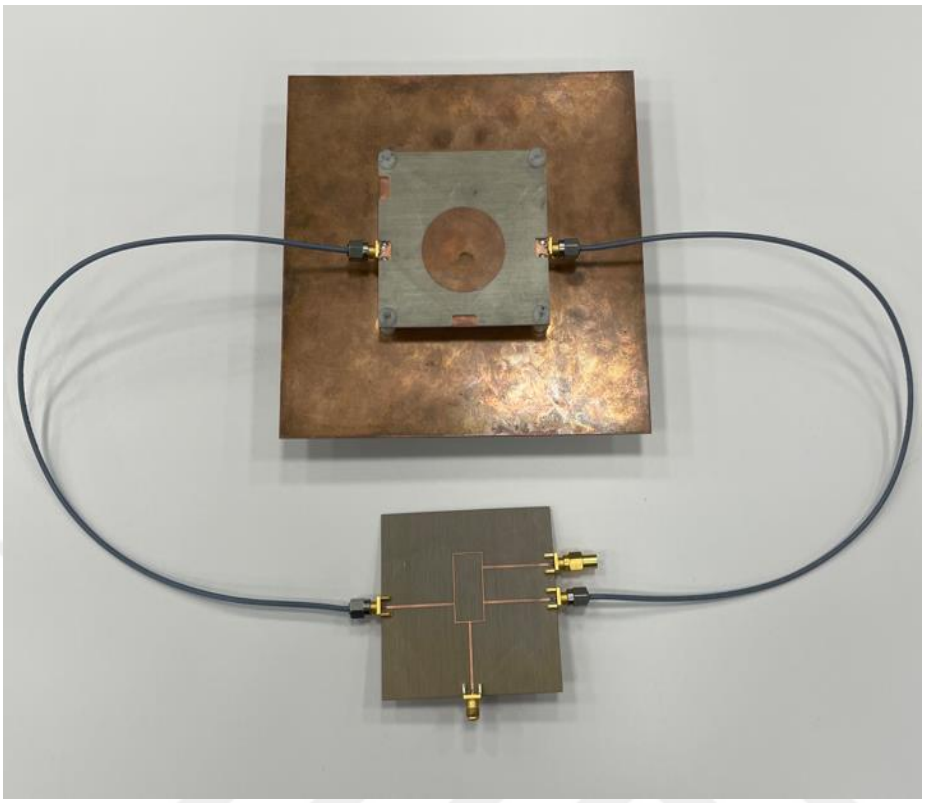

Figure 5.24: The cable connection of the antenna to the rat-race coupler

The return loss measurement results of the situation in which the rat-race coupler and the antenna are integrated with each other, and the rat-race coupler and the antenna are connected by a cable are compared in Figure 5.25 and Figure 5.26 for the ON-ON state and OFF-ON state, respectively.

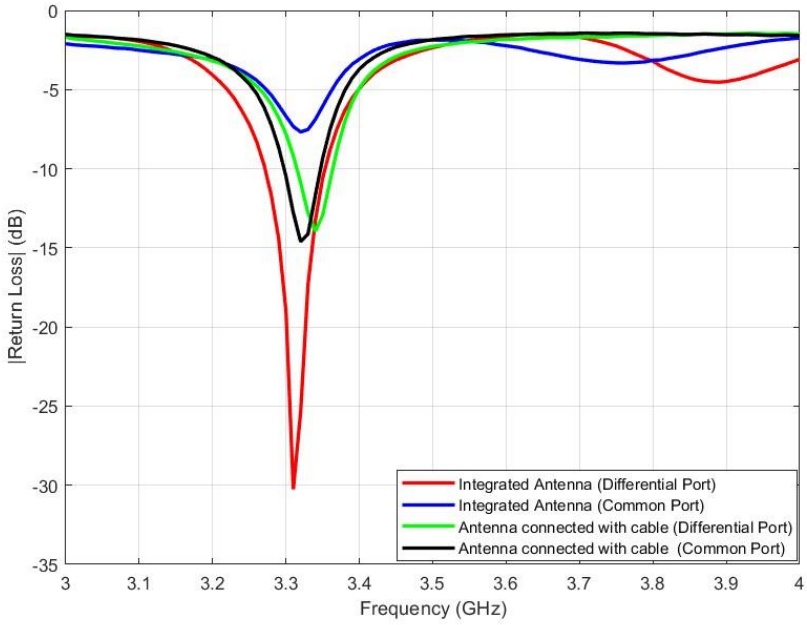

Figure 5.25: Measurement results of the S_{11} parameter of the antenna for switches on the left slot are ON, on the right slot are ON

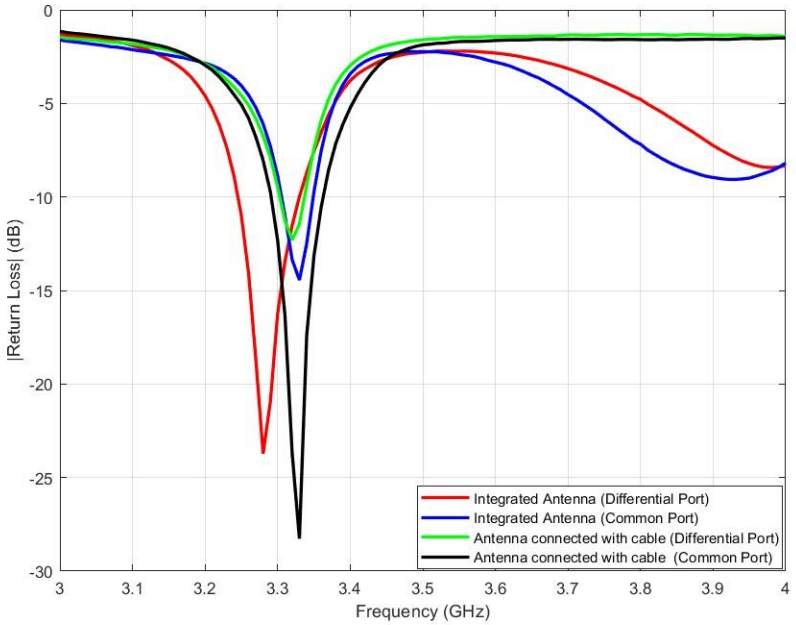

Figure 5.26: Measurement results of the S_{11} parameter of the antenna for switches on the left slot are OFF, on the right slot are ON

As seen in Figure 5.25, the return loss graphs of the situation in which the rat-race coupler and antenna are integrated and the situation in which the rat-race coupler is connected to the antenna with a cable are similar. The common port return loss has shown improvement in the case connected by a cable. In Figure 5.26, the return loss measurement graphs of the situation in which the rat-race coupler and the antenna are integrated and the situation in which the rat-race coupler is connected to the antenna by a cable are in parallel. Similar to the measurement results of the switches in the ON-ON state, the common port return loss in the OFF-ON state also showed improvement in the case connected by a cable.

The structure shown in Figure 5.24 is measured in the SATIMO Spherical Near-Field Measurement System. The measurement setup is shown in Figure 5.27.

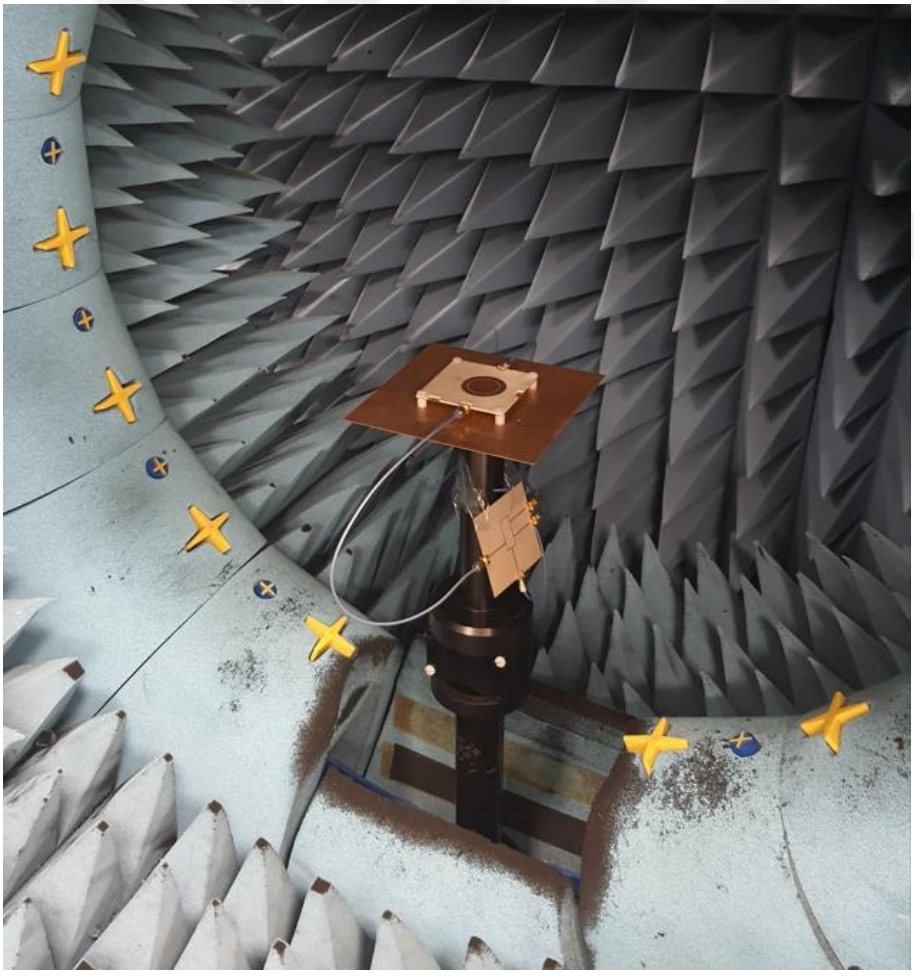

Figure 5.27: The measurement setup

Separate measurements have been taken for different slot configurations shown in Figure 5.2(c) and Figure 5.2(d). Measurement results and simulation results for ON-ON state are compared in Figure 5.28 and Figure 5.29, for differential and common ports, and for OFF-ON state in Figure 5.30 and Figure 5.31 for differential and common ports, respectively.

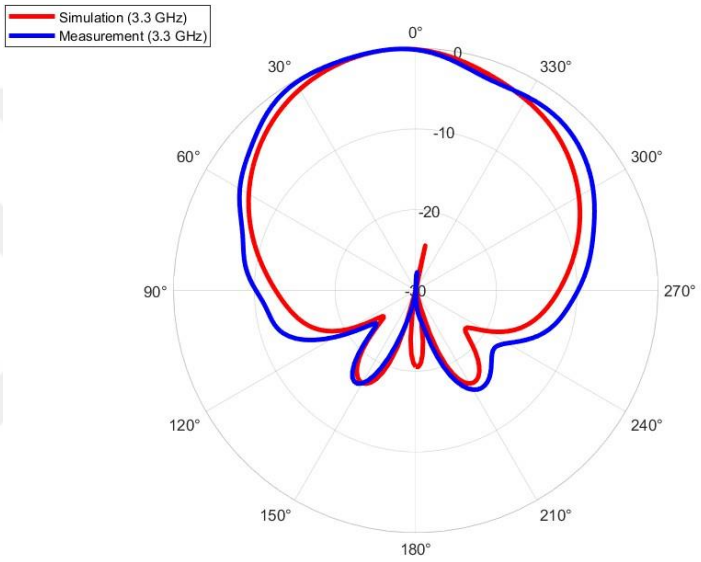

Figure 5.28: Normalized radiation pattern results of the antenna at ϕ=90˚ plane for ON-ON state when the differential port is excited

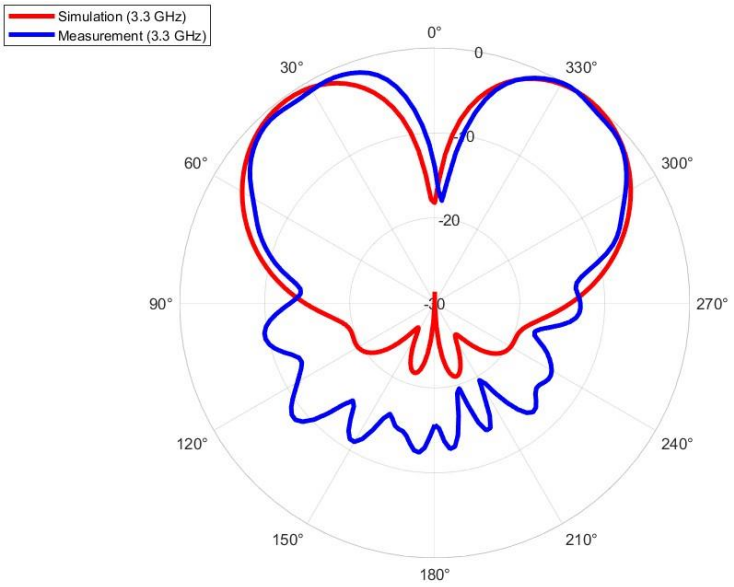

Figure 5.29: Normalized radiation pattern results of the antenna at ϕ=90˚ plane for ON-ON state when the common port is excited

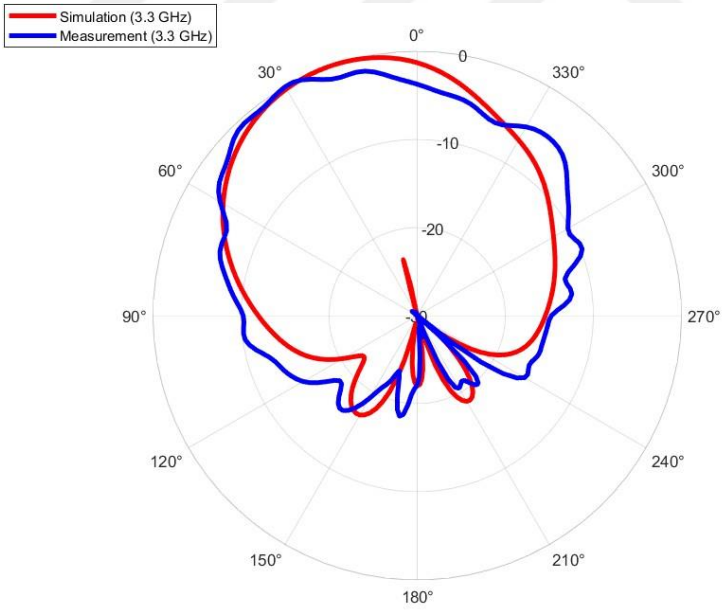

Figure 5.30: Normalized radiation pattern results of the antenna at ϕ=90˚ plane for OFF-ON state when the differential port is excited

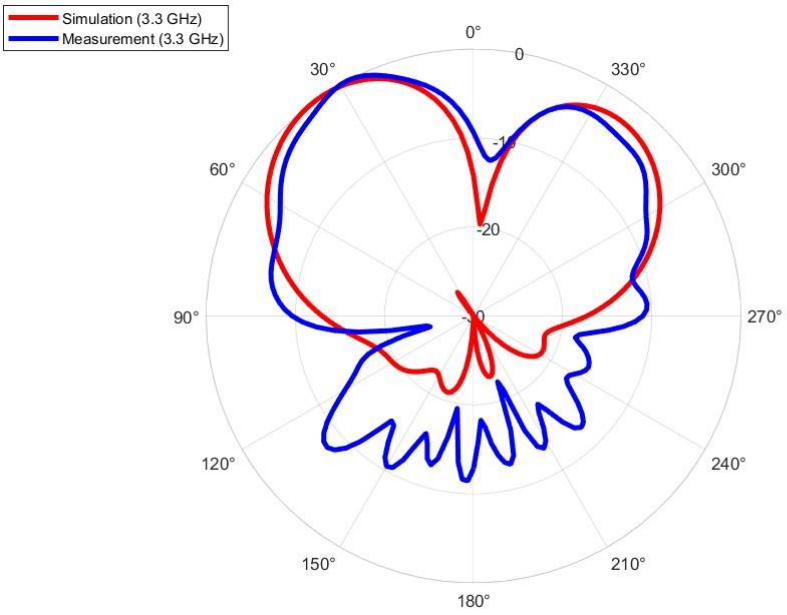

Figure 5.31: Normalized radiation pattern results of the antenna at ϕ=90˚ plane for OFF-ON state when the common port is excited

As can be seen in Figures 5.28, 5.29, 5.30, and 5.31, when the rat-race coupler and the antenna are connected to each other with a cable and the radiation pattern of the antenna is measured, the simulation results and the measurement results are consistent. The simulation and measurement results are presented in Table 5.1 and Table 5.2.

Table 5.1: Comparison of simulation and measurement results when the antenna is fed from common port

Excited Port	State	Radiation Type	Angle at which maximum gain is seen (degrees)	Simulated Gain (dB)	Measured Gain (dB)
Common	ON-ON	Conical	36	8.81	7.26
Common	OFF-ON	Asymmetric Conical	30	9.58	7.64

Table 5.2: Comparison of simulation and measurement results when the antenna is fed from differential port

Excited Port	State	Radiation Type	Angle at which maximum gain is seen (degrees)	Simulated Gain (dB)	Measured Gain (dB)
Differential	ON-ON	Broadside	0	7.15	5.37
Differential	OFF-ON	Off-Broadside	22	7.30	5.58

In order to understand the difference between the measurement results and the simulation results, the insertion loss of the cable connecting the rat race and the antenna is measured. The measurement result is shown in Figure 5.32.

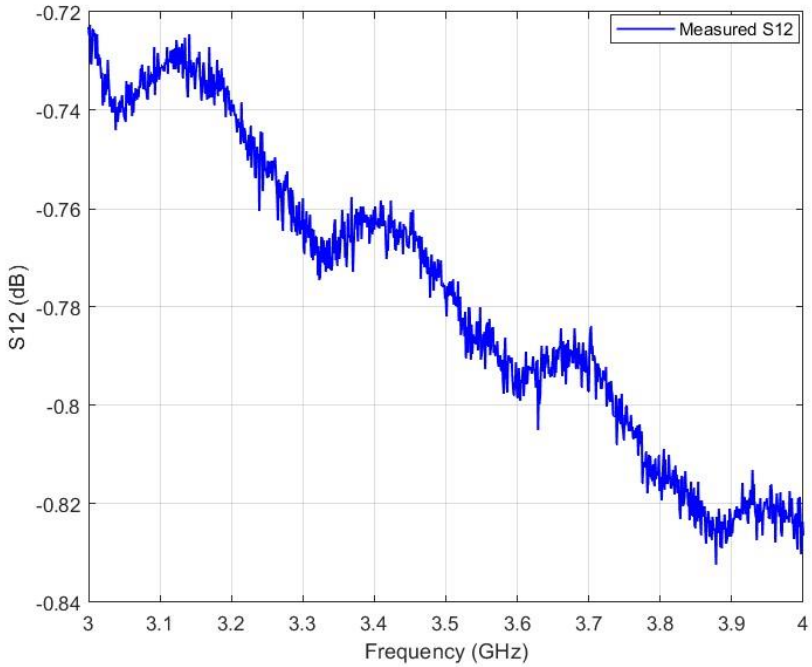

Figure 5.32: Insertion loss of the cable

As seen in Figure 5.32, the cable loss at 3.3 GHz is about 0.77 dB. When the average insertion loss of rat race coupler for common and differential ports are considered (∼0.75dB), the total loss becomes 1.52 dB. The difference between measurement results and simulation results is due to this loss.

In order to better observe the pattern reconfiguration performance of the antenna, measurement results of ON-ON state and OFF-ON state are compared in Figure 5.33 when differential port is excited.

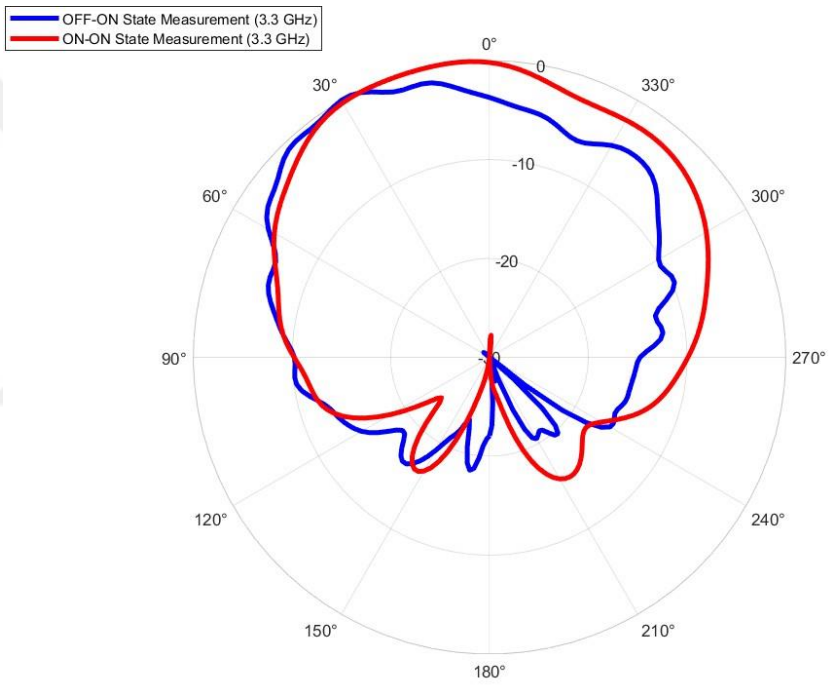

Figure 5.33: Normalized radiation pattern results of the antenna at ϕ=90˚ plane for the switches are ON-ON and OFF-ON states, when the differential port is excited

As seen from Figure 5.33, when the antenna is fed from the differential port, the radiation pattern is obtained in the broadside when both slots are short circuited. On the other hand, the antenna pattern is rotated from the broadside when one of the slots exist.

Measurement results of ON-ON state and OFF-ON state are compared in Figure 5.34, when common port is excited.

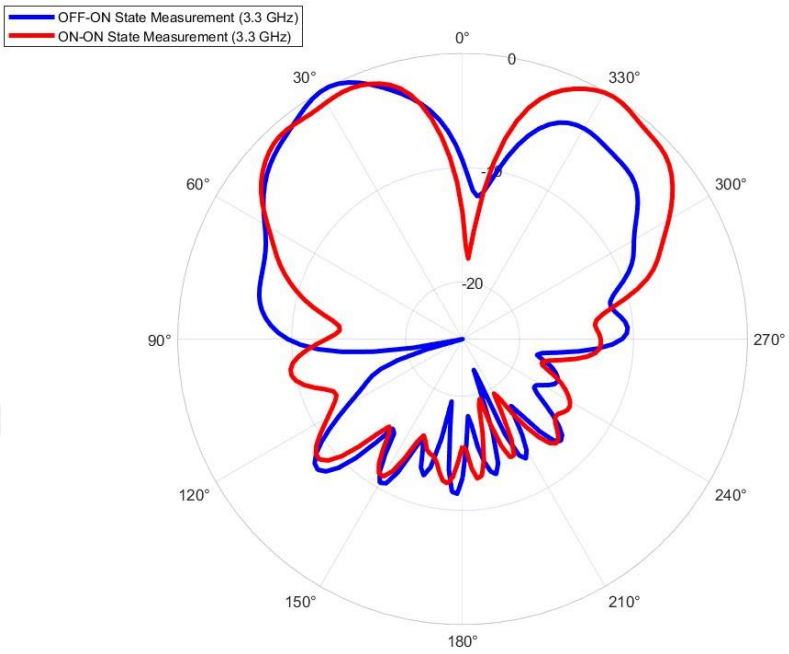

Figure 5.34: Normalized radiation pattern results of the antenna at ϕ=90˚ plane for the switches are ON-ON and OFF-ON states, when the common port is excited

As seen from Figure 5.34, when the antenna is fed from the common port, the conical radiation pattern is obtained when both slot are short circuited. When one of the slots exists, the right side of the initially conical radiation pattern has been suppressed, and the left side has been enhanced as expected. These measurement results show that the radiation pattern of the antenna can be controlled by using slots in the ground plane of the antenna.

CHAPTER 6

CONCLUSION

This thesis focuses on radiation pattern reconfigurable antennas that can be used in 5G Massive MIMO systems. The primary motivation is to prevent the gain reduction caused by the element pattern and array pattern not being in the same direction, which is frequently seen in array antennas. At this point, slots are opened in the ground plane of the antenna to control the element pattern. Through the RF-MEMS switches placed in the opened slots, the element radiation pattern has changed from conical to asymmetrical conical radiation as a result of in-phase feeding. As a result of out-of-phase feeding, the antenna radiation pattern has rotated to a different angle from the broadside radiation. In addition, a rat-race coupler is designed, and the antenna is fed from a single port. The rat-race coupler gives the phase difference automatically, and another port is terminated with 50 Ω.

The antenna designed at 26 GHz within the scope of the thesis is in the structure of a two-layer microstrip antenna. A grounded coplanar waveguide (GCPW) fed from an inductive slot is chosen to excite the antenna. Glass is chosen as the substrate of the GCPW, and the dielectric substrate of the antenna is chosen High Resistivity Silicon (HRS). Through the slots opened on the ground plane and on the circular ring and the RF-MEMS switches placed in these slots, the radiation pattern of the antenna has been reconfigured. The antenna radiation pattern has been reconfigured for six different states when the antenna is fed in-phase and out-of-phase. When the antenna is fed in-phase, the directivity of the antenna increases in a certain direction while it decreases in a symmetrical direction. In other words, an asymmetric radiation pattern is obtained by controlling the RF-MEMS switches. The angle at which the maximum gain of the antenna is observed is ±30˚. Through the slots opened on the outer circular ring, the radiation pattern is directed in a different direction from the broadside

radiation pattern without the need for out-of-phase feeding of the antenna. The rotation angle at which the maximum gain of the antenna is observed is ±38˚.

An agreement has been reached with the METU MEMS Center for producing the ring circular patch antenna designed at 26 GHz. However, this antenna could not be produced due to some production problems and the prolongation of the production process. To verify the concept, the antenna is designed and manufactured on a material with a lower dielectric constant. ROGERS4003 is chosen as the lower substrate and the upper substrate. Also, 3.3 GHz is chosen as the antenna operating frequency. Since the antenna size increases at low frequency, it is planned to control the slots in the ground plane of the antenna with PIN diode switches for pattern reconfiguration. The antenna is excited by the slot coupling technique using two feeds, and a microstrip transmission line is chosen as the feeding structure. In addition, a rat-race coupler has been designed so the antenna can be fed from a single port, and the 180˚ phase difference can be automatically given. The unexcited port is terminated with a 50 Ω matched load. The antenna radiation pattern has been reconfigured for three different states when the antenna is fed in-phase and out-of-phase. When the antenna is fed in-phase, the directivity of the antenna increases in a certain direction while it decreases in a symmetrical direction. In other words, an asymmetric radiation pattern is obtained by controlling the PIN diode switches. When the antenna is fed out-of-phase, the radiation pattern diverts to a different angle from the broadside radiation pattern..

The design, which operates at 3.3 GHz, is fabricated and measured. Scattering parameters, radiation pattern, and gain measurements are taken from the fabricated prototypes. The measurement results of the antenna illustrate a notable agreement with the simulation values.

As a result, the prevention of gain reduction caused by the fact that the array radiation pattern and the element radiation pattern are not in the same direction in the array antennas, which is the primary purpose of the thesis, is achieved by controlling the

element radiation pattern. The element radiation pattern is controlled through the RF-MEMS switches and PIN diode switches placed on the antenna ground plane.

In future work first the design of the antenna operating at 26 GHz will be refined according to the active s-parameter values. Secondly, the reasons behind the observation that the asymmetry created in the radiation pattern of the GCPW fed antenna is better than the asymmetry created in the radiation pattern of the aperture coupled fed antenna, can be investigated. In addition, the reasons why the mode change can not be achieved by opening a slot on the ring in the antenna operating at 3.3 GHz can be investigated.

REFERENCES

[1] Bernhard, Jennifer T. "Reconfigurable antennas." *Synthesis lectures on antennas* 2.1 (2007): 1-66.

[2] Christodoulou, C. G., Tawk, Y., Lane, S. A., & Erwin, S. R. (2012). Reconfigurable antennas for wireless and space applications. *Proceedings of the IEEE*, *100*(7), 2250-2261.

[3] Zhang, S., Huff, G. H., Feng, J., & Bernhard, J. T. (2004). A pattern reconfigurable microstrip parasitic array. *IEEE Transactions on Antennas and Propagation*, *52*(10), 2773-2776.

[4] Luther, J. J., Ebadi, S., & Gong, X. (2012). A microstrip patch electronically steerable parasitic array radiator (ESPAR) antenna with reactance-tuned coupling and maintained resonance. *IEEE Transactions on Antennas and Propagation*, *60*(4), 1803-1813.

[5] Ding, X., & Wang, B. Z. (2013). A novel wideband antenna with reconfigurable broadside and endfire patterns. *IEEE Antennas and Wireless Propagation Letters*, *12*, 995-998.

[6] Chen, S. L., Qin, P. Y., Lin, W., & Guo, Y. J. (2018). Pattern-reconfigurable antenna with five switchable beams in elevation plane. *IEEE Antennas and Wireless Propagation Letters*, *17*(3), 454-457.

[7] Ha, S. J., & Jung, C. W. (2011). Reconfigurable beam steering using a microstrip patch antenna with a U-slot for wearable fabric applications. *IEEE Antennas and Wireless Propagation Letters*, *10*, 1228-1231.

[8] Kishor, K. K., & Hum, S. V. (2014). A pattern reconfigurable chassis-mode MIMO antenna. *IEEE transactions on antennas and propagation*, *62*(6), 3290-3298.

[9] Li, K., & Shi, Y. (2018). A pattern reconfigurable MIMO antenna design using characteristic modes. *IEEE Access*, *6*, 43526-43534.

[10] Dicandia, F. A., Genovesi, S., & Monorchio, A. (2018). Efficient excitation of characteristic modes for radiation pattern control by using a novel balanced inductive coupling element. *IEEE Transactions on Antennas and Propagation*, *66*(3), 1102-1113.

[11] Wei, K., Zhang, Z., Chen, W., & Feng, Z. (2010). A novel hybrid-fed patch antenna with pattern diversity. *IEEE Antennas and Wireless Propagation Letters*, *9*, 562-565.

[12] Jiang, X., Zhang, Z., Li, Y., & Feng, Z. (2014). A novel null scanning antenna using even and odd modes of a shorted patch. *IEEE transactions on antennas and propagation*, *62*(4), 1903-1909.

[13] Selvam, Y. P., Kanagasabai, M., Alsath, M. G. N., Velan, S., Kingsly, S., Subbaraj, S., ... & Karuppiah, M. (2017). A low-profile frequency-and pattern-reconfigurable antenna. *IEEE Antennas and Wireless Propagation Letters*, *16*, 3047-3050.

[14] Lau, K. L., & Luk, K. M. (2005). A wide-band monopolar wire-patch antenna for indoor base station applications. *IEEE Antennas and Wireless Propagation Letters*, *4*, 155-157.

[15] Liu, J., Xue, Q., Wong, H., Lai, H. W., & Long, Y. (2012). Design and analysis of a low-profile and broadband microstrip monopolar patch antenna. *IEEE Transactions on Antennas and Propagation*, *61*(1), 11-18.

[16] Yang, S. L., & Luk, K. M. (2006). Design of a wide-band L-probe patch antenna for pattern reconfiguration or diversity applications. *IEEE Transactions on Antennas and Propagation*, *54*(2), 433-438.

[17] Lin, W., Wong, H., & Ziolkowski, R. W. (2017). Circularly polarized antenna with reconfigurable broadside and conical beams facilitated by a mode switchable feed network. *IEEE Transactions on Antennas and Propagation*, *66*(2), 996-1001.

[18] Liang, Z., Liu, J., Li, Y., & Long, Y. (2015). A dual-frequency broadband design of coupled-fed stacked microstrip monopolar patch antenna for WLAN applications. *IEEE Antennas and Wireless Propagation Letters*, *15*, 1289-1292.

[19] Tran, T. Q., & Sharma, S. K. (2011). Radiation characteristics of a multimode concentric circular microstrip patch antenna by controlling amplitude and phase of modes. *IEEE transactions on antennas and propagation*, *60*(3), 1601-1605.

[20] Çelik, F. T. (2021). *Pattern reconfigurable antenna designs insub-6 ghz band for 5g applications* (Master's thesis, Middle East Technical University).

[21] Balanis, C. A. (2015). *Antenna theory: analysis and design*. John wiley & sons.

[22] Garg, R., Bhartia, P., Bahl, I. J., & Ittipiboon, A. (2001). *Microstrip antenna design handbook.* Artech house.

[23] Giauffret, L., & Laheurte, J. M. (1999). Parametric study of the coupling aperture in CPW–fed microstrip antennas. *IEE Proceedings-Microwaves, Antennas and Propagation*, *146*(3), 169-174.

[24] Tonga, M. (2022). *DESIGN OF A DECOUPLING NETWORK TO IMPROVE ISOLATION BETWEEN TWO PORTS OF MULTI-FUNCTIONAL ANTENNA* (Master's thesis, Middle East Technical University).

[25] Aydın, T. (2020). *Design of pattern reconfigurable antennas by using characteristic mode theory* (Master's thesis, Middle East Technical University).